

SAND REPORT

SAND2004-1030
Unlimited Release
Printed March 2004

Laboratory Constitutive Characterization of Cellular Concrete

Moo Y. Lee, David R. Bronowski, and Robert D. Hardy

Prepared by
Sandia National Laboratories
Albuquerque, New Mexico 87185 and Livermore, California 94550

Sandia is a multiprogram laboratory operated by Sandia Corporation,
a Lockheed Martin Company, for the United States Department of
Energy under Contract DE-AC04-94AL85000.

Approved for public release; further dissemination unlimited.



Issued by Sandia National Laboratories, operated for the United States Department of Energy by Sandia Corporation.

NOTICE: This report was prepared as an account of work sponsored by an agency of the United States Government. Neither the United States Government, nor any agency thereof, nor any of their employees, nor any of their contractors, subcontractors, or their employees, make any warranty, express or implied, or assume any legal liability or responsibility for the accuracy, completeness, or usefulness of any information, apparatus, product, or process disclosed, or represent that its use would not infringe privately owned rights. Reference herein to any specific commercial product, process, or service by trade name, trademark, manufacturer, or otherwise, does not necessarily constitute or imply its endorsement, recommendation, or favoring by the United States Government, any agency thereof, or any of their contractors or subcontractors. The views and opinions expressed herein do not necessarily state or reflect those of the United States Government, any agency thereof, or any of their contractors.

Printed in the United States of America. This report has been reproduced directly from the best available copy.

Available to DOE and DOE contractors from

U.S. Department of Energy
Office of Scientific and Technical Information
P.O. Box 62
Oak Ridge, TN 37831

Telephone: (865)576-8401
Facsimile: (865)576-5728
E-Mail: reports@adonis.osti.gov
Online ordering: <http://www.doe.gov/bridge>

Available to the public from

U.S. Department of Commerce
National Technical Information Service
5285 Port Royal Rd
Springfield, VA 22161

Telephone: (800)553-6847
Facsimile: (703)605-6900
E-Mail: orders@ntis.fedworld.gov
Online order: <http://www.ntis.gov/ordering.htm>



SAND 2004-1030

Unlimited Release

Printed March 2004

Laboratory Constitutive Characterization of Cellular Concrete

Moo Y. Lee, David R. Bronowski, and Robert D. Hardy
Geomechanics Department
Sandia National Laboratories
P.O. Box 5800
Albuquerque, NM 87185-0751

ABSTRACT

To establish mechanical material properties of cellular concrete mixes, a series of quasi-static, compression and tension tests have been completed. This report summarizes the test methods, set-up, relevant observations, and results from the constitutive experimental efforts. Results from the uniaxial and triaxial compression tests established failure criteria for the cellular concrete in terms of stress invariants I_1 and J_2 .

$$\sqrt{J_2} \text{ (MPa)} = 297.2 - 278.7 \exp^{-0.000455 I_1 \text{ (MPa)}} \text{ for the 90-pcf concrete}$$

$$\sqrt{J_2} \text{ (MPa)} = 211.4 - 204.2 \exp^{-0.000628 I_1 \text{ (MPa)}} \text{ for the 60-pcf concrete}$$

ACKNOWLEDGEMENTS

The authors would like to appreciate the support of Allen Shirley and Edward O'Connor of the Naval Surface Warfare Center, Dahlgren, Virginia (NSWCDD), who have funded the laboratory experimental project. The authors also thank to Larry Costin and Mike Riggins for their critical review of this report.

Table of Contents

1. Introduction.....	9
2. Unconfined Compression Tests (UCT)	11
3. Triaxial Compression (TXC) / Hydrostatic Compression Tests (HCT)	15
4. Uniaxial Strain Tests (UXE)	25
5. Triaxial Extension Tests (TXE).....	28
6. Uniaxial Tension Tests (UTT).....	32
7. Conclusions.....	34
References.....	35
Appendix A Cellular Concrete	36
Appendix B Stress-Strain Plots from Uniaxial Compression Testing (UCT) of Cellular concrete (σ_a -axial stress, ε_a -axial strain, ε_l -lateral strain, and ε_v -volumetric strain)	46
Appendix C-1 Stress-Strain Plots from Hydrostatic Compression Tests (HCT) of Cellular concrete (σ_a -axial stress, ε_a -axial strain, ε_l -lateral strain, ε_v -volumetric strain, and P-confining pressure).....	49
Appendix C-2 Stress-Strain Plots from Triaxial Compression (TXC) / Hydrostatic Compression Tests (HCT) of Cellular concrete (σ_a -axial stress, ε_a -axial strain, ε_l -lateral strain, ε_v -volumetric strain, and P-confining pressure).....	52
Appendix D Stress-Strain Plots from Uniaxial Strain Tests (UXE) of Cellular concrete (σ_a -axial stress, ε_a -axial strain, and ε_v -volumetric strain).....	61
Appendix E Stress-Strain-Time and Stress-Strain Plots from Triaxial Extension Tests (TXE) of Cellular concrete (σ_a -axial stress, σ_1 -major principal stress, σ_2 -intermediate principal stress, σ_3 -minor principal stress, σ_{3T} -triaxial extension strength, ε_a -axial strain, ε_l -lateral strain, and P-confining pressure).....	64
Appendix F Stress-Displacement Plots from Uniaxial Tension Tests (UTT) of Cellular concrete (-T : uniaxial tensile strength).....	70
Appendix G List of Data and Supplemental Files Archived in Webfileshare System.....	74

Figures

Figure 1. Stress-strain plot for the uniaxial compression test of specimen FC-UC901.....12

Figure 2. Failed concrete specimens, FC-UC601 (left) and FC-UC901 (right), under uniaxial compression stress condition ($\sigma_1 \neq 0, \sigma_2 = \sigma_3 = 0$). A lateral LVDT is shown with a mounting device for measuring diametral deformations of the specimen.....12

Figure 3. Linear segments of the axial stress (σ_a) - axial strain (ϵ_a) plot obtained during the unconfined compression tests (UCT) for the cellular concrete. The Young’s modulus, E, was obtained as the slope of the best-fit straight line.....13

Figure 4. Linear segments of the lateral strain (ϵ_l) - axial strain (ϵ_a) plot obtained during the unconfined compression tests (UCT) for the cellular concrete. The Poisson’s ratio, ν , is obtained as the slope of the best-fit straight line.....14

Figure 5. Instrumented concrete specimens for triaxial compression (TXC) / hydrostatic compression (HCT) tests. Shown are the axial LVDTs and the Schuler gage for measuring axial and lateral displacements, respectively. The specimen on the left is prepared for confining pressures up to 400 MPa and the specimen on the right is for up to 1,000 MPa confining pressure.15

Figure 6. The pressure-strain plot obtained during hydrostatic compression test (HCT) of the FC-HC900 specimen up to 200 MPa pressure. The graphical representation of the bulk modulus, K, is also indicated as the slope ($\Delta P / \Delta \epsilon_v$) of the unloading and reloading curves.16

Figure 7. The pressure-strain plot obtained during hydrostatic pressurization of the triaxial compression test (HCT) of the FC-HC905 specimen.....17

Figure 8. The stress-strain plot obtained from the FC-TC905 specimen consisting of hydrostatic compression (HCT) up to 380 MPa confining pressure, P, followed by triaxial compression (TXC) until failure of the specimen at 600 MPa in axial stress, σ_a18

Figure 9. The pressure-lateral displacement plot obtained during pre-compaction stage of sample preparation for the low-density 60-series specimens.....18

Figure 10. The differential stress-strain plot obtained during triaxial compression (TXC) / hydrostatic compression (HCT) testing of the FC-TC609 specimen under 800 MPa confining pressure, P.....19

Figure 11. FC-TC911 specimen after triaxial compression (TXC) / hydrostatic compression (HCT) tests under 1,000 MPa confining pressure.20

Figure 12a. Failure criterion of the 90-series cellular concrete represented by the stress invariants, $I_1 (= \sigma_1 + \sigma_2 + \sigma_3)$ and $J_2 (= [(\sigma_1 - \sigma_2)^2 + (\sigma_2 - \sigma_3)^2 + (\sigma_3 - \sigma_1)^2] / 6)$	22
Figure 12b. Failure criterion of the 60-series cellular concrete represented by the stress invariants, $I_1 (= \sigma_1 + \sigma_2 + \sigma_3)$ and $J_2 (= [(\sigma_1 - \sigma_2)^2 + (\sigma_2 - \sigma_3)^2 + (\sigma_3 - \sigma_1)^2] / 6)$	22
Figure 13a. Failure criterion of the 90-series cellular concrete determined in terms of the principal stresses, σ_{1f} axial failure stress and $\sigma_3 (= P)$ confining pressure	23
Figure 13b. Failure criterion of the 60-series cellular concrete determined in terms of the principal stresses, σ_{1f} axial failure stress and $\sigma_3 (= P)$ confining pressure	23
Figure 14. The uniaxial strain test (UXE) set-up consisting of a die, piston, and load cells.	25
Figure 15. The stress-strain plots obtained during uniaxial strain (UXE) testing of the cellular concrete specimens: 60-series (blue dotted) and 90-series (red). The axial strain is effectively same as the volumetric strain under uniaxial strain condition ($\epsilon_a \neq 0, \epsilon_l = 0$). ...	27
Figure 16. The failure of the cellular concrete under uniaxial strain (UXE) testing condition.	27
Figure 17. The triaxial extension test (TXE) set-up and an instrumented specimen with two axial LVDTs and a Schuler gage for the measurements of axial and lateral displacements, respectively.	28
Figure 18. Triaxial extension test (TXE) record for the FC-TE916 specimen showing the test sequences and the corresponding variations of stresses and strains with respect to time.	29
Figure 19. Triaxial extension test (TXE) record for the FC-TE615 specimen showing the test sequences and the corresponding variations of stresses and strains with respect to time.	30
Figure 20. Stress-strain plot obtained during triaxial extension test (TXE) of the FC-TE916 specimen under 200 MPa of confining pressure, P.....	30
Figure 21. Stress-strain plot obtained during triaxial extension test (TXE) of the FC-TE615 specimen under 100 MPa of confining pressure, P.....	31
Figure 22. Two different failure modes of the cellular concrete specimens under the triaxial extension (TXE) test condition: tensile failure in the 90-series concrete specimen (FC-TE916, left) and shear failure in the 60-series specimen (FC-TE615, right).	31
Figure 23. Typical tensile fracture planes induced in the cellular concrete specimen during uniaxial tension tests (UTT). Also shown are the nominal dimensions of the “dog-bone” shaped specimen prepared for UTT testing.....	32

Figure 24. The uniaxial tension test (UTT) set-up consisting of the flexible chain-links and the end-caps cemented to the shaped specimen.....33

Figure 25. The axial load-displacement plots obtained during uniaxial tension testing (UTT) of the cellular concrete specimens.33

Tables

Table 1. Summary of the unconfined compression tests (UCT) of the cellular concrete.....	11
Table 2. Summary of the triaxial compression (TXC) / hydrostatic compression (HCT) tests of the cellular concrete.	24
Table 3. Summary of the axial strain tests (UXE) of the cellular concrete	26
Table 4. Summary of the triaxial extension tests (TXE) of the cellular concrete.....	29
Table 5. Summary of the uniaxial tension tests (UTT) of the cellular concrete.....	32

1. Introduction

This report describes an experimental study that was completed to measure the mechanical material properties of cellular concrete in support of a program sponsored by the Naval Surface Warfare Center, Dahlgren, Virginia (NSWCDD). The objective of this study was to provide realistic modeling parameters of the target material under quasi-static compressive loading conditions so that the impact modeling effort could develop and test its models and codes under different loading conditions.

Sandia Geomechanics Department carried out a series of constitutive mechanical tests consisting of unconfined uniaxial compression tests (UCT), a combination of triaxial compression (TXC) and hydrostatic compression tests (HCT), uniaxial strain tests (UXE), triaxial extension tests (TXE), and uniaxial tension tests (UTT). This report summarizes the test methods, set-up, relevant observations, and results from our experimental efforts.

We received two batches of cellular concrete cores that had two different nominal densities (1.4 g/cm^3 and 1.0 g/cm^3). The higher-density cellular concrete was designated as 90-series test and the lower-density concrete was designated as 60-series test in this report ($1.4 \text{ g/cm}^3 \approx 90 \text{ pcf}$ and $1.0 \text{ g/cm}^3 \approx 60 \text{ pcf}$). These numbers are the nominal values of the densities in lb/ft^3 (pcf). The cellular concrete (see Appendix A) is a composite mixture of cement (Portland Type I), water, and foam. The entrapped small air bubbles in the slurry result in a porous and light-weight foamed concrete, without sand or any other aggregate. This cellular concrete, not only has a lower density than conventional concrete, but it also has a lower strength and an increased penetrability. For each batch of the specimens, the following test matrix was applied to characterize the mechanical properties of the concrete.

- Unconfined Compression Tests (UCT)
 - Three strain-controlled unconfined uniaxial compression tests
- Triaxial Compression (TXC) / Hydrostatic Compression Tests (HCT)
 - Tests #1 and #2 with 100 MPa confining pressure
 - Tests #3 and #4 with 200 MPa confining pressure
 - Tests #5 and #6 with 400 MPa confining pressure
 - Tests #7 and #8 with 600 MPa confining pressure
 - Tests #9 and #10 with 800 MPa confining pressure
 - Tests #11 and #12 with 1000 MPa confining pressure
- Uniaxial Strain Tests (UXE)
 - Tests #13 and #14 up to 600 MPa confining pressure
- Triaxial Extension Tests (TXE)
 - Tests #15 with 100 MPa confining pressure
 - Tests #16 with 200 MPa confining pressure
 - Tests #17 with 400 MPa confining pressure
- Uniaxial Tension Tests (UTT)
 - Three strain-controlled uniaxial tension tests

2. Unconfined Compression Tests (UCT)

The cellular concrete core was prepared in the form of a right circular cylinder with nominal dimensions of 51 mm in diameter and 102 mm in length. The dimensions fall within the range of length-to-diameter ratio (2 to 2.5) recommended in ASTM D4543 (“Standard Practice for Preparing Rock Core Specimens and Determining Dimensional and Shape Tolerances”). The ends of the specimen were ground flat within 0.025 mm tolerance. Samples were visually inspected for significant flaws and general straightness of circumferential surfaces. The dimensions of the prepared specimens are listed in Table 1 with bulk densities and the strength results.

Table 1. Summary of the unconfined compression tests (UCT) of the cellular concrete.

Specimen ID	Diameter (mm)	Length (mm)	Weight (g)	Density (g/cm ³)	C ₀ (MPa)
FC-UC901	50.67	101.22	279.24	1.37	44
FC-UC902	50.63	101.37	283.88	1.39	48
FC-UC601	50.56	101.93	198.01	0.97	9
FC-UC602	50.57	101.52	199.18	0.98	13

Figure 1 shows a typical stress-strain plot resulting from an unconfined uniaxial compression test. The axial displacements of the specimen were measured from the machine stroke and the lateral displacements were measured using the LVDT mounted on the specimen perpendicular to the loading axis. Experimental apparatus used for the compression tests meets or exceeds the requirements of ASTM2938 (“Standard Test Method for Unconfined Compressive Strength of Intact Rock Core Specimens”). Specimens were loaded at a constant displacement rate of 10⁻¹ mm/s which corresponds to a strain rate of 10⁻³ /s. The specimens were loaded until the peak load was reached. The axial stress (σ_a) is plotted against axial (ϵ_a) and lateral (ϵ_l) strains, respectively (Figure 1). The volumetric strain, calculated as ($\epsilon_v = \epsilon_a + 2\epsilon_l$), is also shown on the plot. The specimen response during unconfined uniaxial compressive loading typically includes an initial nonlinear “toe” followed by linear elastic loading to approximately 75% of peak stress. The unconfined uniaxial compressive strength of the concrete was calculated from the following equation:

$$C_0 = P_u / \pi r^2$$

where C_0 is the unconfined uniaxial compressive strength of the concrete in MPa; P_u is the peak load in N; and r is the radius of the specimen in mm.

The results from the uniaxial compression tests are summarized in Table 1. Stress-strain plots from all four tests are given in Appendix B. Figure 2 shows the failed concrete specimens under uniaxial compressive load. The lower-density specimen (FC-UC601) shows an axial splitting (left). In contrast, the higher density specimen (FC-UC901) shows a conjugate shear failure surfaces inclined to the loading axis.

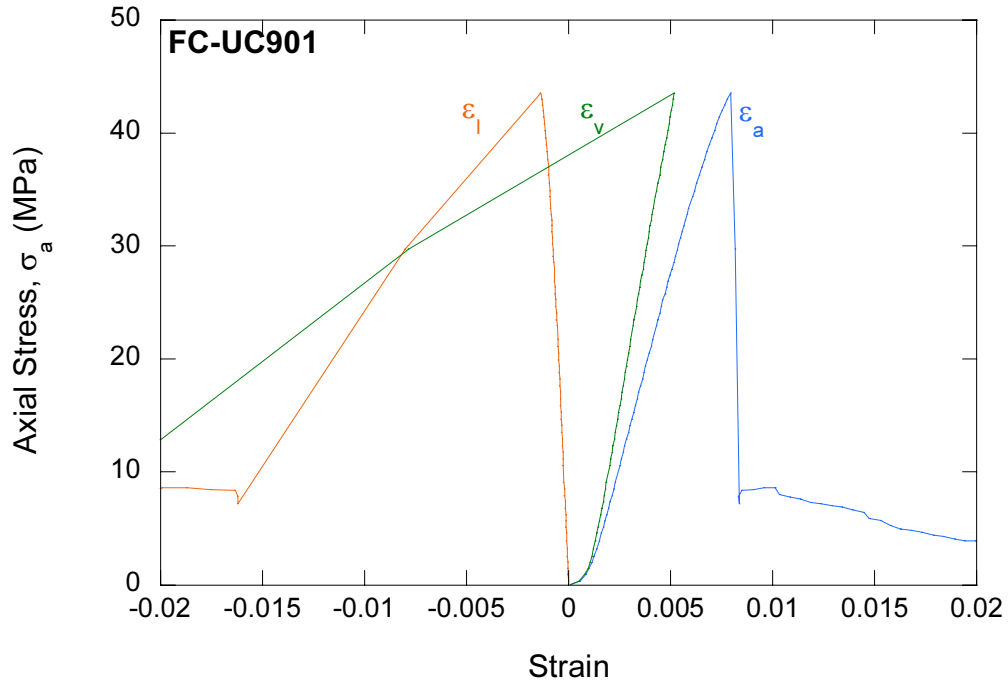


Figure 1. Stress-strain plot for the uniaxial compression test of specimen FC-UC901.

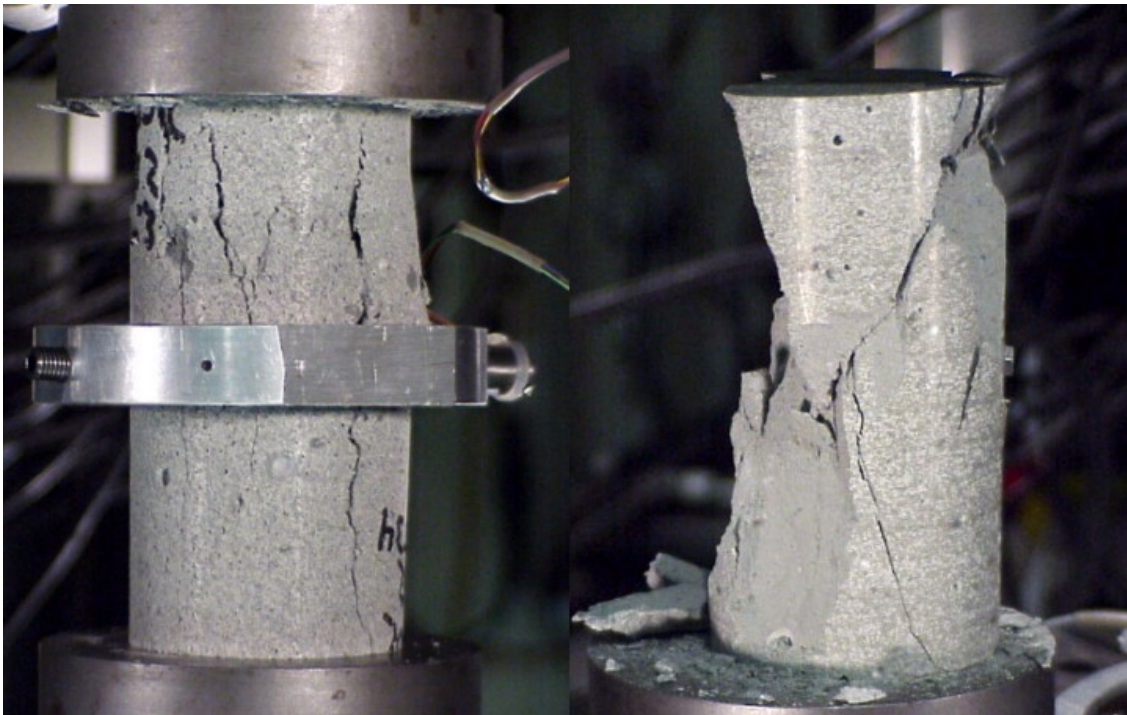


Figure 2. Failed concrete specimens, FC-UC601 (left) and FC-UC901 (right), under uniaxial compression stress condition ($\sigma_1 \neq 0, \sigma_2 = \sigma_3 = 0$). A lateral LVDT is shown with a mounting device for measuring diametral deformations of the specimen.

The proportional constant between stress and strain in the elastic portion of compression tests defines the Young's modulus, E :

$$E = \sigma_a / \varepsilon_a$$

where σ_a is the axial stress and ε_a is the axial strain. The Young's modulus was determined using least square fits of a straight line (or linear regression analysis) to the stress-strain data. Figure 3 shows the segment of stress-strain plots and the fitted straight line of all uniaxial compression tests between 10 and 75 % of C_0 . The Young's modulus for the 90-series tests varied from 6.8 to 7.4 GPa, whereas, the Young's modulus for the 60-series specimens varied from 2.9 to 3.3 GPa.

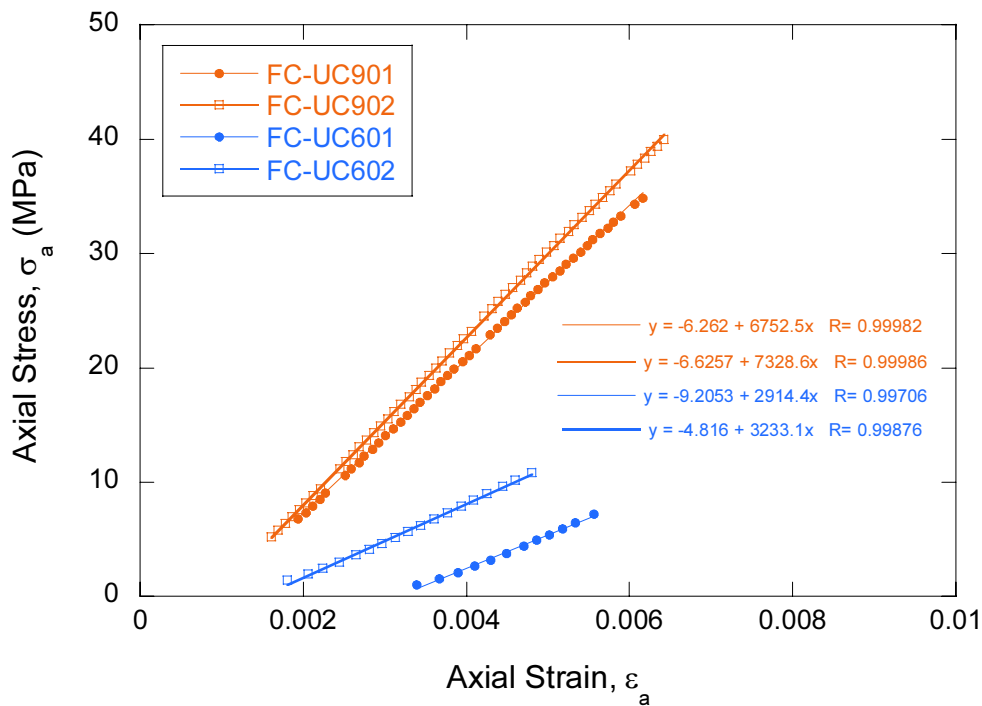


Figure 3. Linear segments of the axial stress (σ_a) - axial strain (ε_a) plot obtained during the unconfined compression tests (UCT) for the cellular concrete. The Young's modulus, E , was obtained as the slope of the best-fit straight line.

Poisson's ratio, defined as $\nu = |\varepsilon_l| / |\varepsilon_a|$, was obtained from the stress-strain plot. The linear loading segments of the stress-strain plot, shown in Appendix B, were isolated for the ε_l - ε_a plot shown in Figure 4. The absolute value of the slope of the best-fit line represents Poisson's ratio. The Poisson's ratio for the 90-series specimens varied from 0.18 to 0.19. The Poisson's ratio for the 60-series specimens had a wide varying range from 0.13 to 0.16.

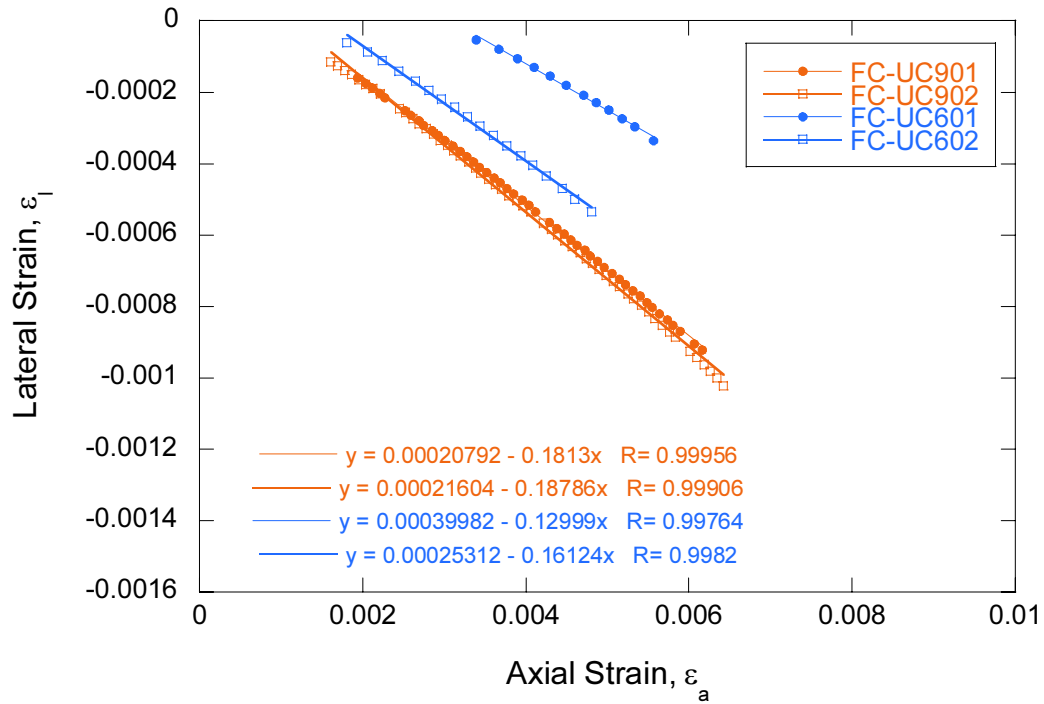


Figure 4. Linear segments of the lateral strain (ϵ_l) - axial strain (ϵ_a) plot obtained during the unconfined compression tests (UCT) for the cellular concrete. The Poisson's ratio, ν , is obtained as the slope of the best-fit straight line.

3. Triaxial Compression (TXC) / Hydrostatic Compression Tests (HCT)

The cylindrical specimens for the triaxial compression (TXC) / hydrostatic compression (HCT) tests were prepared following the same sample preparation procedures as in the uniaxial compression tests. After the specimen was fabricated to meet the recommendations in ASTM D4543, two axial LVDTs and a Schuler gage (Schuler, 1978) were mounted on the specimen to measure axial and the lateral displacements, respectively (Figure 5). We used two types of pressure vessels capable of operating at confining pressures up to 400 MPa and 1000 MPa, respectively. The axial load applied to the specimen was measured by the external load cell for all tests with confining pressures up to 400 MPa. For confining pressures over 400 MPa, an internal load cell was also used to measure the axial load on the specimen to avoid errors from friction between the piston and the pressure vessel. The experimental apparatus used for the compression tests meets or exceeds the requirements of ASTM2664 (“Standard Test Method for Triaxial Compressive Strength of Undrained Rock Core Specimens without Pore Pressure Measurements”).

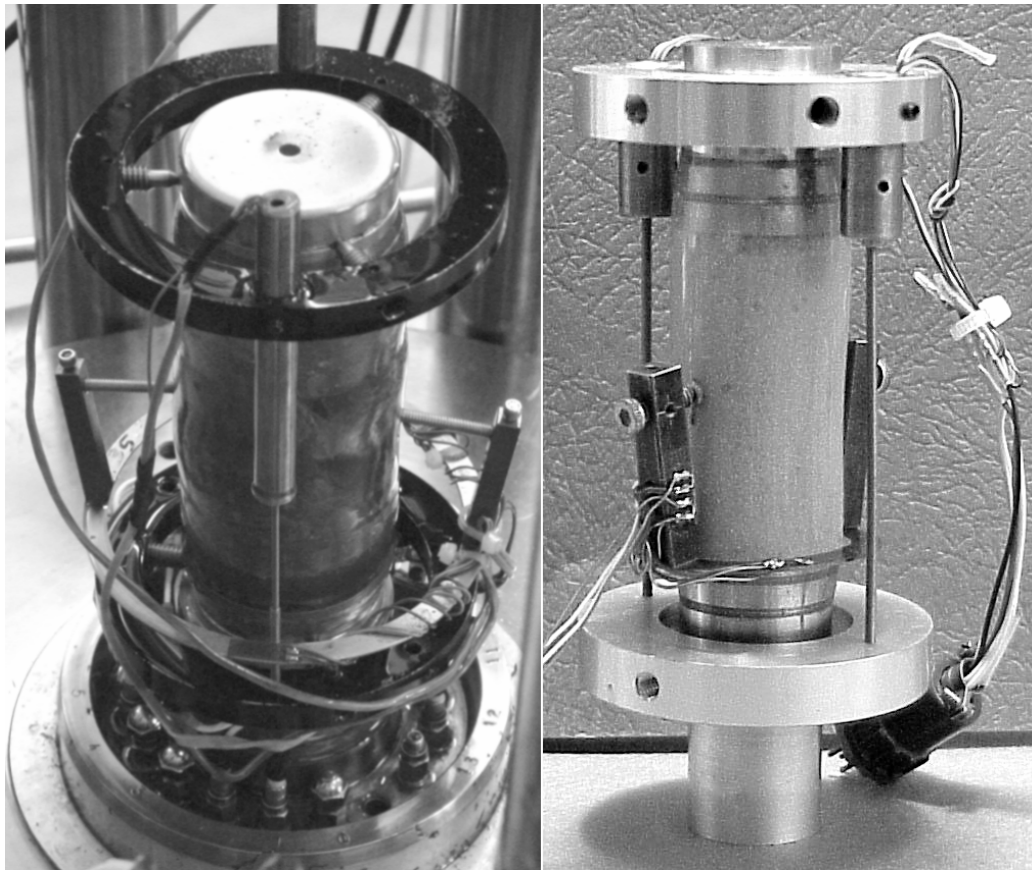


Figure 5. Instrumented concrete specimens for triaxial compression (TXC) / hydrostatic compression (HCT) tests. Shown are the axial LVDTs and the Schuler gage for measuring axial and lateral displacements, respectively. The specimen on the left is prepared for confining pressures up to 400 MPa and the specimen on the right is for up to 1,000 MPa confining pressure.

Hydrostatic Compression Tests

The machined specimen was placed between cylindrical end-caps of same diameter. The specimen assembly was enclosed in a shrinkable tubing and then coated with an approximately 1 mm thick impervious polyurethane membrane. To maintain uniform thickness of the membrane during curing the specimen assembly was turned on a lathe along the axial centerline of the assembly. The shrinkable tubing coated with flexible membrane allows the confining pressure to be applied hydrostatically on the specimen and at the same time prevents the confining fluid from infiltrating into the specimen. The instrumented specimen assembly (Figure 5) was placed in a triaxial pressure vessel. The vessel is equipped with feed-throughs (see Figure 5) for transmitting data from the strain gages and the internal load-cell to the data acquisition system. After the specimen is placed in the pressure vessel, hydraulic pressure is applied to a predetermined level of confining pressure. The servo-controller maintains the pressure level ($\sigma_1=\sigma_2=\sigma_3=P$; where σ_1 , σ_2 , and σ_3 are the maximum, intermediate, and minimum principal stresses, respectively).

During the hydrostatic compression test, unloading and reloading of the pressure were conducted. The slope of the unloading and reloading loop may determine the bulk modulus, K , defined as the ratio between the hydrostatic pressure P and the volumetric strain ϵ_v it produces (Jaeger and Cook, 1969). In unloading-reloading loop, the bulk modulus can be represented as the ratio of incremental quantities.

$$K = \Delta P / (\Delta \epsilon_v)$$

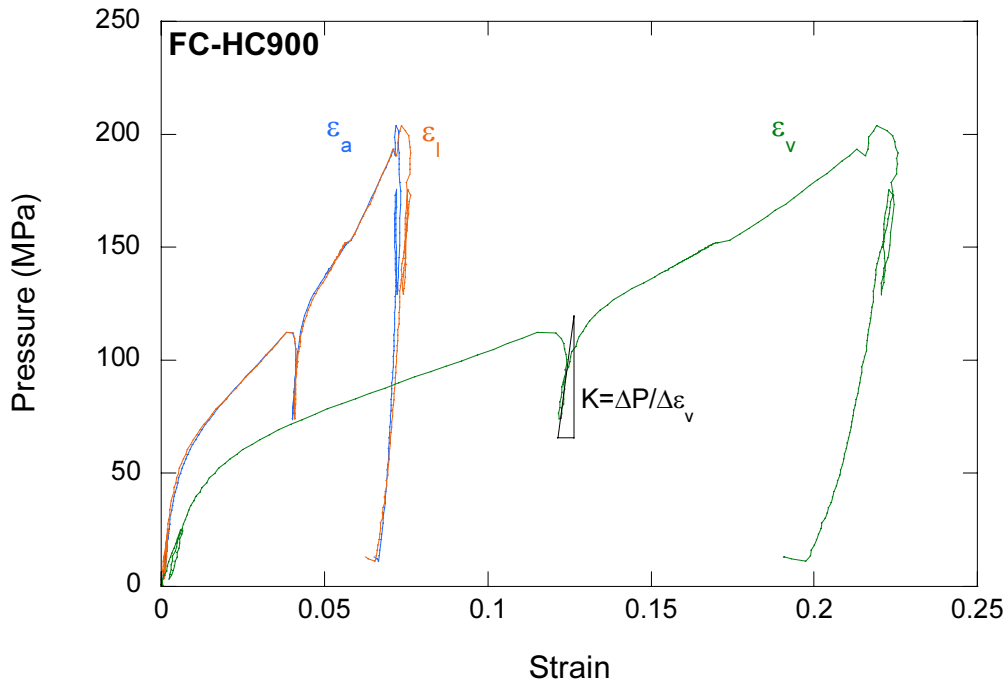


Figure 6. The pressure-strain plot obtained during hydrostatic compression test (HCT) of the FC-HC900 specimen up to 200 MPa pressure. The graphical representation of the bulk modulus K is also indicated as the slope ($\Delta P / \Delta \epsilon_v$) of the unloading and reloading curves.

Figure 6 shows the pressure-strain plot for the FC-HC900 specimen. This test was the only hydrostatic compression test conducted independently from a triaxial compression test. All other hydrostatic compression tests were conducted as a part of a triaxial compression test. Test records from hydrostatic compression are shown in Appendix C-1. The initial segment of hydrostatic pressurization up to the set confining pressure is used as a hydrostatic compression test. Figure 7 shows an example of the hydrostatic compression test in conjunction with a triaxial compression test. The bulk modulus values for the selected unloading-reloading loops are summarized in Table 2.

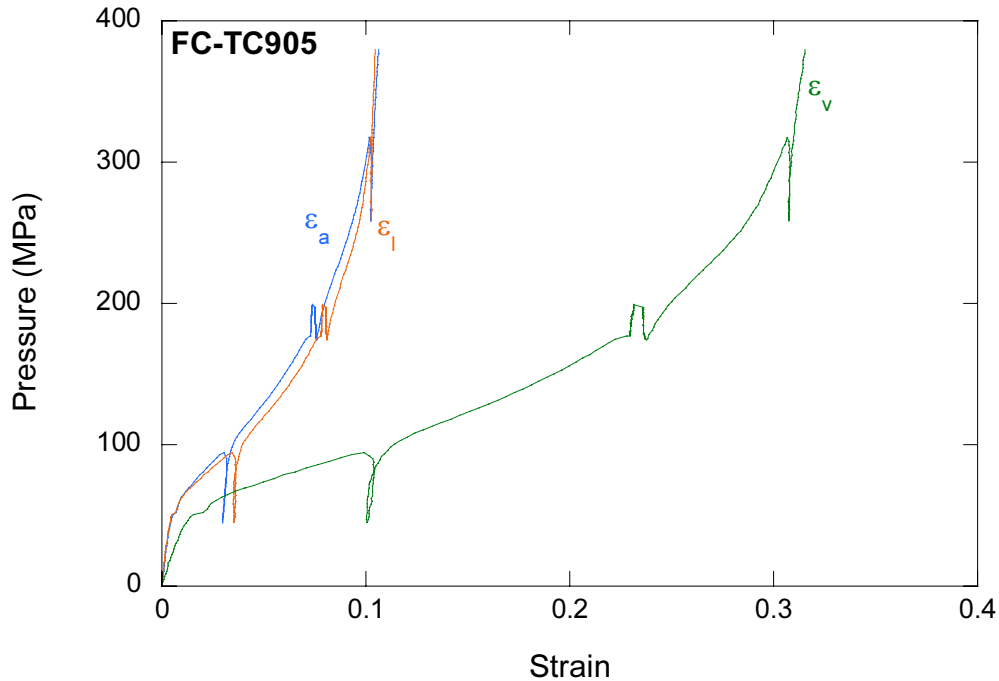


Figure 7. The pressure-strain plot obtained during hydrostatic pressurization of the triaxial compression test (HCT) of the FC-HC905 specimen.

Triaxial Compression Tests

After the confining pressure, P , is stabilized, the specimen was loaded axially at a constant axial strain rate of 10^{-3} /s. For triaxial compression tests, the specimens were loaded until peak load was reached. The experimental apparatus used for the compression tests meets or exceeds the requirements of ASTM2664 for the triaxial compression tests. An example of the strains (ϵ_a - axial, ϵ_l - lateral, and ϵ_v - volumetric) vs. axial stress plot, recorded during testing of FC-TC905 is shown in Figure 8.

Due to large deformations in the lower-density 60-series specimens under high confining pressures, the impermeable jacket punctures frequently around the joint between the specimen and the end-cap. Thus, the larger diameter (50 mm) specimen was pre-compacted under hydrostatic pressures up to 45 MPa. Then, the pre-compacted specimen was removed from the pressure vessel and machined to fit the smaller diameter (25 mm) end-caps. Figure 9 shows the

lateral deformation of the specimens under hydrostatic pressure during the pre-compaction stage of sample preparation.

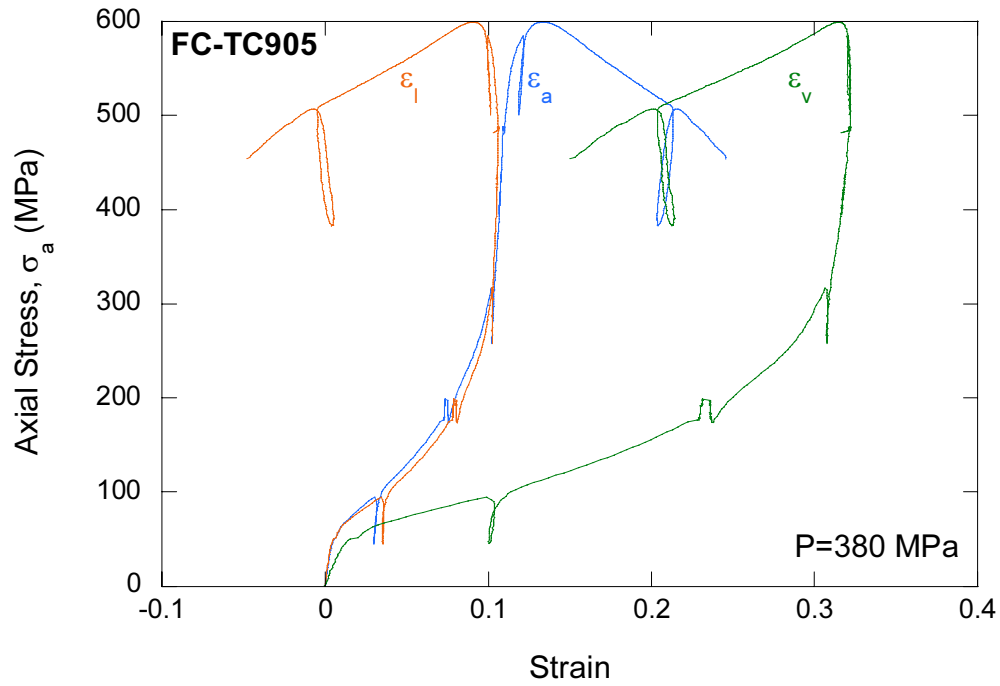


Figure 8. The stress-strain plot obtained from the FC-TC905 specimen consisting of hydrostatic compression (HCT) up to 380 MPa confining pressure, P , followed by triaxial compression (TXC) until failure of the specimen at 600 MPa in axial stress, σ_a .

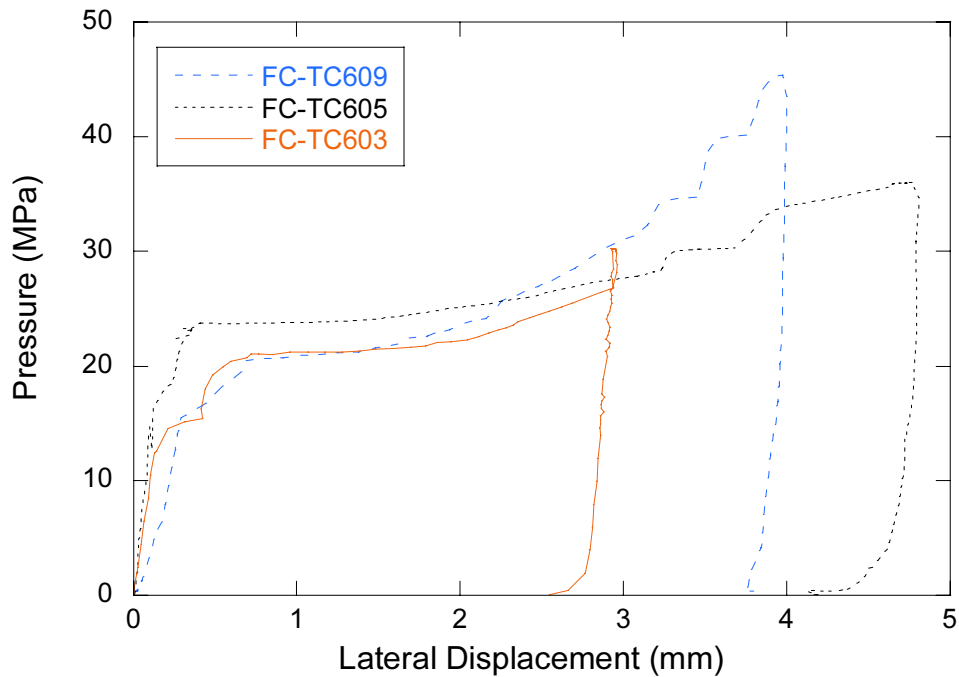


Figure 9. The pressure-lateral displacement plot obtained during pre-compaction stage of sample preparation for the low-density 60-series specimens.

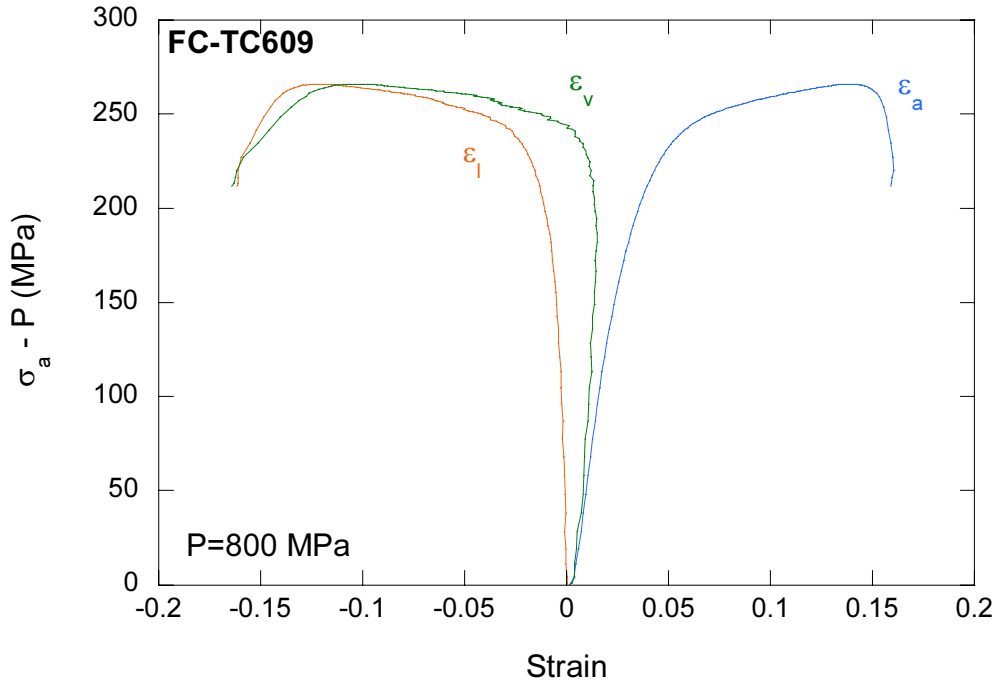


Figure 10. The differential stress-strain plot obtained during triaxial compression (TXC) / hydrostatic compression (HCT) testing of the FC-TC609 specimen under 800 MPa confining pressure, P.

For triaxial testing at high confining pressure (>400 MPa), we presented the results in terms of differential stress, $\sigma_a - P$. A typical test record is shown in Figure 10.

As shown in Figures 8 and 9, the specimens experienced the lateral strains more than 10 % during the triaxial compression phase of testing. Therefore, the axial stress, σ_a , at each load step, was calculated based on the current cross-sectional area of the specimen. The diametral displacements, measured by the Schuler gage, were used to calculate the changes in cross-sectional area of the specimen. The results are summarized in Table 2 and the test records are shown in Appendix C-2. The corrected stress values were used for all triaxial compression tests except for the FC-TC904 test in which the Schuler gage malfunctioned. To make reasonable corrections to the FC-TC904 data, a similar test series, FC-TC903, was selected to obtain the correction factor. The ratio between the corrected σ_f and the uncorrected σ_f was 1.2 in the FC-TC903 test and the same correction factor was applied to the FC-TC904 data to obtain the corrected value of σ_f .

Figure 11 shows a failed specimen under triaxial compression. The inclined opening shows the shear failure surface evident in most of the failed specimens. The gap between the upper end-cap and the specimen shows the results from significant amount of volume reduction (approximately 30% for 90-series tests and 50% for 60-series tests).

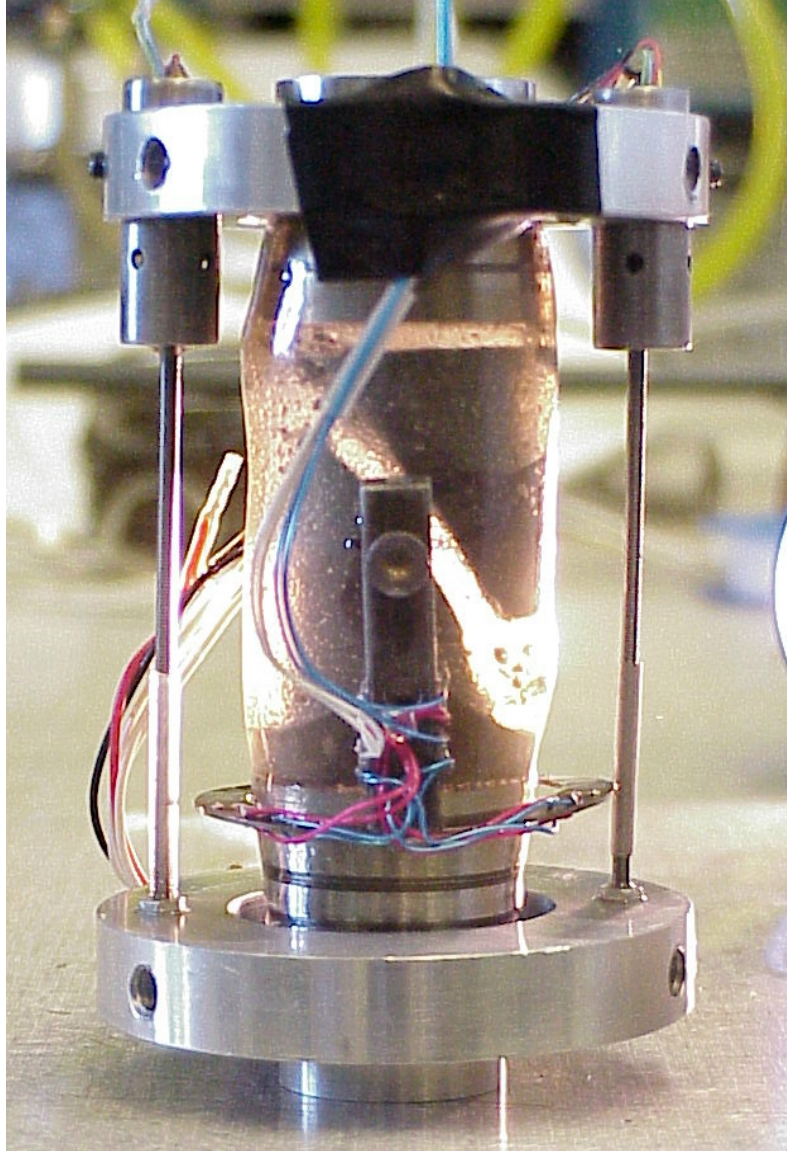


Figure 11. FC-TC911 specimen after triaxial compression (TXC) / hydrostatic compression (HCT) tests under 1,000 MPa confining pressure.

Table 2 summarizes the results from the triaxial compression tests. Results from the triaxial tests were used to formulate a cap plasticity model (Sandler and Rubin, 1979). The cap model is described in terms of two stress invariants: I_1 -the first invariant of the Cauchy stress and J_2 - the second invariant of the deviator stress. In the triaxial compression tests, where the axial stress was the major principal stress (σ_1) and the confining pressure P was acting as σ_2 and σ_3 , mean stress invariant I_1 and the square root of the deviator invariant J_2 can be described as,

$$I_1 = \sigma_1 + \sigma_2 + \sigma_3 = \sigma_1 + 2P$$

$$\sqrt{J_2} = \sqrt{\frac{(\sigma_1 - \sigma_2)^2 + (\sigma_2 - \sigma_3)^2 + (\sigma_3 - \sigma_1)^2}{6}} = \frac{(\sigma_1 - P)}{\sqrt{3}}$$

The values of I_1 and $\sqrt{J_2}$ for different confining pressures are listed in Table 2. During the shear failure of the specimens, the state of stress can be represented as the shear failure envelope represented empirically by the following exponential equation (Sandler and Rubin, 1979 and Fossum et. al., 1995).

$$\sqrt{J_2} = A - B \exp^{-C I_1}$$

where A, B, and C are unknown parameters to be determined for different materials.

We used a nonlinear regression analysis to determine the unknown parameters A, B, and C, which minimized the sum of the squares of errors between the model-predicted values and the observed $J_2^{0.5}$ values for different I_1 values. For the two batches of cellular concrete, the shear failure envelopes are best represented by the following equations (Figures 12a and 12b):

$$\begin{aligned} \sqrt{J_2} \text{ (MPa)} &= 297.2 - 278.7 \exp^{-0.000455 I_1 \text{ (MPa)}} \quad \text{for the 90-series tests} \\ \sqrt{J_2} \text{ (MPa)} &= 211.4 - 204.2 \exp^{-0.000628 I_1 \text{ (MPa)}} \quad \text{for the 60-series tests} \end{aligned}$$

The failure strength data from the triaxial compression tests may also be described in terms of the principal stresses.

$$\sigma_{1f} = C_{0p} + q\sigma_3$$

where σ_{1f} is the predicted major principal stress σ_1 at failure, C_{0p} is the predicted value of uniaxial compressive strength C_0 , σ_3 is the minor principal stress generated by the confining pressure, and q is the slope of the best-fit straight line.

For the cellular concrete, the shear failure envelopes are best represented by the following linear equations (Figures 13a and 13b):

$$\begin{aligned} \sigma_{1f} \text{ (MPa)} &= 89.4 + 1.353 \sigma_3 \text{ (MPa)} \quad \text{for the 90-series tests} \\ \sigma_{1f} \text{ (MPa)} &= 42.9 + 1.355 \sigma_3 \text{ (MPa)} \quad \text{for the 60-series tests} \end{aligned}$$

Due to the nonlinearity near the origin of the plot shown in Figure 13, the predicted value of uniaxial compressive strength, C_{0p} identified as the vertical intercept, is quite larger than the measured one shown in Table 1 ($C_{0p} \gg C_0$). It appears that the above failure criteria based on the principal stress are only valid for the confining pressures larger than 100 MPa.

The slope of the best-fit linear lines for two batches of concrete specimens are practically identical and can be related to the coefficient of internal friction μ as follows.

$$q = [(\mu^2 + 1)^{0.5} + \mu]^2$$

Thus, the coefficient of internal friction, μ , for both batches of the specimens are approximately 0.15.

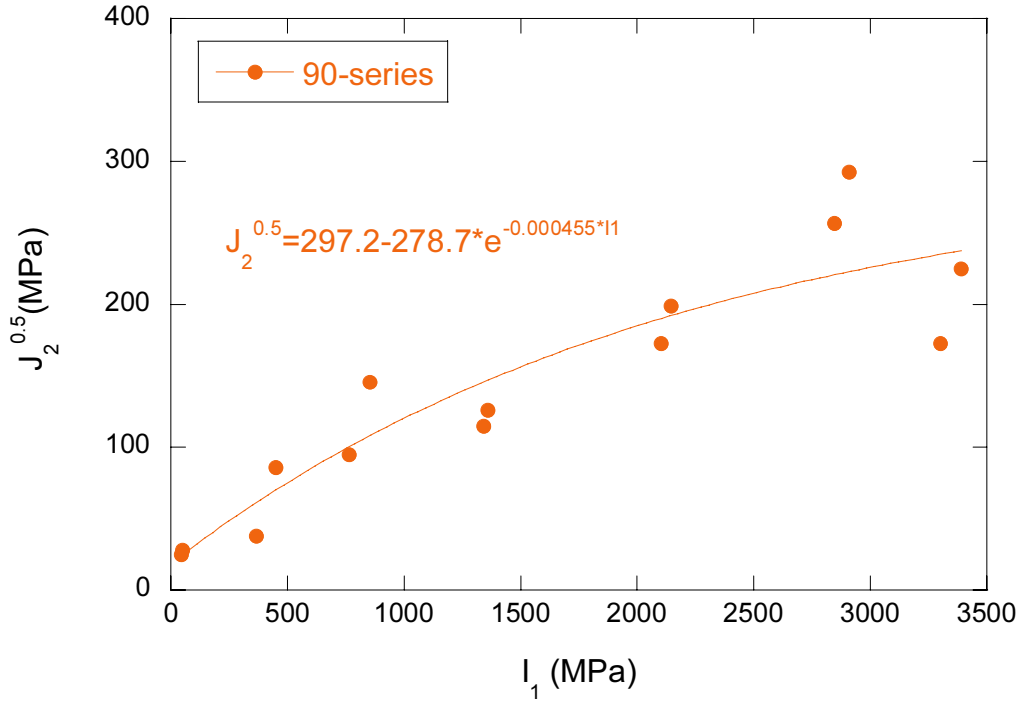


Figure 12a. Failure criterion of the 90-series cellular concrete represented by the stress invariants I_1 , $(=\sigma_1+\sigma_2+\sigma_3)$ and J_2 $(=[(\sigma_1-\sigma_2)^2 + (\sigma_2-\sigma_3)^2 + (\sigma_3-\sigma_1)^2]/6)$.

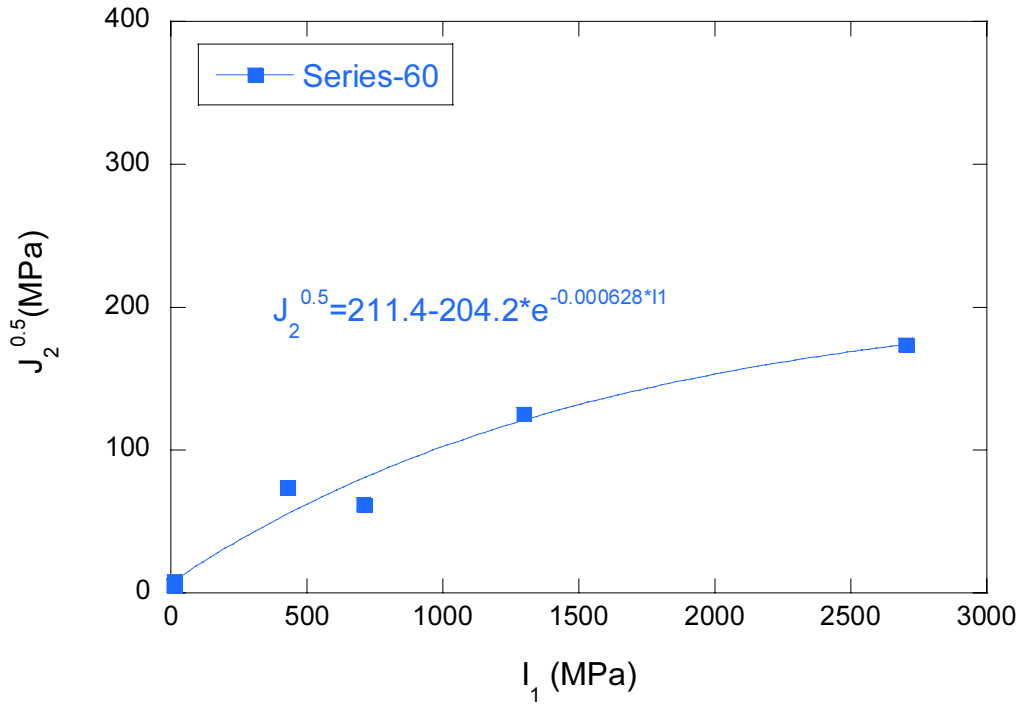


Figure 12b. Failure criterion of the 60-series cellular concrete represented by the stress invariants I_1 , $(=\sigma_1+\sigma_2+\sigma_3)$ and J_2 $(=[(\sigma_1-\sigma_2)^2 + (\sigma_2-\sigma_3)^2 + (\sigma_3-\sigma_1)^2]/6)$.

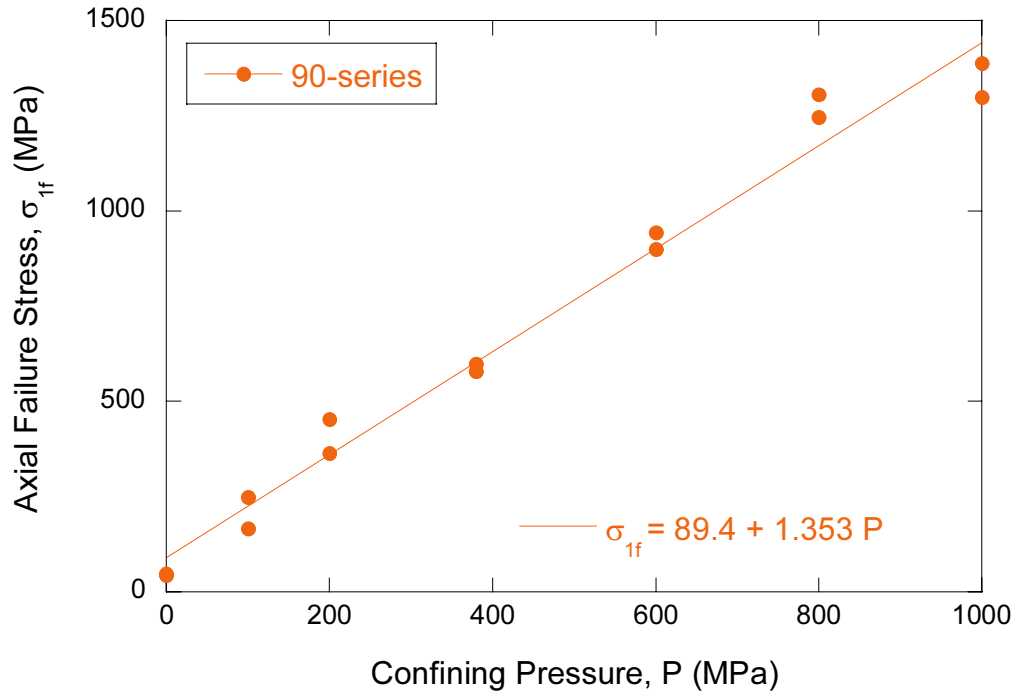


Figure 13a. Failure criterion of the 90-series cellular concrete determined in terms of the principal stresses, σ_{1f} axial failure stress and $\sigma_3 (=P)$ confining pressure.

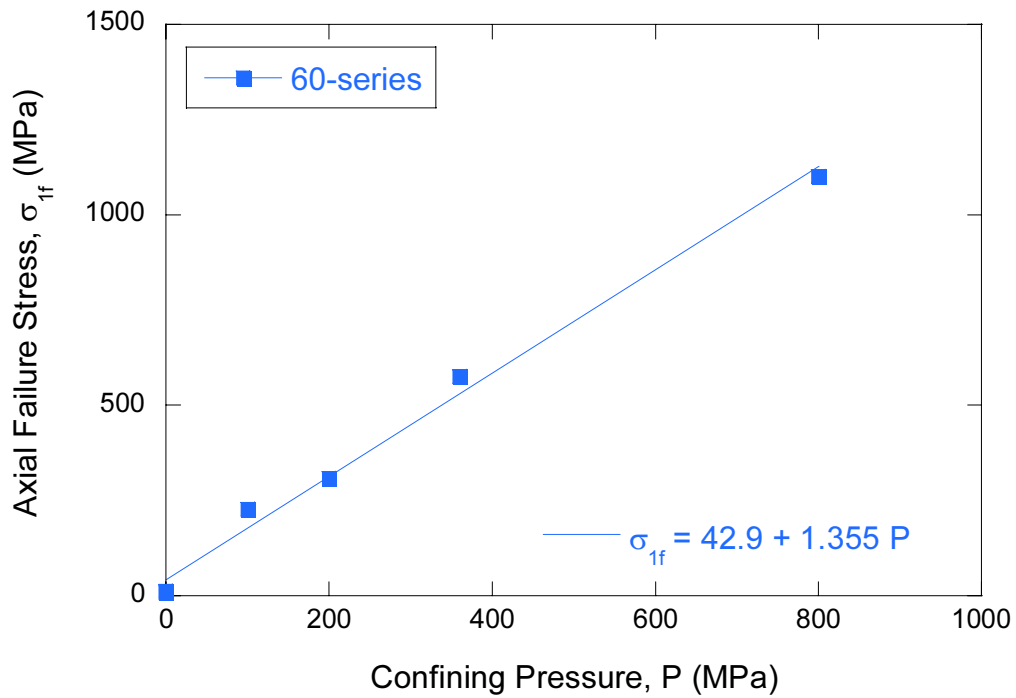


Figure 13b. Failure criterion of the 60-series cellular concrete determined in terms of the principal stresses, σ_{1f} axial failure stress and $\sigma_3 (=P)$ confining pressure.

Table 2. Summary of the triaxial compression (TxC) / hydrostatic compression (HCT) tests of the cellular concrete.

Specimen no.	Diameter (mm)	Length (mm)	Weight (g)	Density (g/cm ³)	K(ϵ_{vk}) (GPa)	ϵ_{vk}	P (MPa)	σ_{1f} (MPa)	I_1 (MPa)	$\sqrt{J_2}$ (MPa)
FC-HC900*	50.79	101.57	295.35	1.44	6.9	0.12	NA	44	NA	NA
FC-UC901**	50.67	101.22	279.24	1.37			0	44	44	25
FC-UC902**	50.63	101.37	283.88	1.39			0	48	48	28
FC-TC901	50.72	101.42	294.67	1.44	16.1	0.06	100	166	366	38
FC-TC902	50.72	101.37	292.33	1.43	6.2	0.08	100	249	449	86
FC-TC903	50.77	101.70	308.50	1.50	6.4	0.15	200	364	764	95
FC-TC904	50.70	101.57	295.76	1.44			200	453	853	146
FC-TC905	50.83	101.63	309.79	1.50	17.1	0.31	380	599	1359	126
FC-TC906	50.77	101.70	308.50	1.50	8.4	0.23	380	580	1340	115
FC-TC907	24.40	47.02	30.83	1.40			600	944	2144	199
FC-TC908	24.37	48.44	32.18	1.42			600	900	2100	173
FC-TC909	24.37	48.26	31.18	1.38			800	1246	2846	257
FC-TC910	24.37	48.18	31.71	1.41			800	1307	2907	293
FC-TC911	24.38	47.02	30.39	1.38	21.8	0.43	1000	1389	3389	225
FC-TC912	24.35	46.94	31.04	1.42	16.9	0.40	1000	1300	3300	173
FC-UC601**	50.56	101.93	198.01	0.97			0	9	9	5
FC-UC602**	50.57	101.52	199.18	0.98			0	13	13	8
FC-TC601	50.75	101.60	214.86	1.05			100	228	428	74
FC-TC603***	50.75	101.50	209.43	1.02			200	308	708	62
FC-TC605***	50.67	101.47	183.20	0.90			360	576	1296	125
FC-TC609***	44.44	88.72	134.90	0.98	3.1	0.38	800	1102	2702	174

*-hydrostatic compression test; **-unconfined uniaxial compression test; ***-pre-compacted specimen

K(ϵ_{vk})-bulk modulus K measured at volumetric strain ϵ_{vk}

σ_{1f} -failure stress, P-confining pressure

$I_1 = \sigma_1 + 2P$

$\sqrt{J_2} = (\sigma_1 - P) / \sqrt{3}$

4. Uniaxial Strain Tests (UXE)

The uniaxial strain compression test is designed to maintain zero radial strain while increasing the compressive axial load. The volumetric strain, ϵ_v , is measured as a function of the axial stress. Since the lateral strains are suppressed, the volumetric strain is equal to the axial strain, ϵ_a . The uniaxial strain tests were performed using a die compaction test set-up as shown in Figure 14. The test set-up consists of a die, a punch, a linear variable displacement transformer (LVDT) to measure axial deformation of the specimen, a total load-cell to measure the axial load applied to the specimen, and a frictional load-cell to measure the frictional force between the specimen, the punch and the die body. The load applied to the specimen is calculated from the total load minus the frictional load. Right cylinder specimens were used for the uniaxial strain tests. The diameter of the specimen was 28.45 mm to fit the bore of the die and the length of the specimen was approximately from 18 to 19 mm. Table 3 shows the dimensions of the specimens. All four test-records are shown in Appendix D.

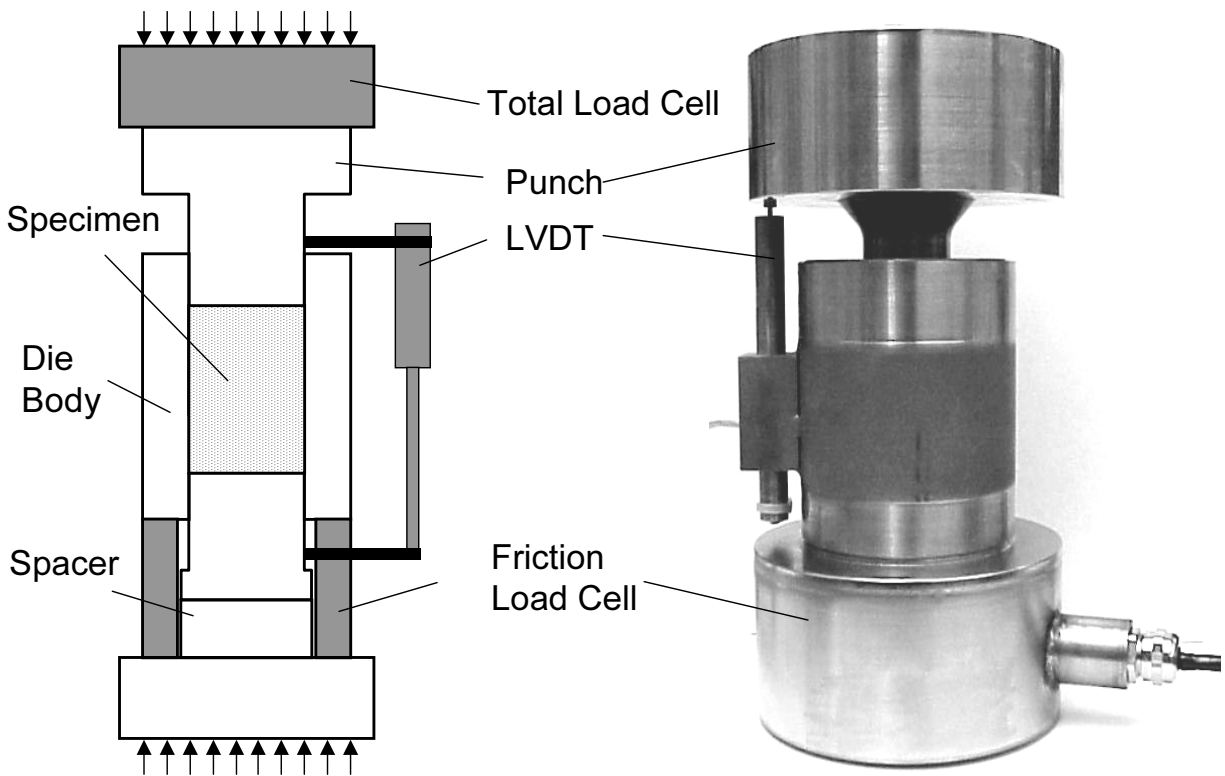


Figure 14. The uniaxial strain test (UXE) set-up consisting of a die, piston, and load cells.

Table 3. Summary of the uniaxial strain tests (UXE) of the cellular concrete.

Specimen ID	Diameter (mm)	Length (mm)	Weight (g)	Density (g/cm ³)
FC-UX913	28.45	19.30	17.16	1.40
FC-UX914	28.45	17.88	15.79	1.39
FC-UX613	28.45	18.95	11.03	0.92
FC-UX614	28.45	19.25	11.59	0.95

Four uniaxial strain tests (two 90-series and two 60-series specimens) were conducted up to 600 MPa axial stress, σ_a . The axial stress-volumetric strain plots, consisting of three segments, are shown in Figures 15 and 16. The first segment is the elastic response of the material with a steep increase in σ_a until the specimen fails at a compressive strength σ_f . The peak stress is usually accompanied by a small amount of stress drop (Figure 16) that may indicate a formation of compaction bands, a common phenomenon in porous materials (Olsson, 1999). The next segment is where the localized failure propagates throughout the specimen converting the intact elastic material into a nonlinear fractured material. This segment is characterized by an increase of ε_v without significantly increasing the applied stress. The last segment is the compaction of the fractured material characterized by a rapid increase in the applied stress without significantly increasing ε_v . In this last segment, the porous spaces are effectively all collapsed and only the matrix material remains. Therefore, regardless of the initial porosities of the specimens, the slope of the curves are very close each other. Under the uniaxial strain test conditions, the value of σ_f varies from 11 to 18 MPa for the 60-series specimens. The 90-series specimens have much higher strengths that range from 59 to 62 MPa.

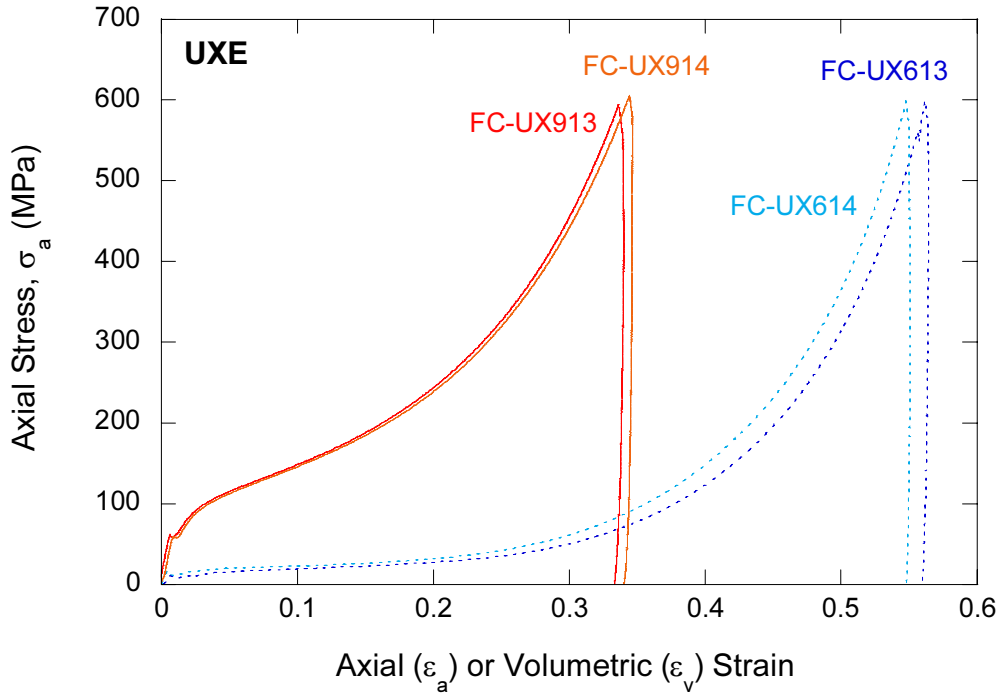


Figure 15. The stress-strain plots obtained during uniaxial strain (UXE) testing of the cellular concrete specimens: 60-series (blue dotted) and 90-series (red). The axial strain is effectively same as the volumetric strain under uniaxial strain condition ($\epsilon_a \neq 0, \epsilon_l = 0$).

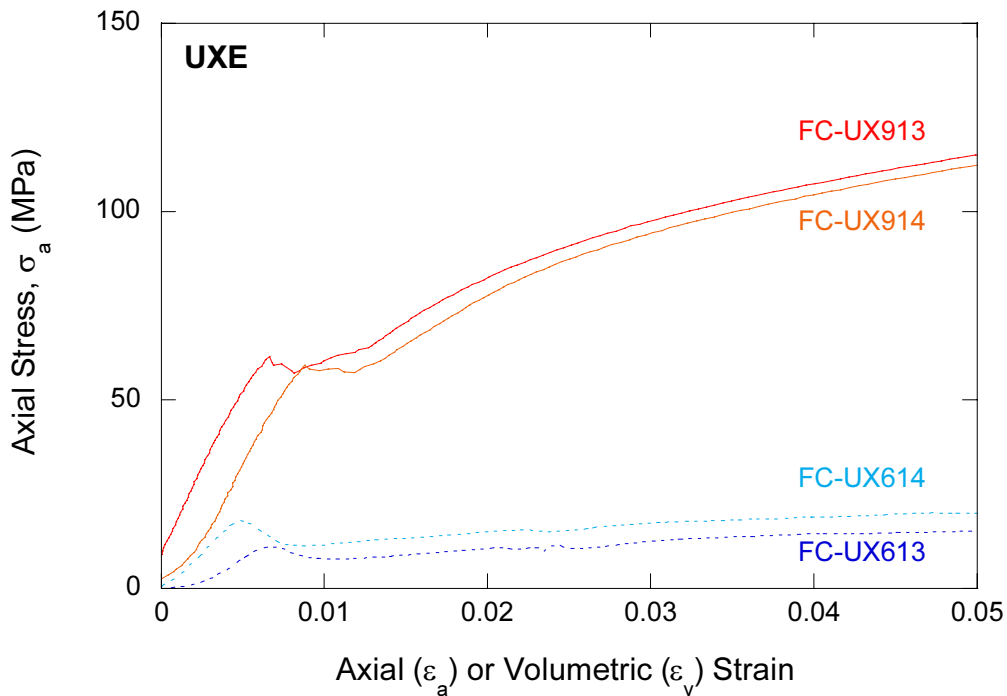


Figure 16. The failure of the cellular concrete under uniaxial strain (UXE) testing condition.

5. Triaxial Extension Tests (TXE)

In the triaxial extension tests, the axial stress applied to the specimen is the minimum principal stress and the confining pressure is acting as the major and the intermediate principal stresses. To create this peculiar stress condition, $\sigma_1 = \sigma_2 > \sigma_3$, in the triaxial pressure cell, we have to prevent the confining pressure acting on the ends of the specimen. This is accomplished by preventing the hydraulic fluid entering the interface between the specimen and the end-caps using a shrinkable tubing and the impermeable coating of polyurethane layer on the specimen assembly. The remaining interfaces between the end-caps and the pistons were sealed by “O” rings (Figure 17). Now, the confining pressure can be increased without increasing σ_3 simultaneously. The axial displacements were measured by two 180° apart axial LVDTs and the lateral displacements were measure by a Schuler gage.

The concrete core was machined in the form of right circular cylinders. The dimensions of the specimens are listed in Table 4 and all test records are shown in Appendix E. For lower-density specimens (FC-TE615 and FC-TE616), the specimen was pre-compacted under 30 MPa of hydrostatic pressure. Then, the compacted specimen was machined to have the nominal dimension of 45 mm in diameter and 90 mm in length.

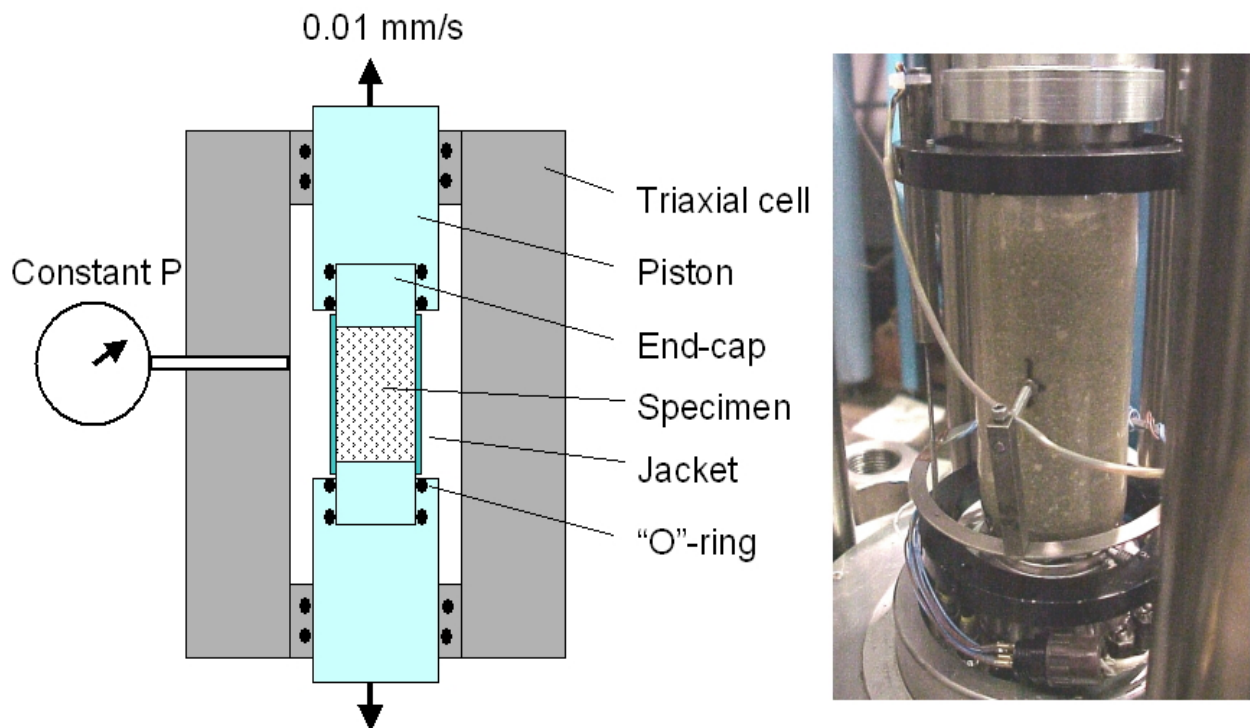


Figure 17. The triaxial extension test (TXE) set-up and an instrumented specimen with two axial LVDTs and a Schuler gage for the measurements of axial and lateral displacements, respectively.

Table 4. Summary of the triaxial extension tests (TXE) of the cellular concrete.

Specimen ID	Confining Pressure (MPa)	Diameter (mm)	Length (mm)	Weight (g)	Density (g/cm ³)	σ_{3f} (MPa)
FC-TE915	100	50.73	101.57	295.78	1.44	66
FC-TE916	200	50.68	101.38	287.23	1.40	85
FC-TE917	400	50.67	101.56	287.74	1.41	297
FC-TE615	100	44.50	93.03	174.18	1.20	66
FC-TE616	200	44.37	91.38	171.32	1.21	81

Figures 18 and 19 show the variations of the axial stress, confining pressure, and the axial strain during the triaxial extension test of the cellular concrete. After the specimen is placed in the triaxial compression cell, the confining pressure was increased to a set level. The axial stress was also increased in tandem with the confining pressure causing the specimen to deform isotropically. Once the hydrostatic stress condition is established to the predetermined pressure, the piston applying the axial stress on the specimen was pulled back at a constant displacement rate of 0.01 mm/sec while maintaining the confining pressure constant (Figures 20 and 21). This will cause the axial stress to drop below the level of confining pressure to create the stress condition of triaxial extension ($\sigma_1 = \sigma_2 > \sigma_3$). The specimen will elongate and at critical stress (triaxial extension strength or σ_{3f}) the specimen fails. For 90-series specimens, the material failed after the specimen elongated approximately 4 % in length. The failure surface was perpendicular to the axis of σ_3 implying the tensile failure mode of the specimen (Figure 22). However, in 60-series specimens, the material failed after going through about 10 % axial elongation. The failure surface was inclined to the axis of σ_3 with slickenside present on the failure surface signifying the shear failure mode of the specimen (Figure 22).

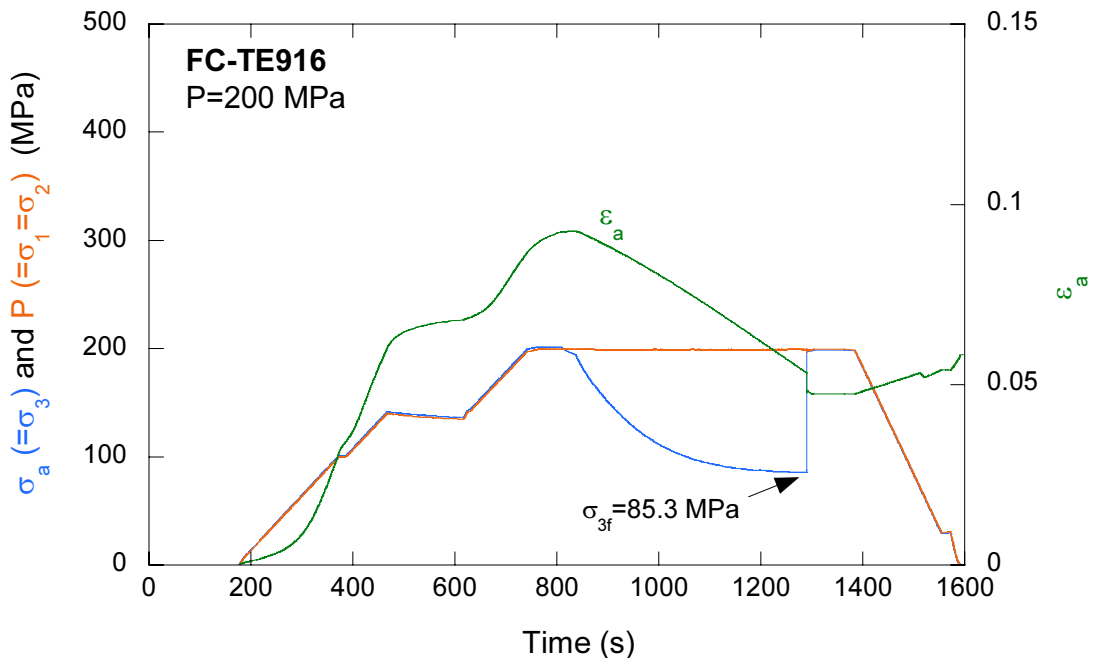


Figure 18. Triaxial extension test (TXE) record for the FC-TE916 specimen showing the test sequences and the corresponding variations of stresses and strains with respect to time.

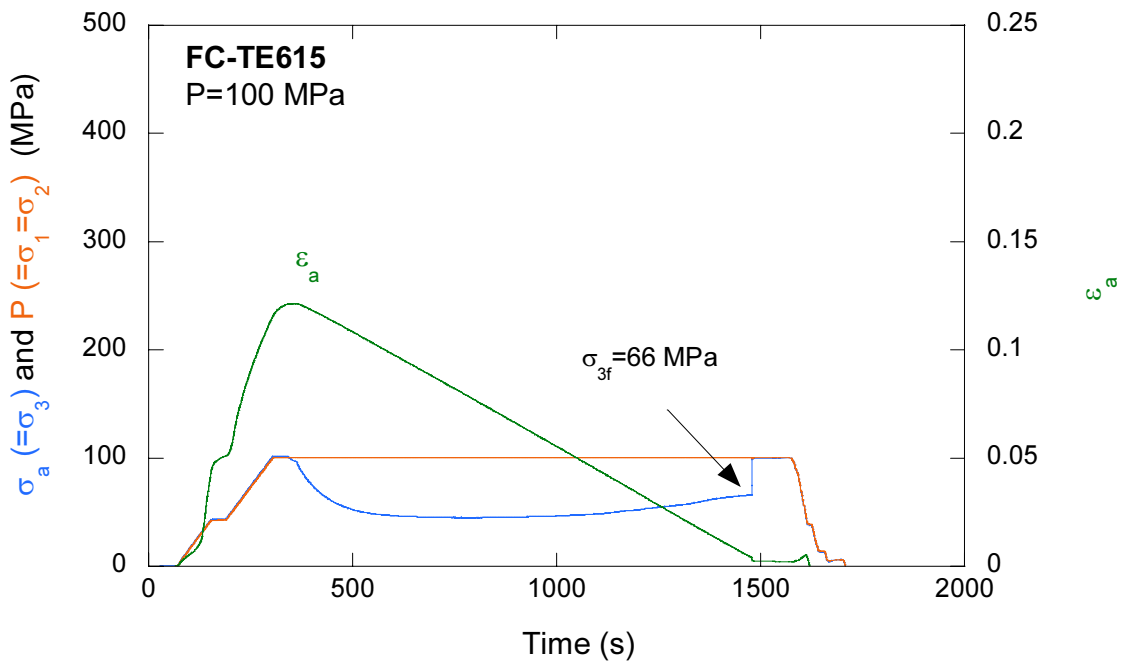


Figure 19. Triaxial extension test (TXE) record for the FC-TE615 specimen showing the test sequences and the corresponding variations of stresses and strains with respect to time.

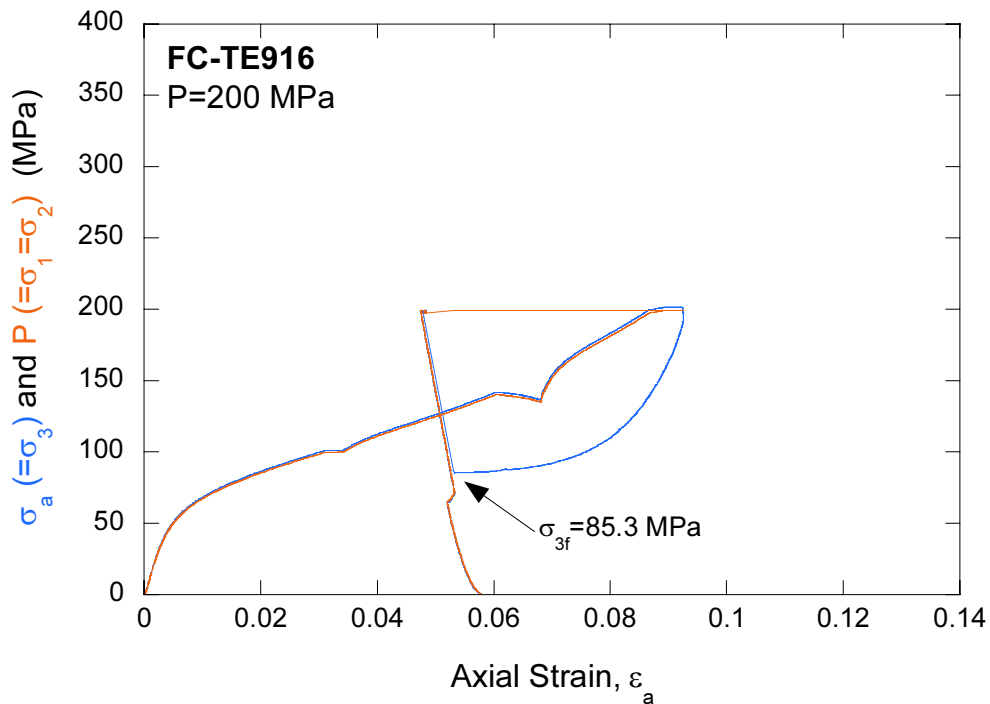


Figure 20. Stress-strain plot obtained during triaxial extension test (TXE) of the FC-TE916 specimen under 200 MPa of confining pressure, P.

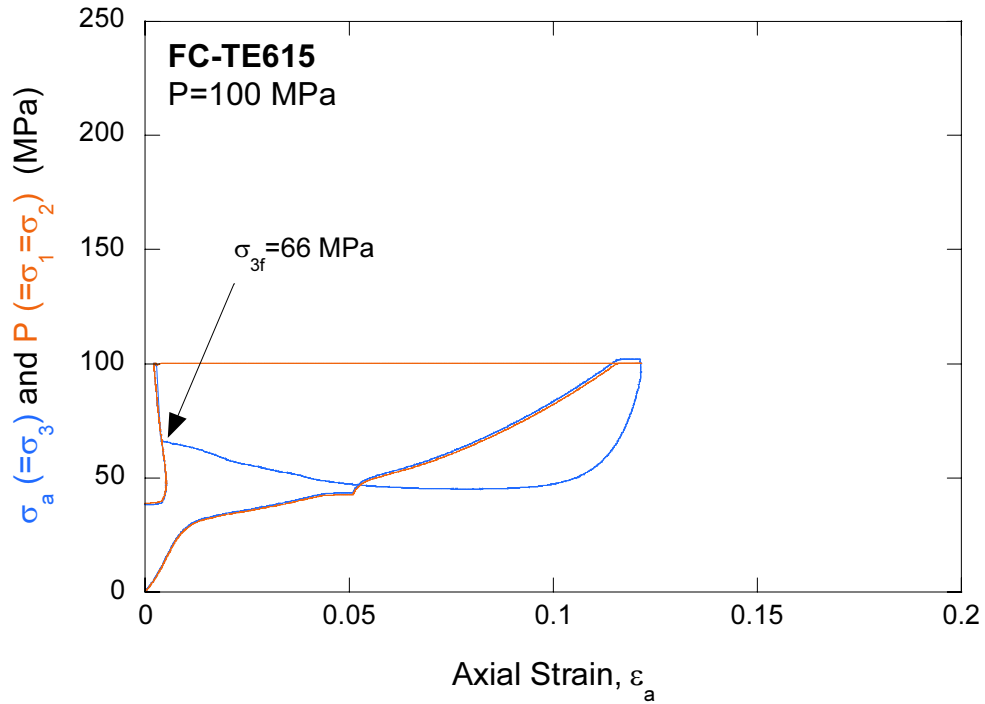


Figure 21. Stress-strain plot obtained during triaxial extension test (TXE) of the FC-TE615 specimen under 100 MPa of confining pressure, P.



Figure 22. Two different failure modes of the cellular concrete specimens under the triaxial extension (TXE) test condition: tensile failure in the 90-series concrete specimen (FC-TE916, left) and shear failure in the 60-series specimen (FC-TE615, right).

6. Uniaxial Tension Tests (UTT)

To measure the tensile strength of the cellular concrete specimens directly, six shaped specimens (three from the 60-series and three from the 90-series) were prepared. Figure 23 shows the shape and the nominal dimensions of the “dog-bone” shaped specimen. The dimensions and the measured tensile strengths of the specimens are listed in Table 5 and all stress-displacement test records are shown in Appendix F.

The diameter of the specimen was exactly same as the diameter of the end-caps to ensure concentricity of the specimen with the axis of the pulling load. The ends of the specimen were cemented to the end-caps. These end-caps were connected to the pulling pistons through the flexible chain-links (Figure 24). The flexible chain-links minimize the bending moment applied to the specimen. The minor diameter of the specimen is located in the middle of the specimen away from the stress concentration cause by the end-caps.

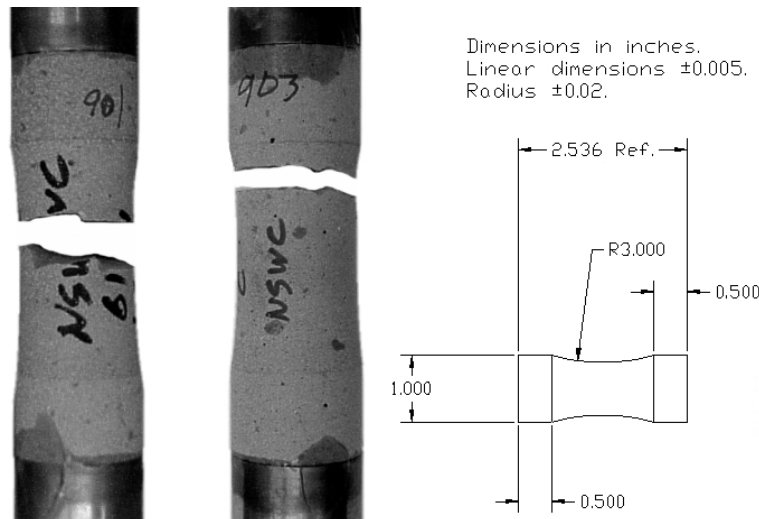


Figure 23. Typical tensile fracture planes induced in the cellular concrete specimen during uniaxial tension tests (UTT). Also shown are the nominal dimensions of the “dog-bone” shaped specimen prepared for UTT testing

Table 5. Summary of the uniaxial tension tests (UTT) of the cellular concrete.

Specimen ID	Diameter (mm)	Length (mm)	Weight (g)	Density (g/cm ³)	-T (MPa)
FC-UT901	22.84	68.88	48.19	1.68	1.65
FC-UT902	22.80	57.00	36.95	1.29	1.56
FC-UT903	22.81	72.10	46.68	1.63	1.65
FC-UT601	22.76	67.26	30.91	1.08	1.15
FC-UT602	22.78	66.67	30.76	1.07	1.25
FC-UT603	22.76	65.34	30.36	1.06	1.05

The tensile load was applied to the specimen at a constant tensile strain rate of $10^{-3}/s$. The tensile strength of the material was calculated from the following equation:

$$-T = P_t / \pi^2 r$$

where $-T$ is the direct tensile strength in MPa; P_t is the peak tensile load in N; r is the minor diameter of the specimen in mm. Figure 25 shows the displacement-tensile load plots for all uniaxial tension test specimens. Unlike the shear failure occurred under compressive loading, the tensile failure plane was typically formed perpendicular to the loading axis (Figure 23).



Figure 24. The uniaxial tension test (UTT) set-up consisting of the flexible chain-links and the end-caps cemented to the shaped specimen.

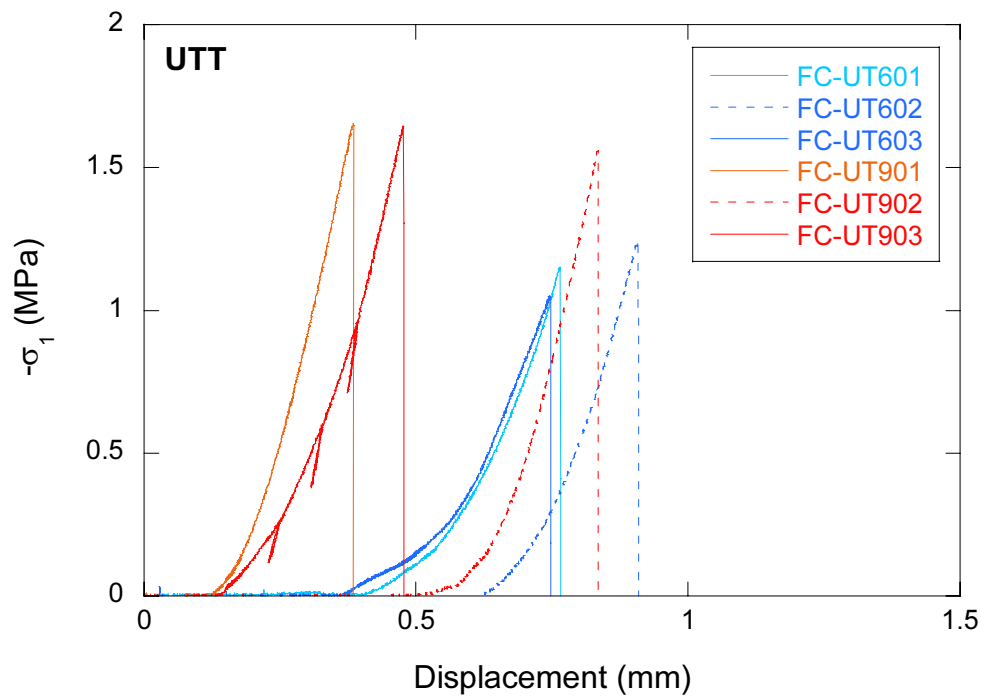


Figure 25. The axial load-displacement plots obtained during uniaxial tension testing (UTT) of the cellular concrete specimens.

7. Conclusions

To establish mechanical material properties of the cellular concrete, a series of quasi-static, compression and tension tests have been completed. The results from laboratory constitutive experiments can be summarized as follows:

- The material properties database for the cellular concrete has been established based on five types of laboratory tests: unconfined compression tests (UCT), triaxial compression (TXC) / hydrostatic compression tests (HCT), uniaxial strain tests (UXE), triaxial extension tests (TXE), and uniaxial tension tests (UTT) tension test.
- Under the triaxial compression stress conditions ($\sigma_1 > \sigma_2 = \sigma_3 = P$), the cellular concrete compacts and then dilates.
- Results from the uniaxial and triaxial compression tests were used to characterize the cellular concrete based on the cap plasticity model (Sandler and Rubin, 1979).

$$\sqrt{J_2} \text{ (MPa)} = 297.2 - 278.7 \exp^{-0.000455 I_1 \text{ (MPa)}} \text{ for the 90-series tests}$$

$$\sqrt{J_2} \text{ (MPa)} = 211.4 - 204.2 \exp^{-0.000628 I_1 \text{ (MPa)}} \text{ for the 60-series tests}$$

- Under the uniaxial strain test conditions ($\epsilon_a \neq 0, \epsilon_l = 0$), the value of σ_f varies from 11 to 18 MPa for the 60-series specimens. The 90-series specimens have much higher strengths that range from 59 to 62 MPa.
- Under the triaxial extension stress conditions ($\sigma_1 = \sigma_2 > \sigma_3$), the 90-series specimens specimen failed in tension after the specimen elongated approximately 4 % in length, whereas, the 60-series specimens failed in shear after going through about 10 % axial elongation.
- Based on the uniaxial tension tests, the tensile strength of the concrete was 1.6 ± 0.05 (MPa) for the 90-series specimens and 1.2 ± 0.10 (MPa) for the 60-series specimens.

References

- ASTM D2664, Standard Test Method for Triaxial Compressive Strength of Undrained Rock Core Specimens without Pore Pressure Measurements, American Society for Testing and Materials, 1995.
- ASTM D2938, Standard Test Method for Unconfined Compressive Strength of Intact Rock Core Specimens, American Society for Testing and Materials, 1995.
- ASTM D4543, Standard Practice for Preparing Rock Core Specimens and Determining Dimensional and Shape Tolerances, American Society for Testing and Materials, 1995.
- Fossum, A.F., Senseny P.E., Pfeifle T.W. and K.D. Mellegard, Experimental Determination of Probability Distributions for Parameters of a Salem Limestone Cap Plasticity Model, *Mechanics of Materials*, 21, 119-137, 1995.
- Jaeger, J.C. and N.G.W., Cook, *Fundamentals of Rock Mechanics*, 169-173, Methuen, London, England, 1969.
- Olsson, W. A., Theoretical and experimental investigation of compaction band in porous rock, *J. Geophys. Res.*, 104, 7219-7228, 1999.
- Sandler, I.S. and D. Rubin, An Algorithm and a Modular Subroutine for the Cap Model, *Int. J. Numer. and Anal. Mech. Geomech.*, 3, 173-186, 1979.
- Schuler, K.W. Lateral-deformation gage for rock-mechanics testing, *experimental Mechanics*, Vol. 18, No. 12, 477-480, 1978.

APPENDIX A

Cellular Concrete

(Modified from a draft of the end of the year report *High Speed Ordnance Technology* to the Office of Naval Research submitted in October 2003 for inclusion in the NSWCDD Surface Weapons Technology Program End of Year 2003 Progress Report, Timothy Spivak, NSWCDD/G22)

Cellular concrete is a composite mixture of cement (Portland Type I), water, and foam. Foam is produced using a foam generator that converts a mixture of foam concentrate and water into thick and usably stable foam. By mixing this foam with cement and water, small air bubbles are entrapped in the slurry resulting in a porous and light-weight concrete, without sand or any other aggregate. With the goal of preparing for a foamcrete target pour, initial foamcrete experiments explored the effect on density of variables including foam concentrate to water ratio, mixing time, curing time, batch to batch consistency, mix consistency, pour consistency, bubble distribution, and slurry temperature. In addition, properties of the foam generator were identified for a few different foam concentrate to water ratios including foam density, mass and volume flow rates, and expansion ratio.

This experimental effort began with a characterization of the foam and the foam generator using the 40:1 water to foam concentrate ratio recommended by the foam generator manufacturer. For this foam mixture, the average foam density was found to be 2.61 lbm/ft³ with a standard deviation of 0.03 lbm/ft³. The mass flow rate of the foam generator was found to be 1.14 lbm/sec with a standard deviation of 0.02 lbm/sec. The volume flow rate was found to be 0.437 ft³/sec with a standard deviation of 0.009 ft³/sec. The expansion ratio (the density based ratio of foam produced by the foam generator to foam solution put into the foam generator) was found to be approximately 24:1. Therefore, with the 2 – 80 gallon tanks of the foam generator completely filled with foam solution, 142 cubic yards of foam could be generated, and it would take at least 2.4 hours to empty both tanks. For this experiment only one tank was filled and incrementally emptied into a 55 gallon drum in order to measure density and flow rates. For subsequent experiments only small volumes of foam concentrate were used.

A potlife experiment investigated the effect of mixing time on foamcrete density for 3 different water to foam concentrate ratios; 10:1, 20:1, and 40:1. The water to cement ratio for this experiment and all successive density experiments was held constant at 0.447:1. The objective of this experiment was to measure the change in density of these 3 different batches of foamcrete over a mixing period of one hour. The result can be seen in Figure A-1 below. As each batch was mixed, air was removed from the slurry, causing an increase in density. For the 40:1 foam solution, the change occurred much faster than for the other two concentrations. Because the 20:1 and 10:1 concentrations behaved similarly and because the 20:1 concentration consumes less concentrate than the 10:1, the 20:1 solution concentration was used for successive experiments.

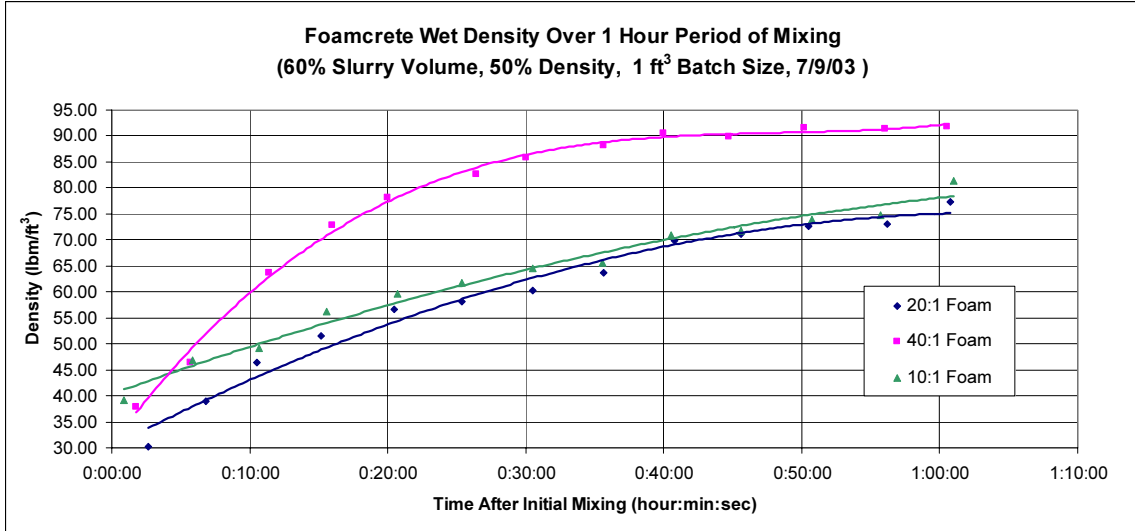


Figure A-1. Potlife Experiment Results

An experiment was performed to evaluate the air bubble distribution, pour consistency, and mix consistency of foamcrete. A full batch (2.5ft^3) of foamcrete was mixed and used to evaluate these three variables. In order to qualify the behavior of air bubbles and the consistency of those air bubbles through the height of a target pour in a 4ft tall columnar target, a 5" O.D. and 4ft tall clear plastic cylinder was filled with foamcrete with a scoop and allowed to cure. Upon inspection and dissection of this column of foamcrete, a significant variation in density was measured from the top to the bottom of the column, a change of approximately 10 lbm/ft^3 . These results can be seen in Figure A-2. For this reason, plans were made to pour real targets in four layers, allowing each layer to slightly cure before pouring the next layer.

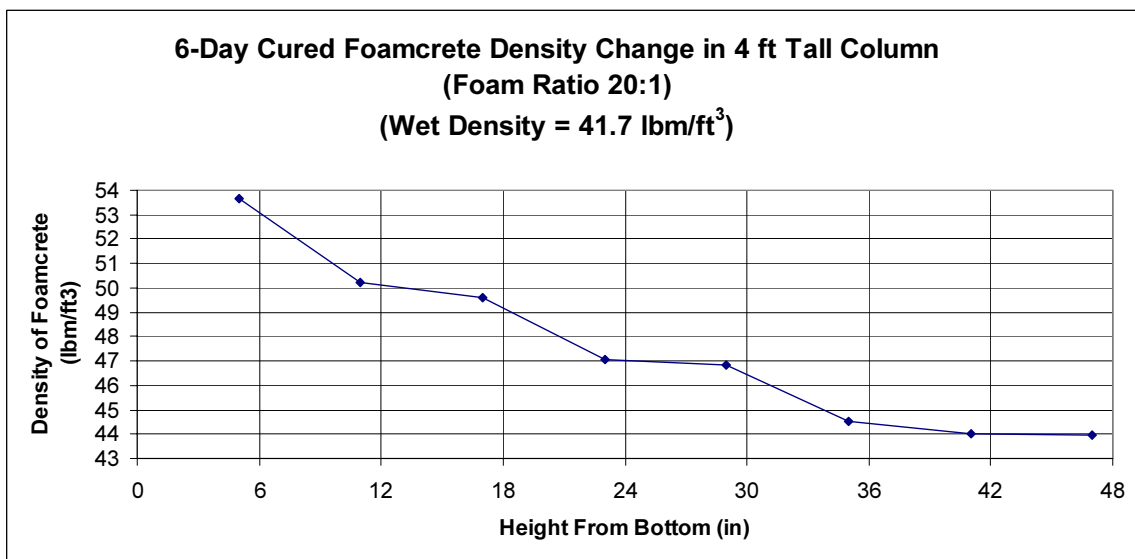


Figure A-2. Pour Consistency Results

Bubble distribution in this column was observed to be wide both spatially and in size. The spatial distribution was somewhat quantified by measuring the density of small segments of the column. Intuitively, a significantly greater amount of air was at the top of the column than at the bottom, once the cylinder cured based on Figure A-2. In addition the cut segments were sliced and observed to have some rather large bubbles and other very small bubbles entrapped as can be seen in Figure A-3.



Figure A-3. Bubble Distribution Results

Mix consistency was also measured during this experiment by pouring a wheelbarrow full of foamcrete and measuring the density of the material taken from four quadrants of the wheelbarrow. The data from this experiment can be seen in Table A-1. There was some variation of density in the mix; however, the pour consistency was a greater concern.

Table A-1. Mix Consistency Results

Location of Sample (Quadrant):	Foamcrete Density (lbm/ft³):
Front Right	46.90721649
Rear Left	45.65292096
Rear Right	44.14089347
Front Left	49.94845361

An anomaly of this experiment and of the previous potlife experiment was that the initial measured densities were much less than expected. In order to explain this, a volume verification experiment was quickly performed using a 5 gallon bucket, a stirring rod, and small amount of cement and water. The previous experiment had resulted in much lower initial densities than expected. The goal for initial density had been 70 lbm/ft³ (~50% of the density of 5,000 psi Concrete); however, an initial density of 42 lbm/ft³ was measured. This indicated that there may have initially been less cement volume in the mixer than intended. In order to verify this suspicion, the volume of water and cement mixture was measured using the same water to cement ratio as previously used. This experiment confirmed that the cement volume used for the previous experiments was only 60% of the volume that was intended for those experiments. This explained the low initial densities. For the bubble/pour/mix experiment, initial density was 60% of the target density.

In the case of the potlife experiment the initial densities were even lower, because a small batch size (1ft³) was used and because a significant amount of slurry (cement and water mixture) was sticking to the inside wall of the mixer, not mixing with the foam. To remedy this problem, the mixer was buttered prior to mixing successive batches and full batch sizes (2.5ft³) were used. Buttering is performed by mixing a small batch of slurry in the mixer and then dumping that mixture out, leaving the inside of the mixer coated with slurry prior to mixing a full batch.

Upon the discovery of solutions to these problems, a decision was made to repeat the potlife experiment using only the 20:1 foam concentration. The results of the original potlife experiment are relative because they were performed in the same manner, meaning that the decision to use a 20:1 ratio for successive experiments is still valid. Thus only the 20:1 experiment needed to be repeated in order to define the effect of mixing time on a 70lbm/ft³ mixture. The 20:1 potlife experiment was repeated and the result of this experiment is compared to the result of the previous experiment in Figure A-4. As can be seen from this figure, the change in density over an hour of mixing time was less significant for the 70 lbm/ft³ foamcrete than it was for the 30 lbm/ft³ foamcrete.

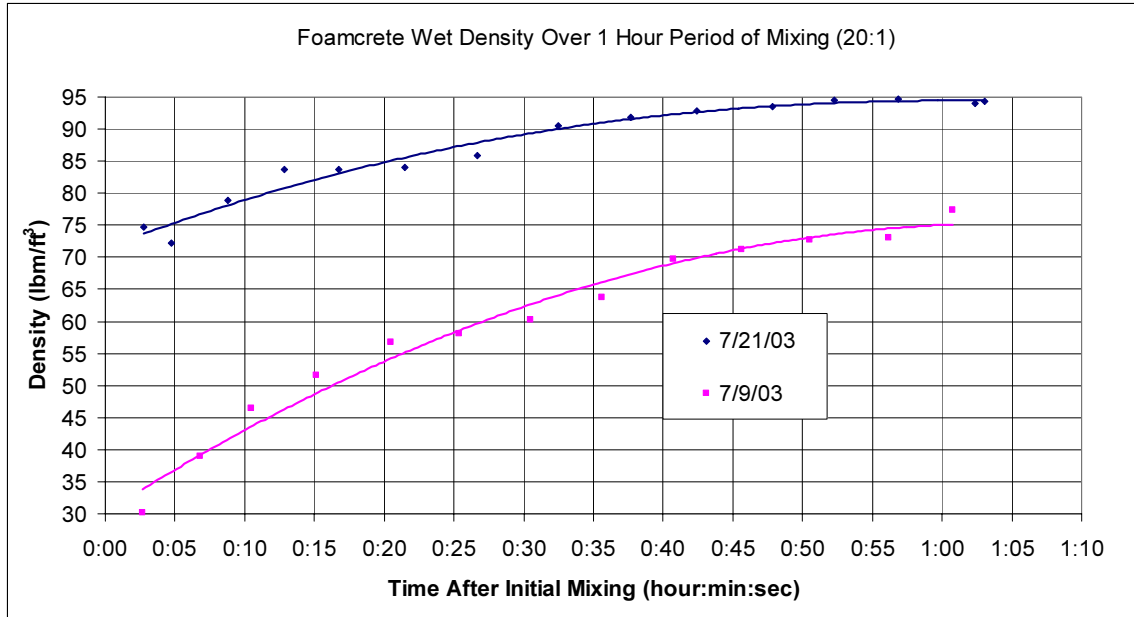


Figure A-4. 20:1 Potlife Results

Several test cylinders from these density experiments were cured and strength tested; however, the quality of the tested material was thought to be poor due to the long mixing times. Mixing this material was thought to reduce strength by damaging the crystalline structure of the foamcrete. In order to quantify the strength of 70 lbm/ft³ foamcrete, a batch of 4”x 8” unconfined compressive strength cylinders were made on 23 July 2003. These early mix cylinders were poured immediately after the foam was mixed with the cement slurry, and this material was not exposed to long mixing periods. 12 cylinders were poured with an average wet density of 63.2 lbm/ft³ and a standard deviation of 2.2 lbm/ft³. Three cylinders were tested at each curing time of 7 days, 14 days, 28 days, and 56 days. The results of these initial strength tests can be seen in Figure A-5. The average strength rises with curing time, but seems to level off somewhere between 28 and 56 days at approximately 900 psi.

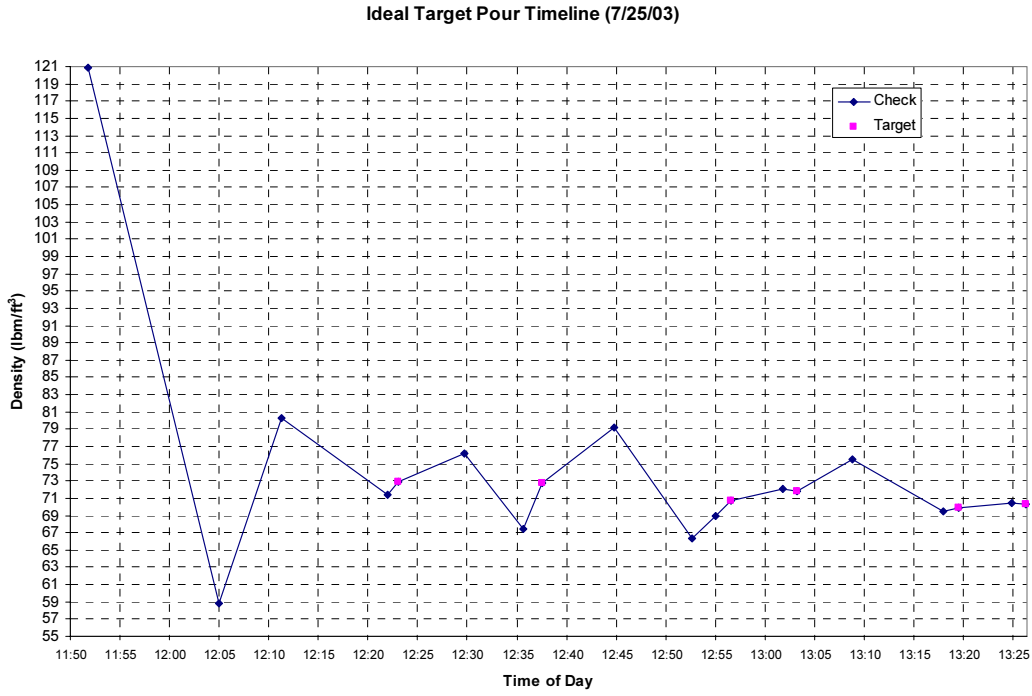


Figure A-6. Ideal Simulated Pour Experiment Results

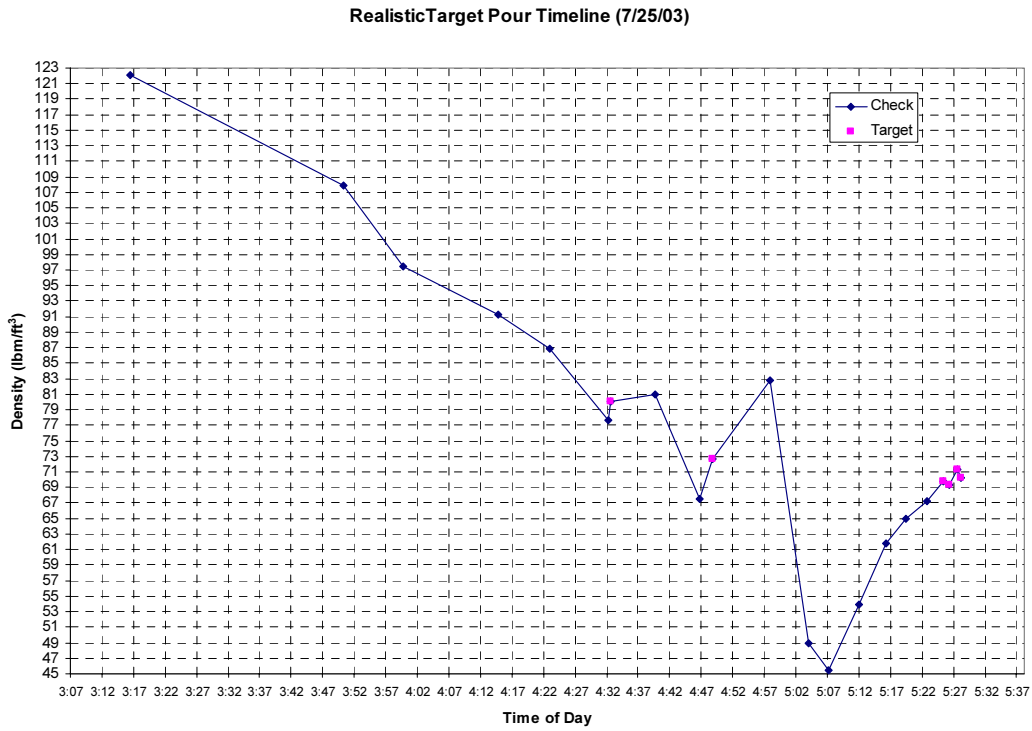


Figure A-7. Realistic Simulated Pour Experiment Results

Following the simulated pours, a few additional questions remained. One was the question of how long each layer of a layered target should be allowed to cure before pouring another layer on top. Too long of a curing time was likely to prevent bonding between layers and possibly cause problems for shock wave transmission through the target. Too short of a curing time was likely to disturb the top surface of lower layers of the target. This question was answered by another experiment. A batch of foamcrete was mixed in the mixer and three 5-gallon buckets were partially filled to represent the bottom layer of a foamcrete target. At three time intervals (30 minutes, 1 hour, and 3 hours) water was poured on top of the targets in order to assess the interaction between the water (representing wet foamcrete) and the top surface of the foamcrete. The results of this experiment illustrated by the runoff in Figure A-8 lead to the selection of 3 hours as the curing time interval between each layer of the target. At the two hour interval a finger test was performed and the surface of the target was still the consistency of thick mashed potatoes, and because the experiment was limited to only one remaining target, water was not poured until the 3 hour interval. It is possible that 2.5 hours or some shorter interval may be optimal.



Figure A-8. Surface Pour Interaction Experiment Results

Another issue that needed to be resolved before the real target pour was that of the difference in volume yield between the Home Depot brand cement used in several of the experiments and the cement used by the cement truck supplier, Rowe Concrete. For this experiment, a few batches of Rowe Cement were mixed in small quantities at the same water to cement ratio previously used, and the yielding volume was measured. This data was compared to that from the previous Home Depot cement volume verification experiment. The results of this experiment are given in Figure A-9. From this chart, weights of water and cement can be selected in order to produce the desired volume of slurry.

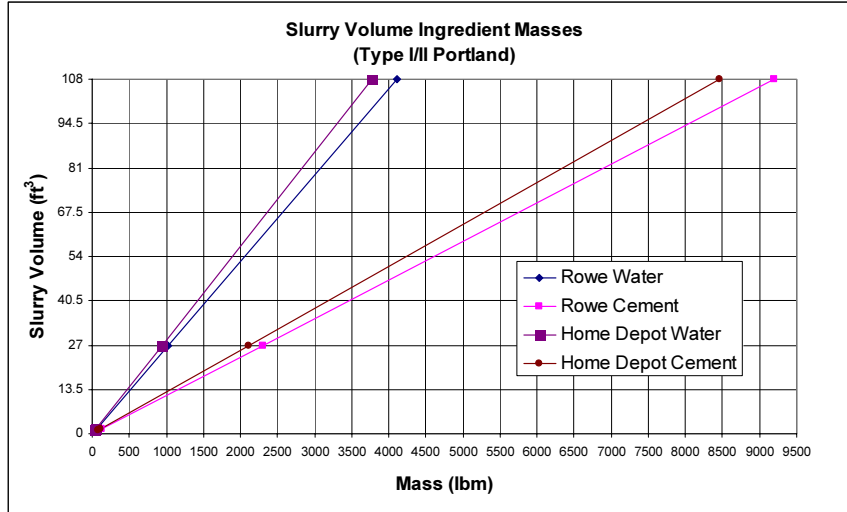


Figure A-9. Slurry Volume Yield Experiment Results

One final piece of information need prior to an actual target pour was the continuous flow rate and density of the foam generator using the 20:1 foam concentrate solution. In previous experiments, the flow rate and density were measured over short durations of foam shoots. For the cement truck longer foam shoots were anticipated, and any variation in flow rate or density of the foam needed to be identified. The results of this experiment are summarized in Table A-2, and as expected, these characteristics of the 20:1 foam were slightly different than those of the 40:1 foam originally characterized.

– Table A-2. Continuous 20:1 Foam Concentrate Experiment Results

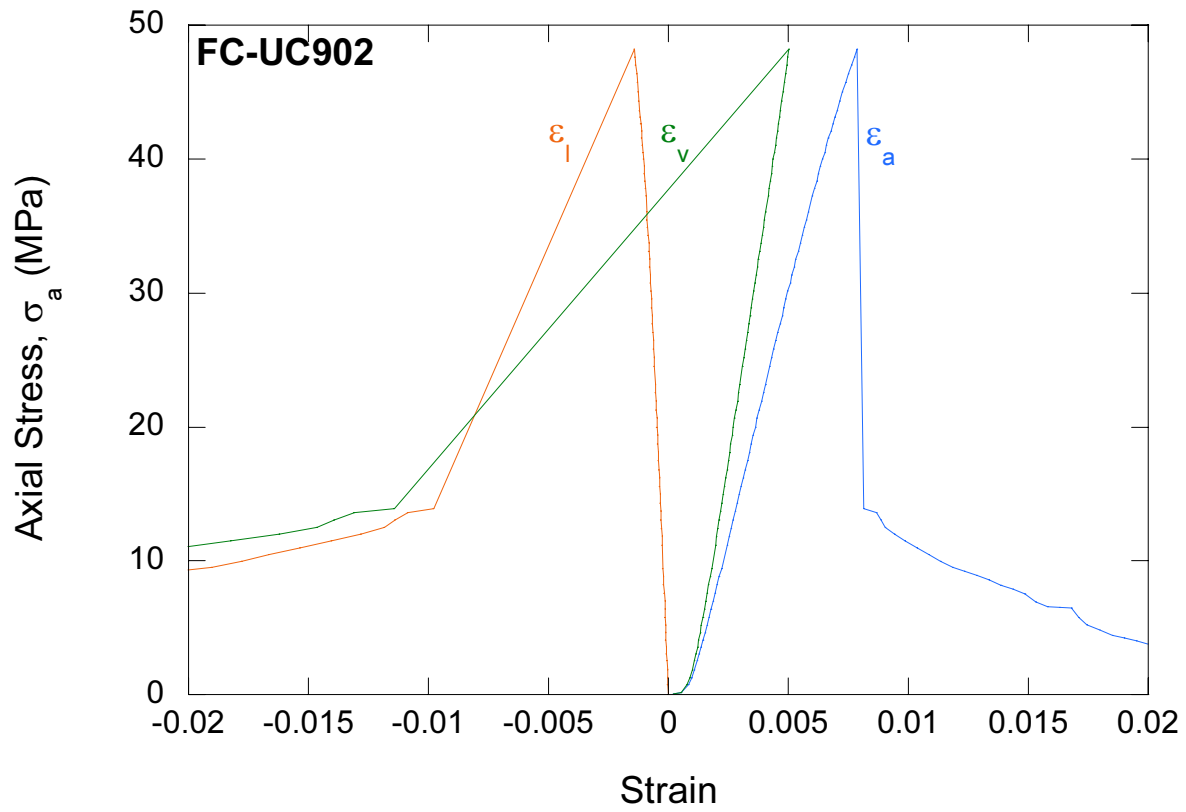
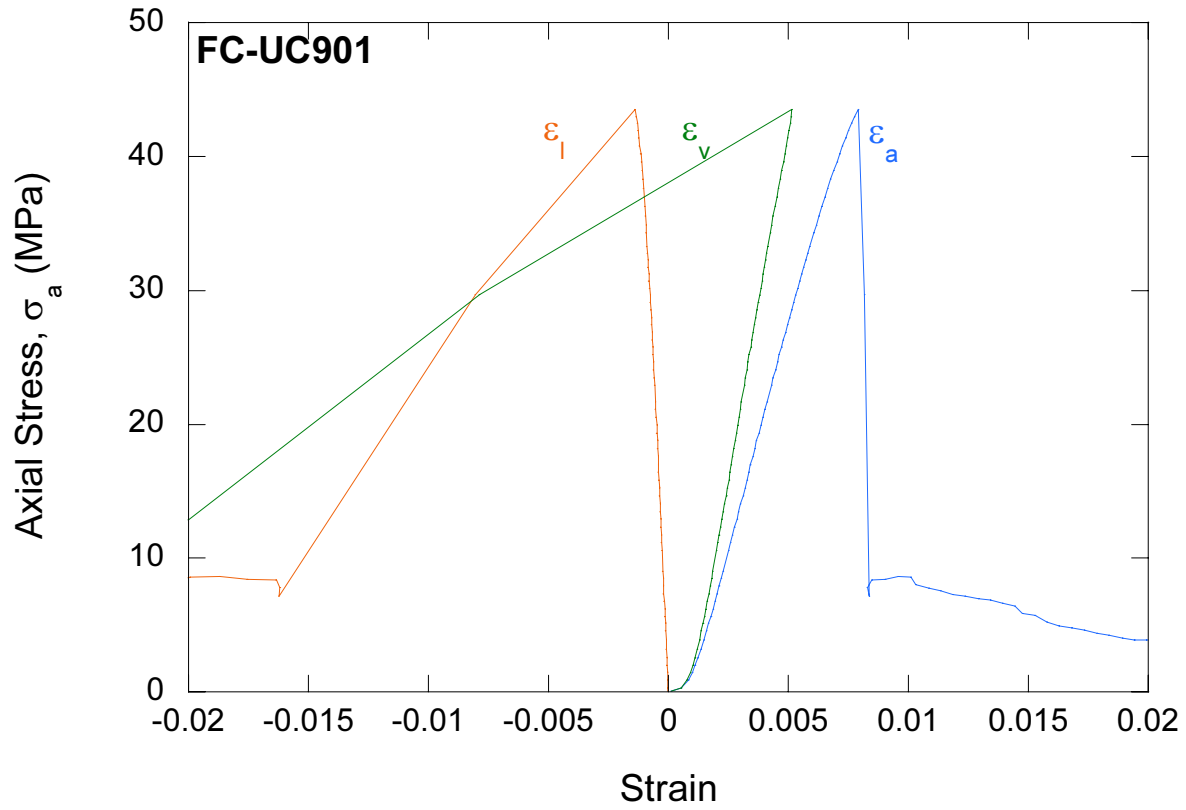
Average Foam Density (lbm/ft³)	3.007764
Standard Deviation	0.060975
Average Mass Flow Rate (lbm/sec)	1.260954
Standard Deviation	0.082391
Average Volume Flow Rate (ft³/sec)	0.419048
Standard Deviation	0.021759

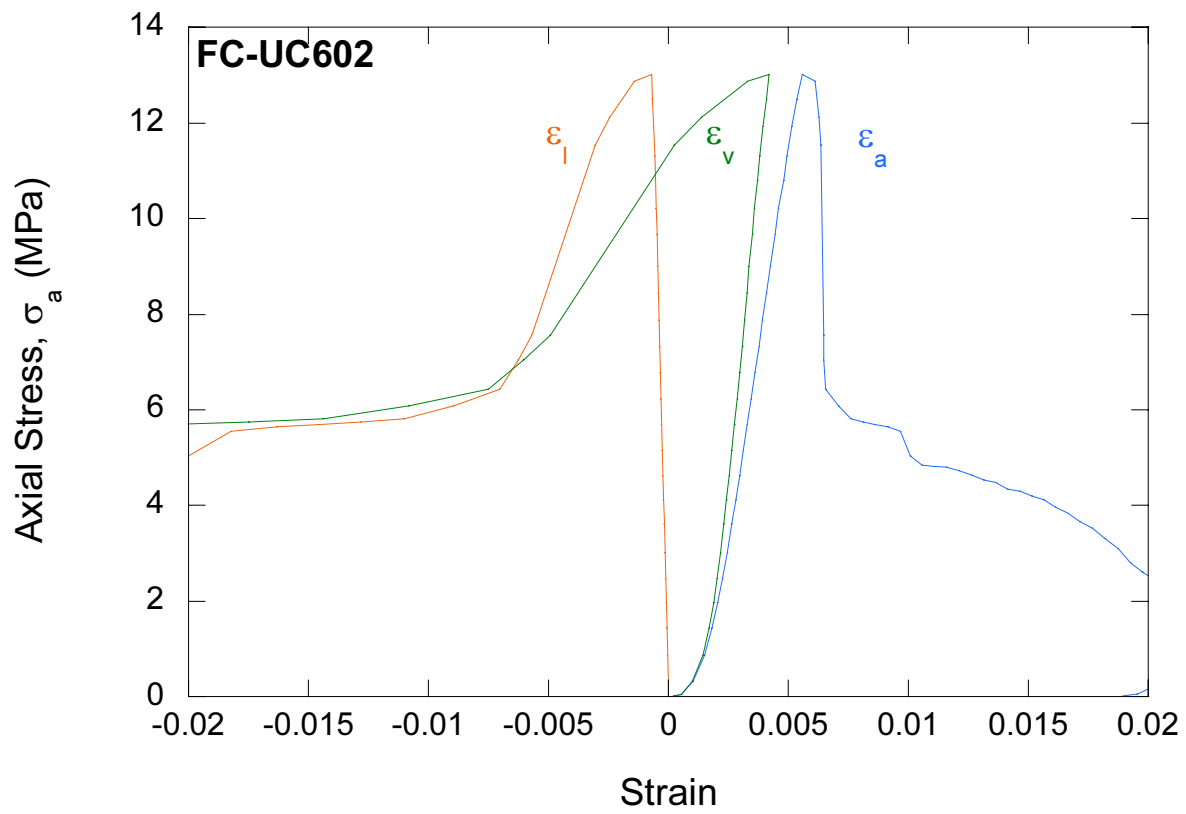
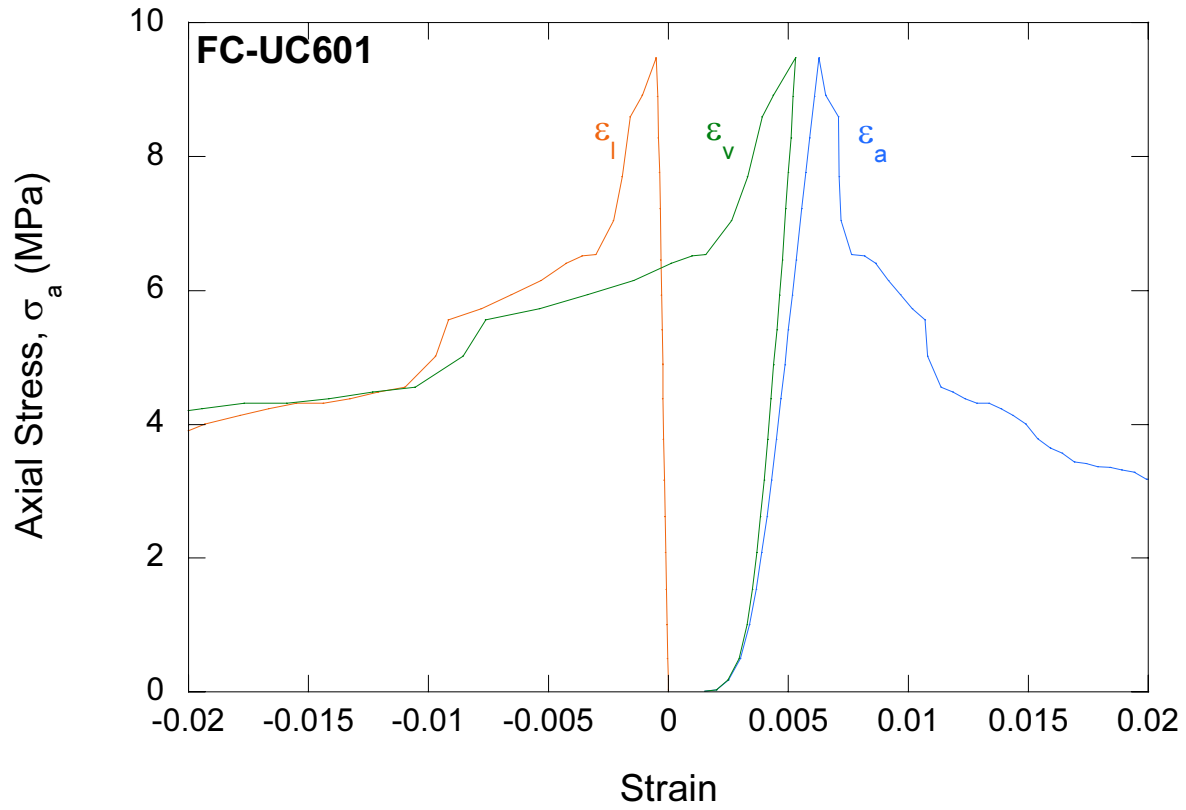
With the initial objective to control density, a goal was set to pour six, 30” (outer diameter) x 48” (height), cylindrical foamcrete targets with a density of 67 lbm/ft³ at the end of this series of density control experiments. This initial goal was met by pouring each target in four, 12” layers, with a resulting average density across all 24 layers of 66.33 lbm/ft³ and with a standard deviation of 0.39 lbm/ft³. At the conclusion of the density control experimental series, a cellular concrete production procedure has been defined, and a production capability has been demonstrated.

APPENDIX B

Stress-Strain Plots from Uniaxial Compression Testing (UCT) of Cellular concrete

(σ_a -axial stress, ε_a -axial strain, ε_l -lateral strain, and ε_v -volumetric strain)

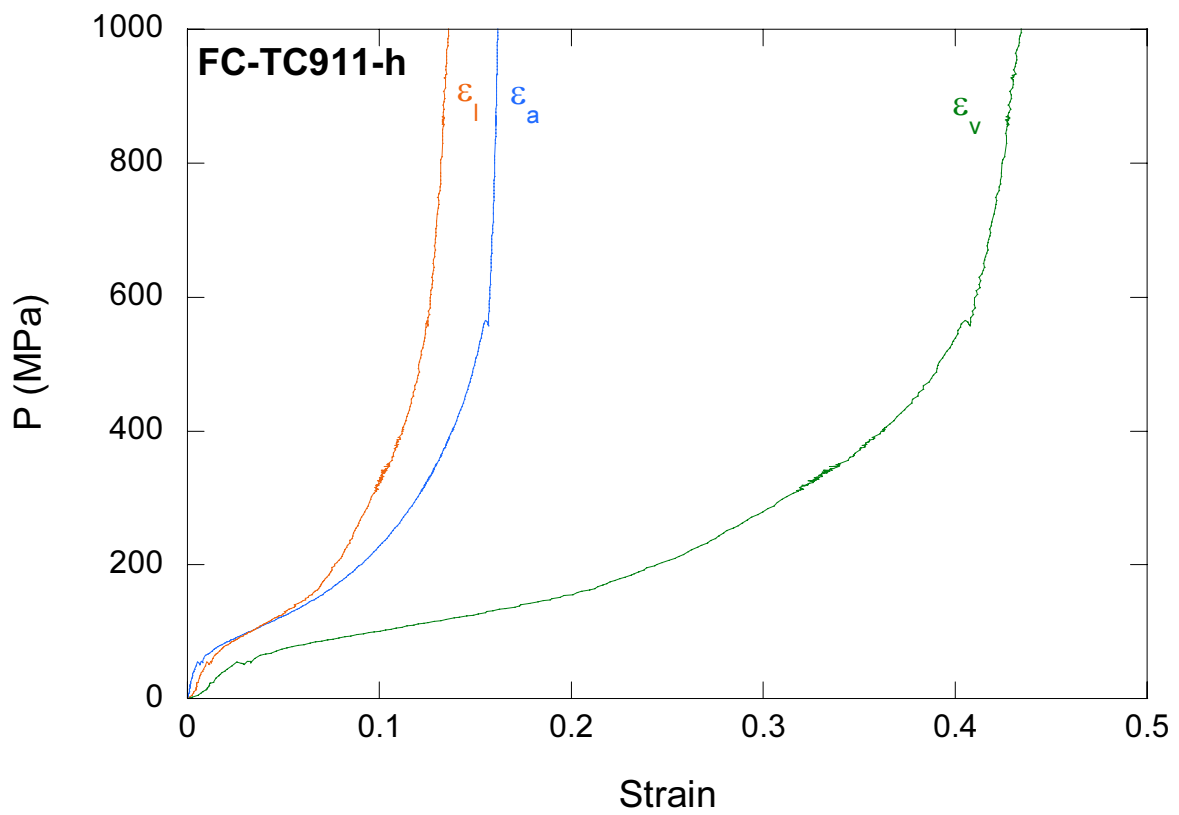
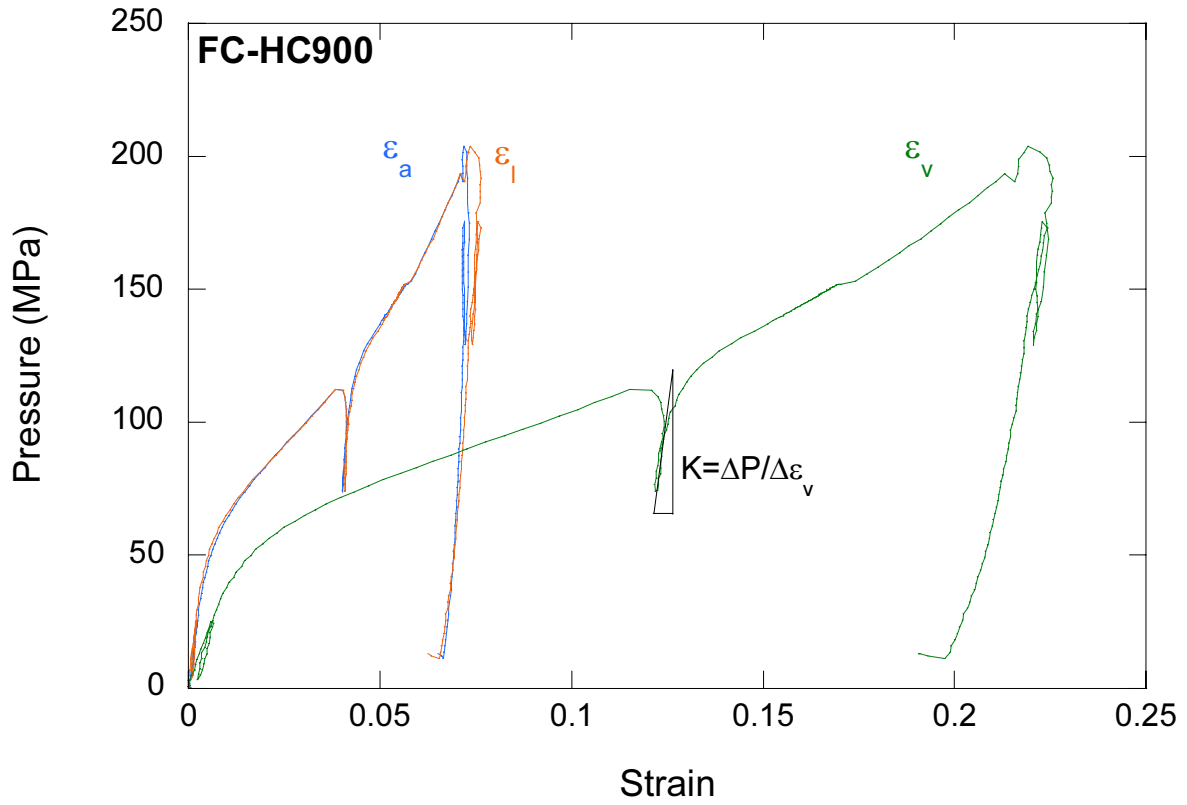


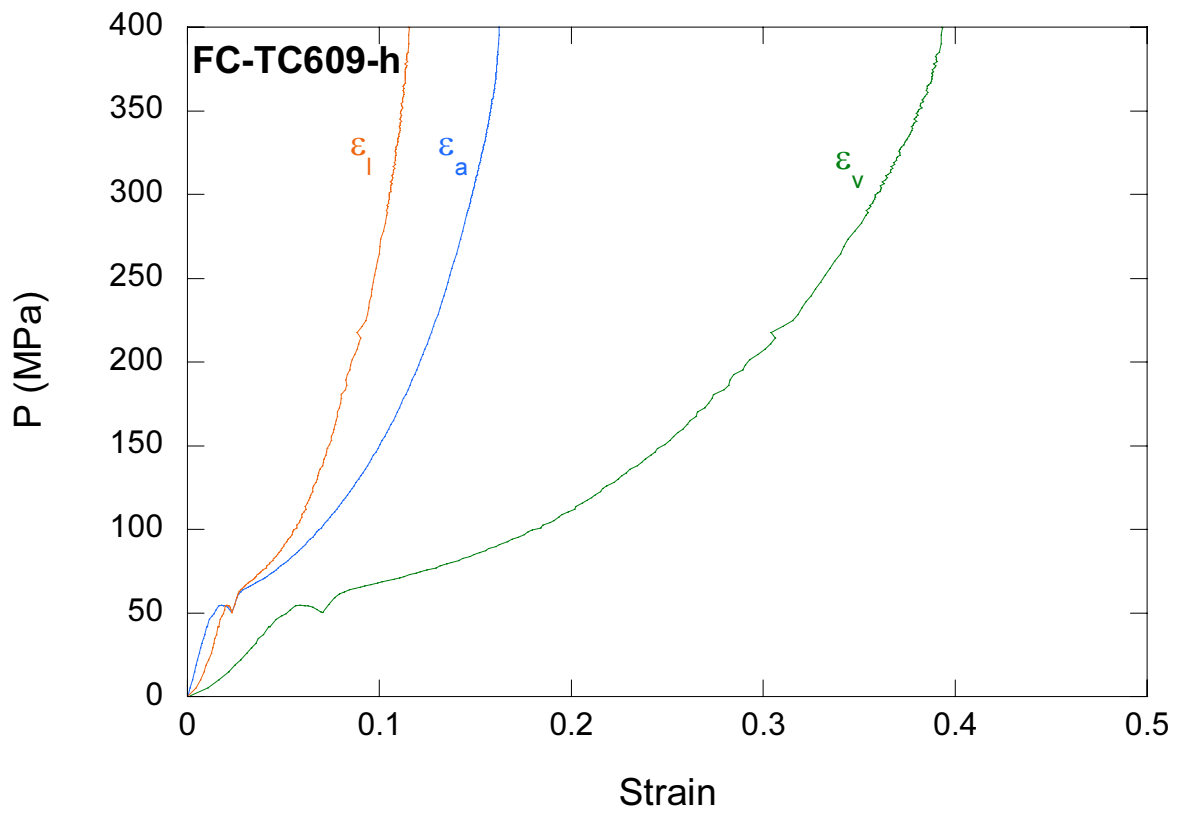
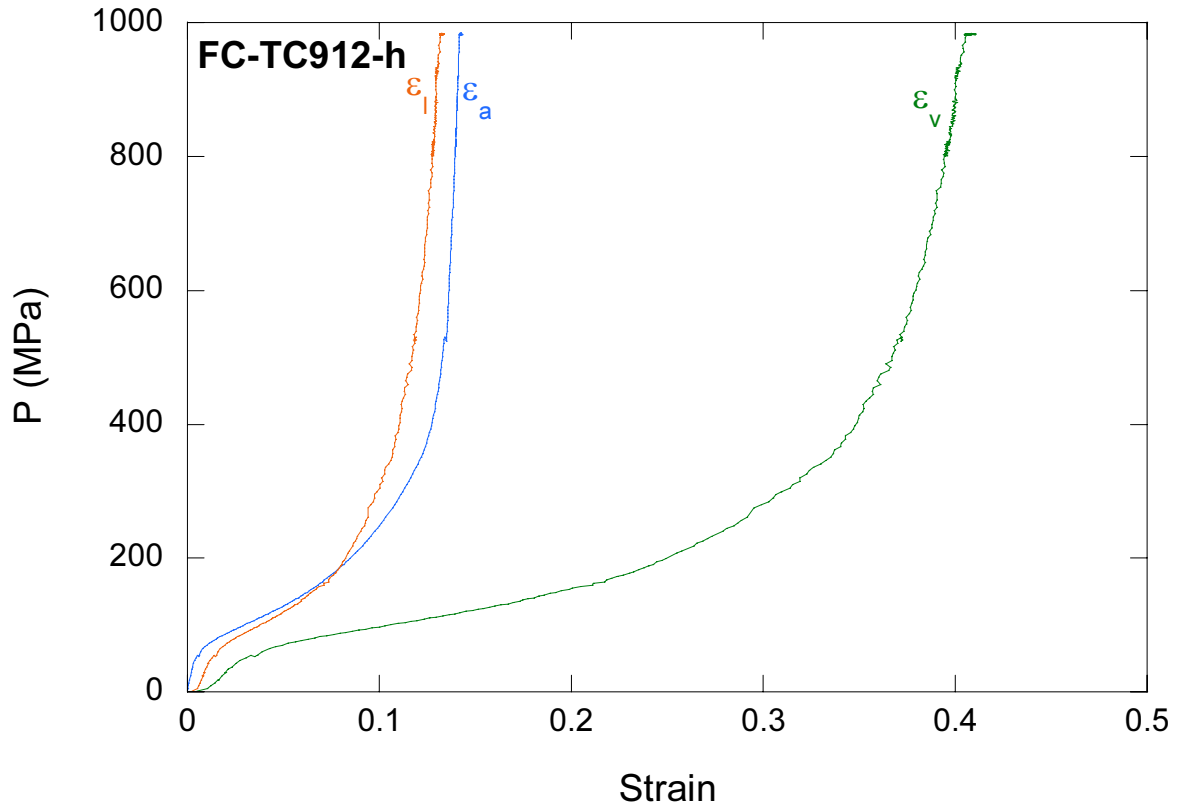


APPENDIX C-1

Stress-Strain Plots from Hydrostatic Compression Tests (HCT) of Cellular Concrete

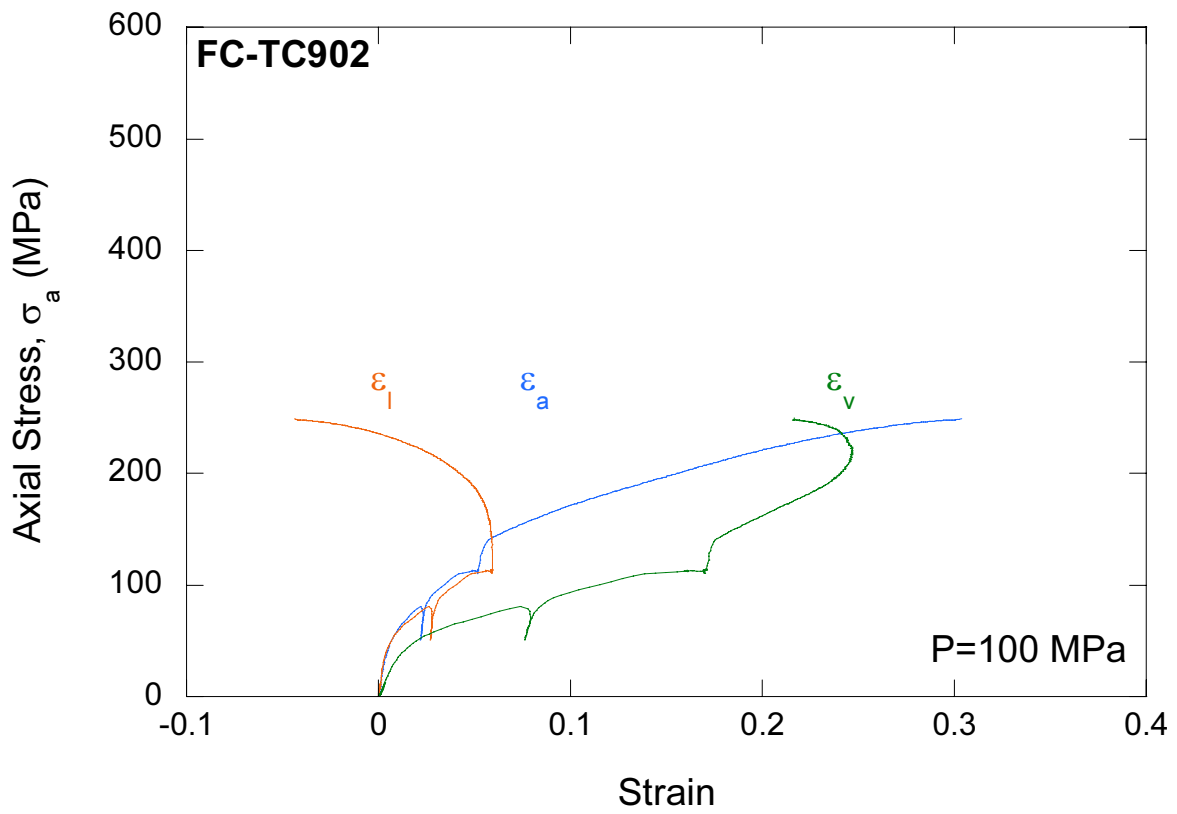
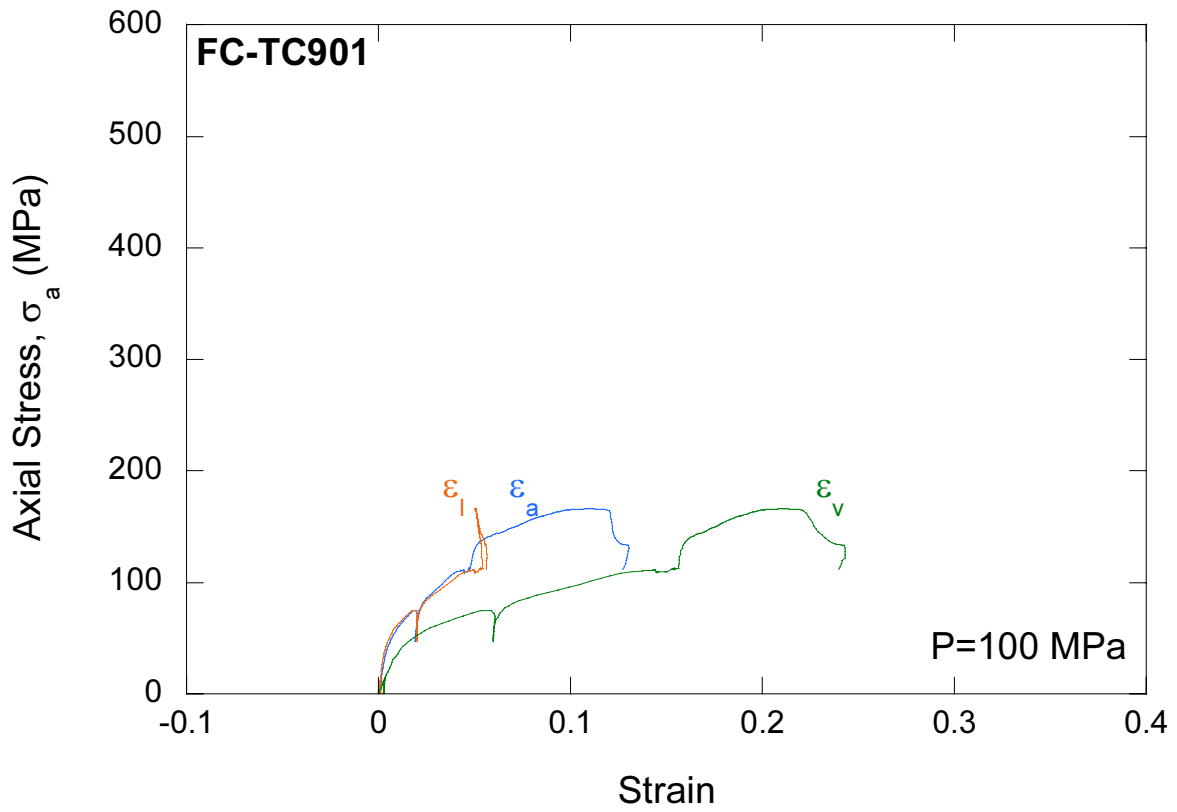
(σ_a -axial stress, ε_a -axial strain, ε_l -lateral strain, ε_v -volumetric strain, and P-confining pressure)

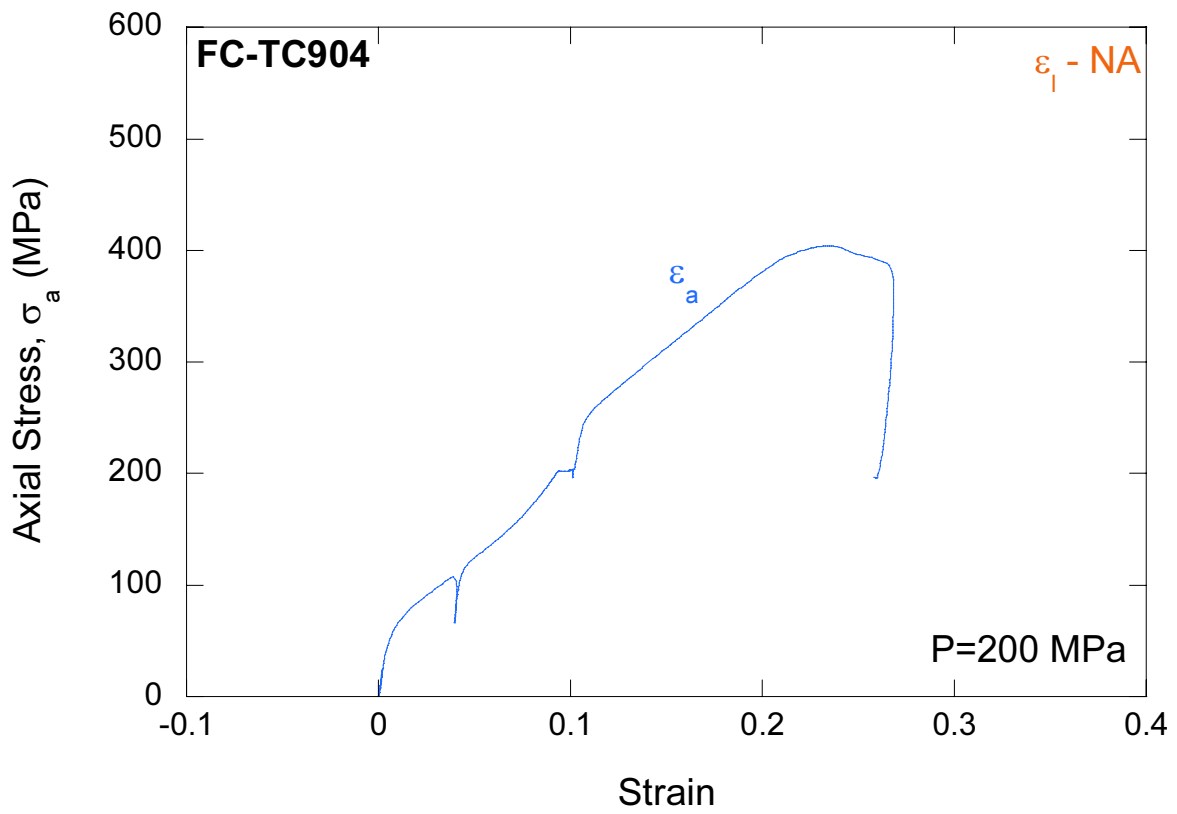
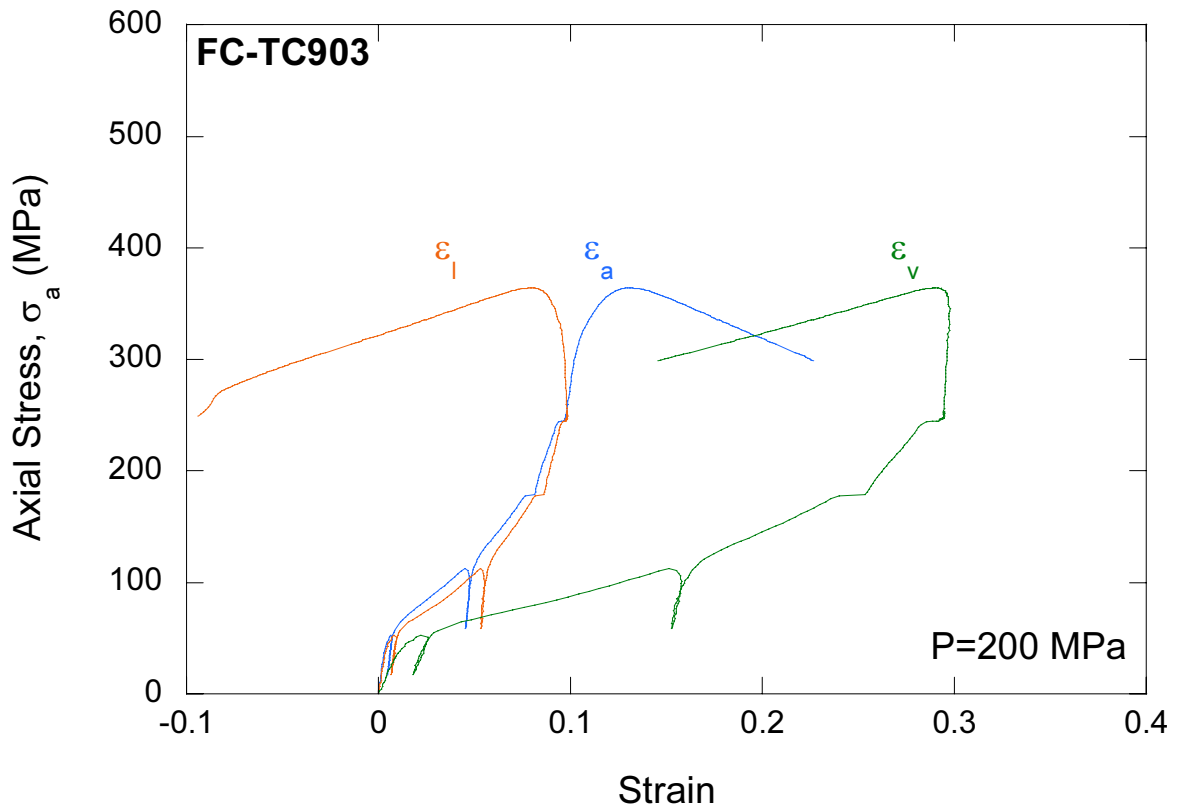


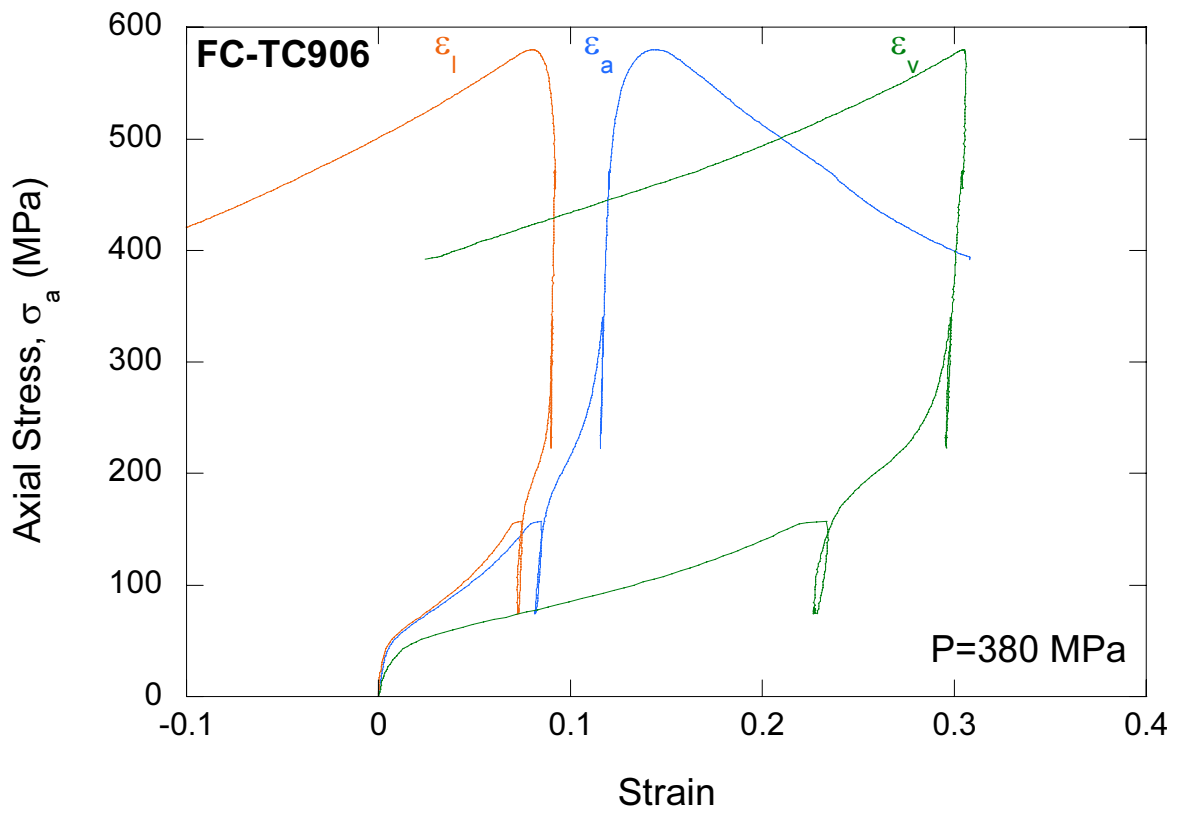
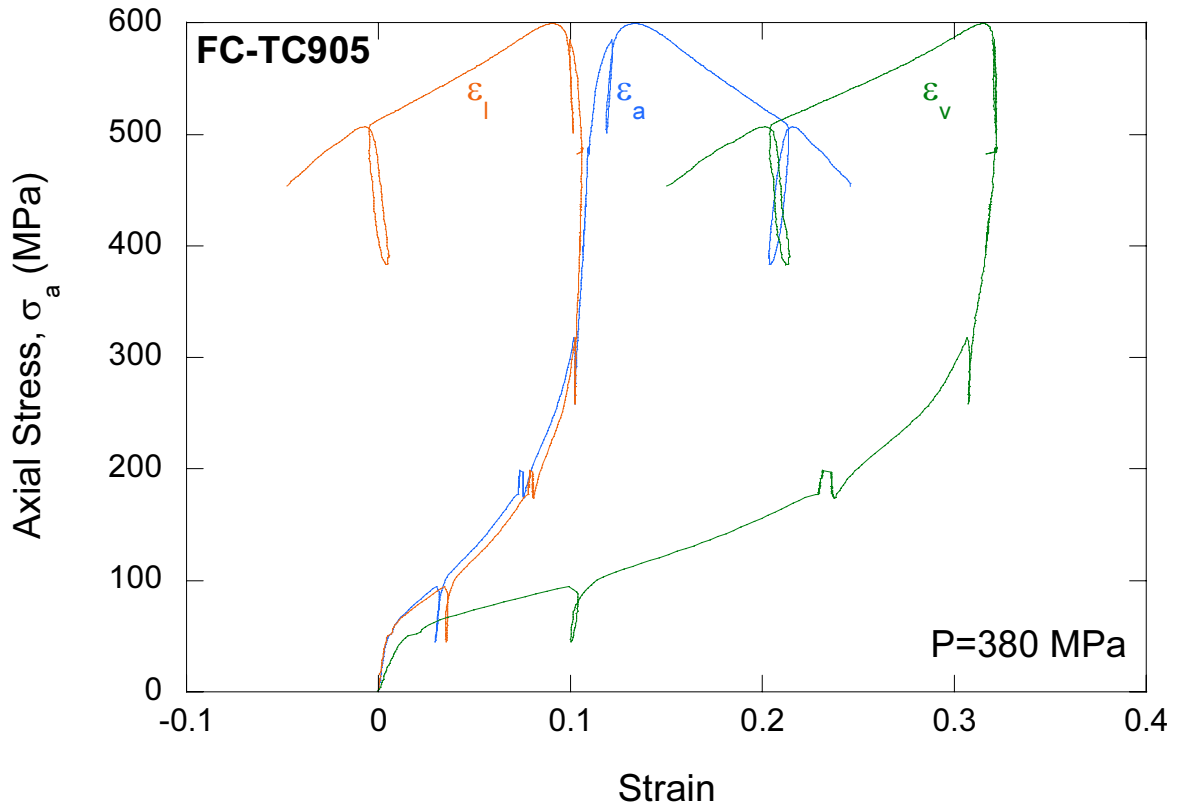


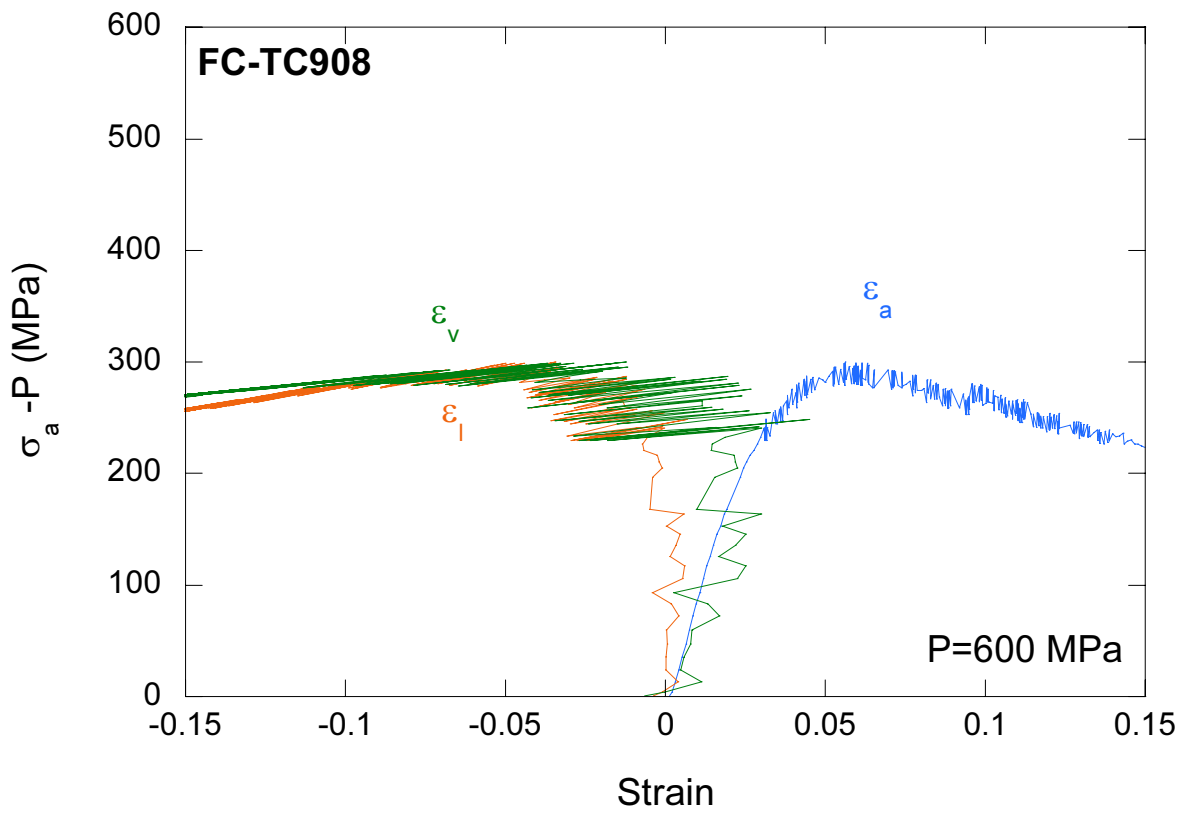
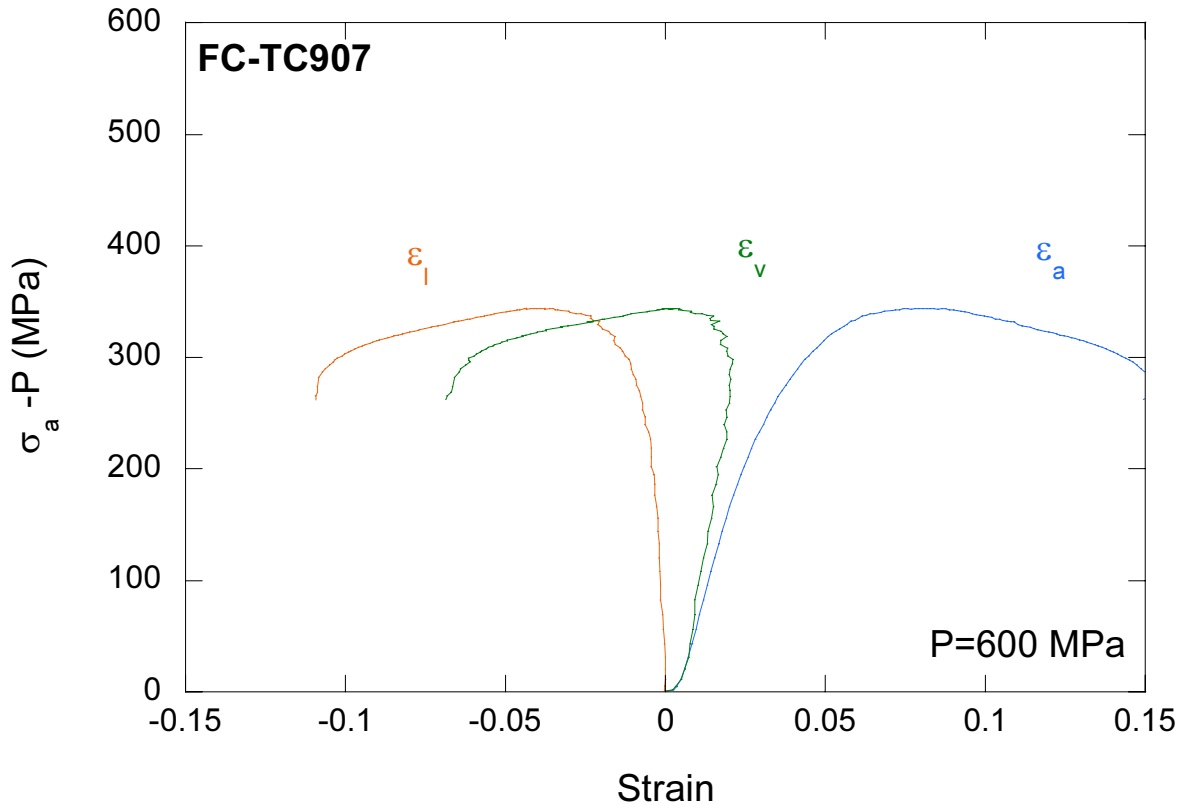
APPENDIX C-2

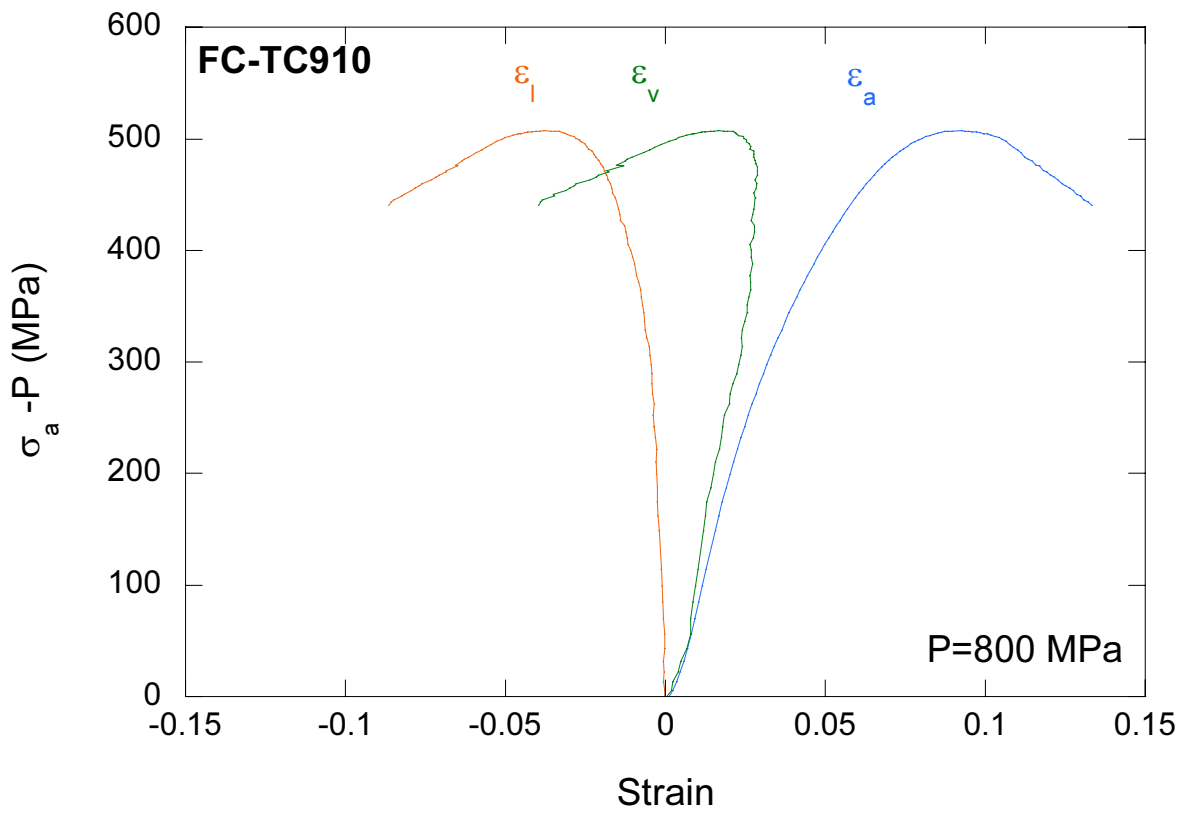
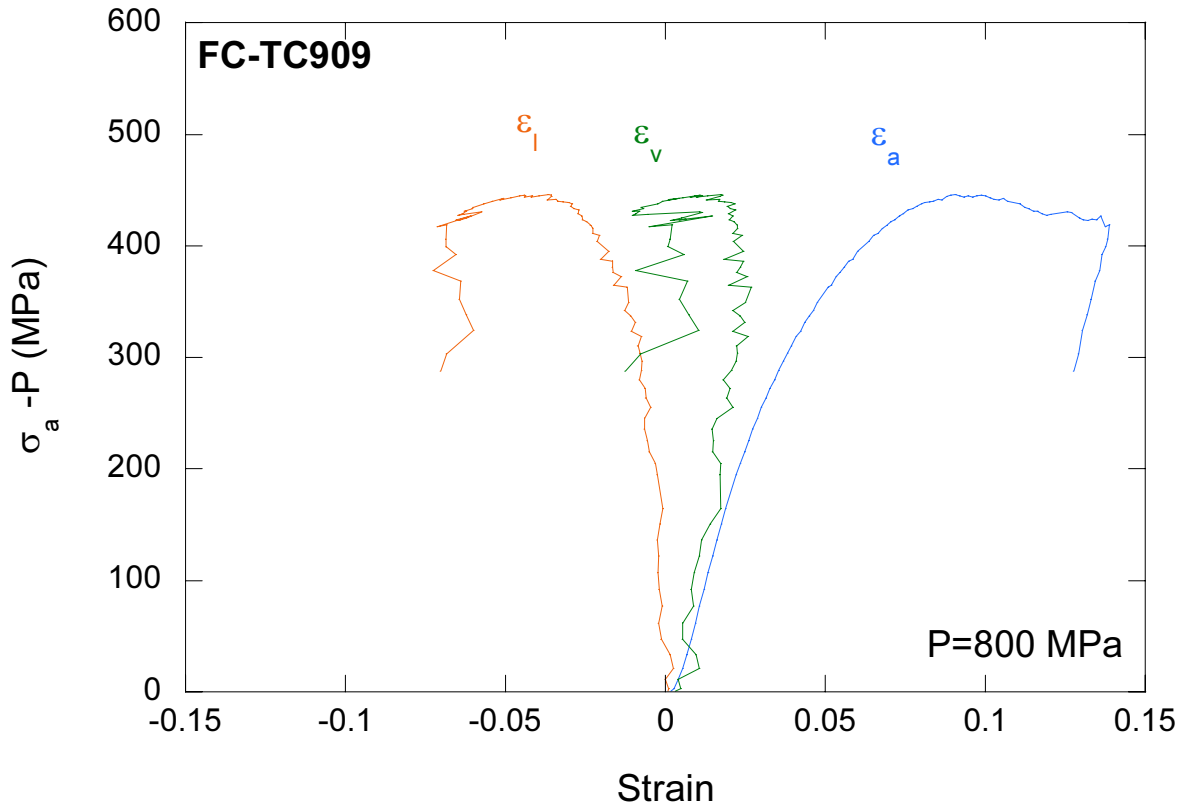
Stress-Strain Plots from Triaxial Compression (TXC) / Hydrostatic Compression Tests (HCT) of Cellular Concrete (σ_a -axial stress, ε_a -axial strain, ε_l -lateral strain, ε_v -volumetric strain, and P- confining pressure)

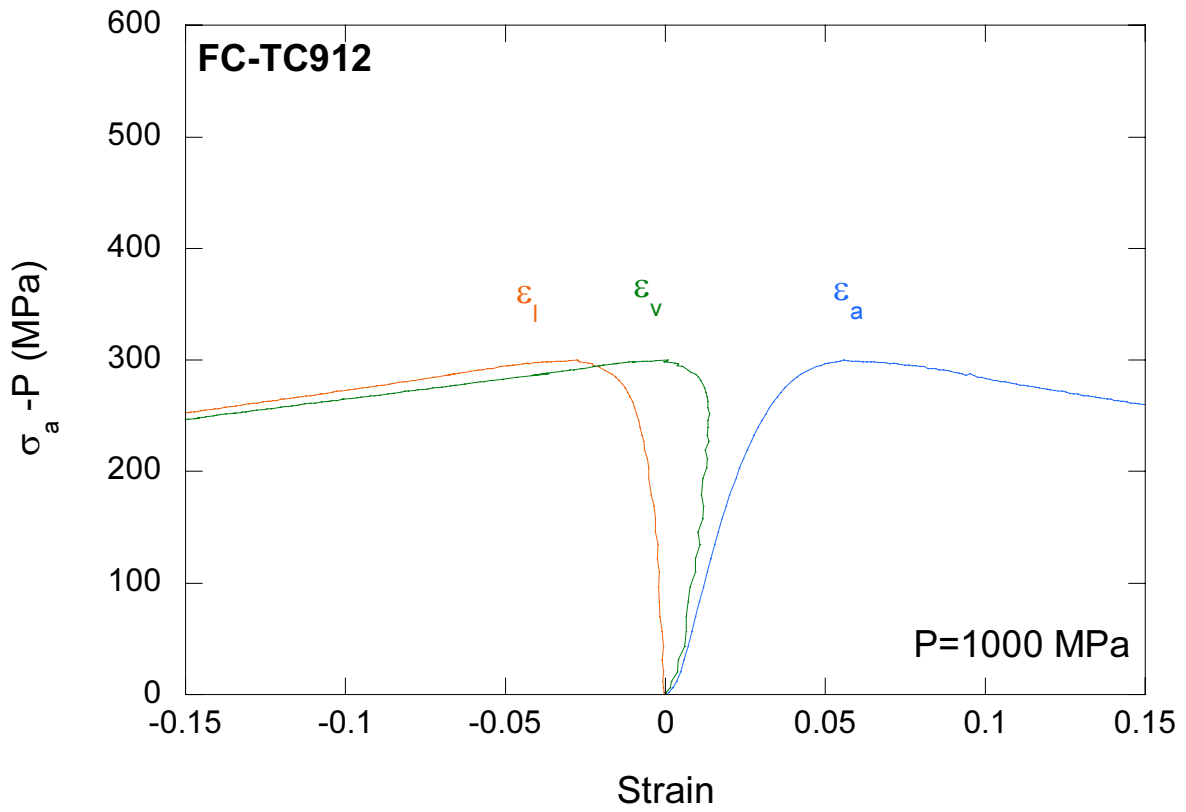
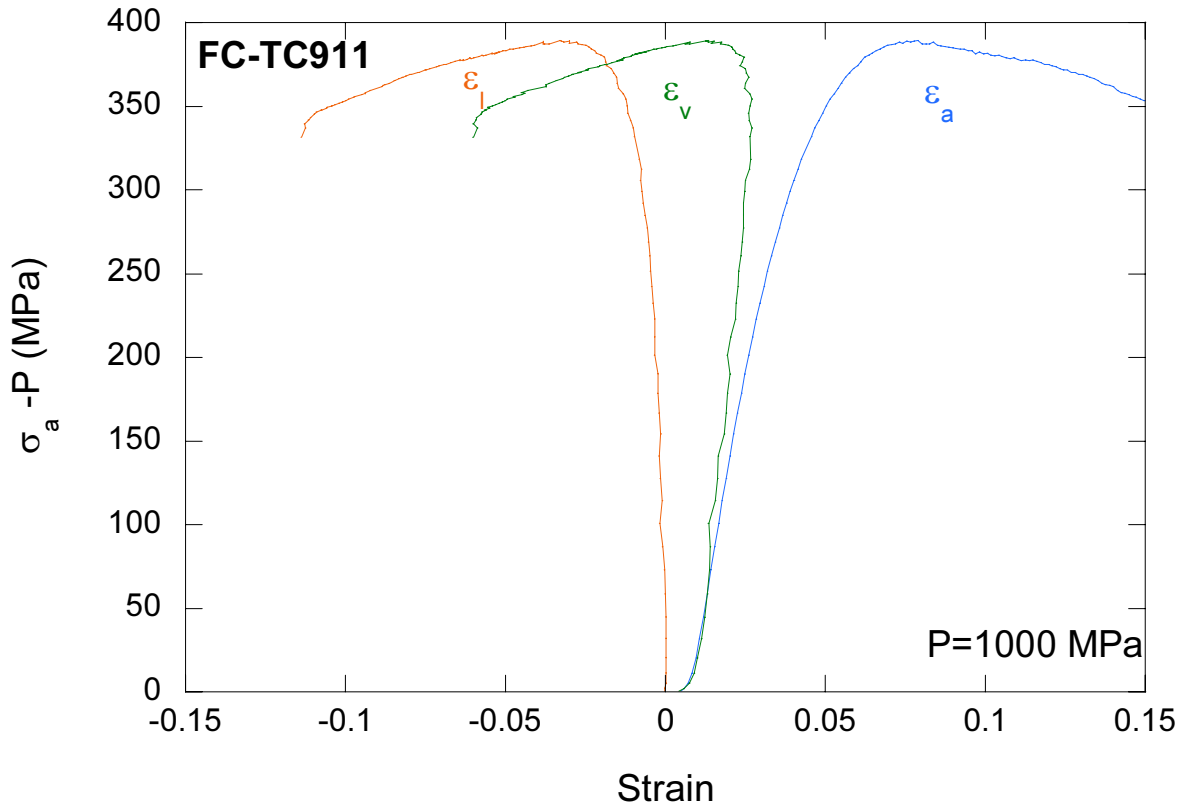


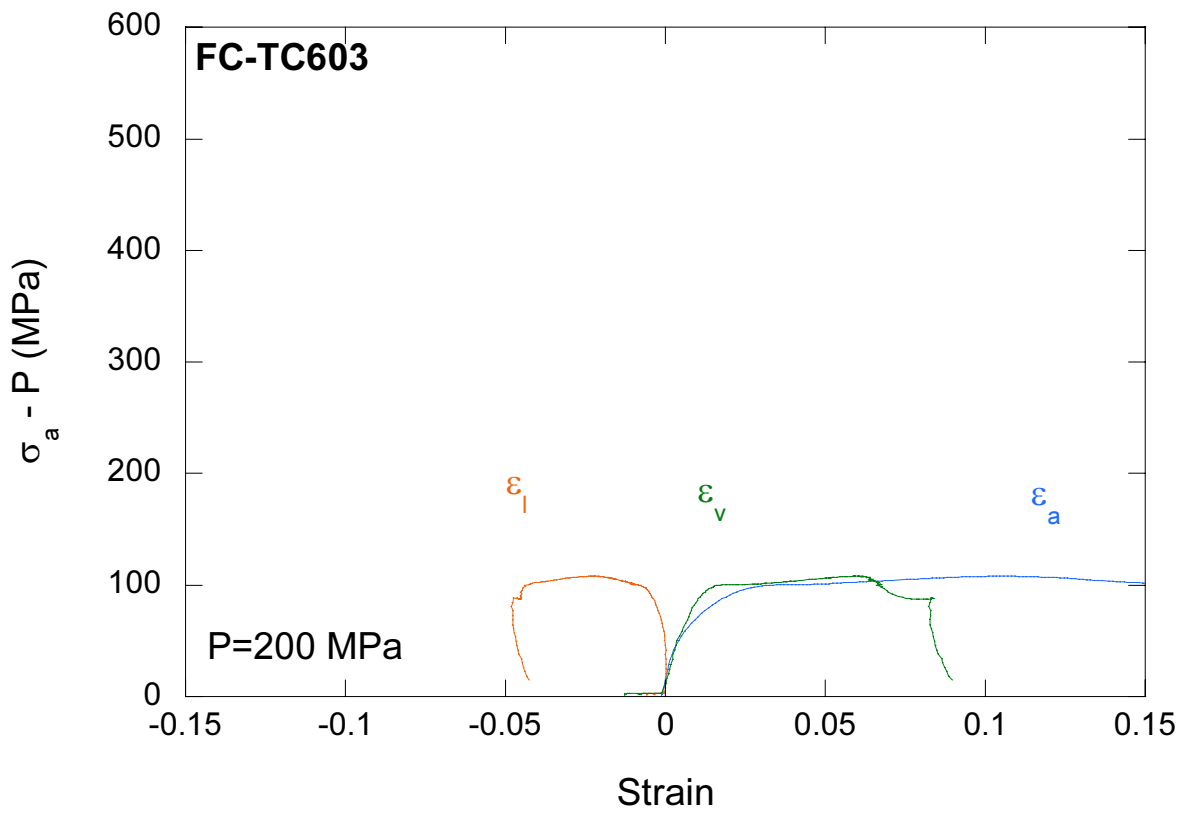
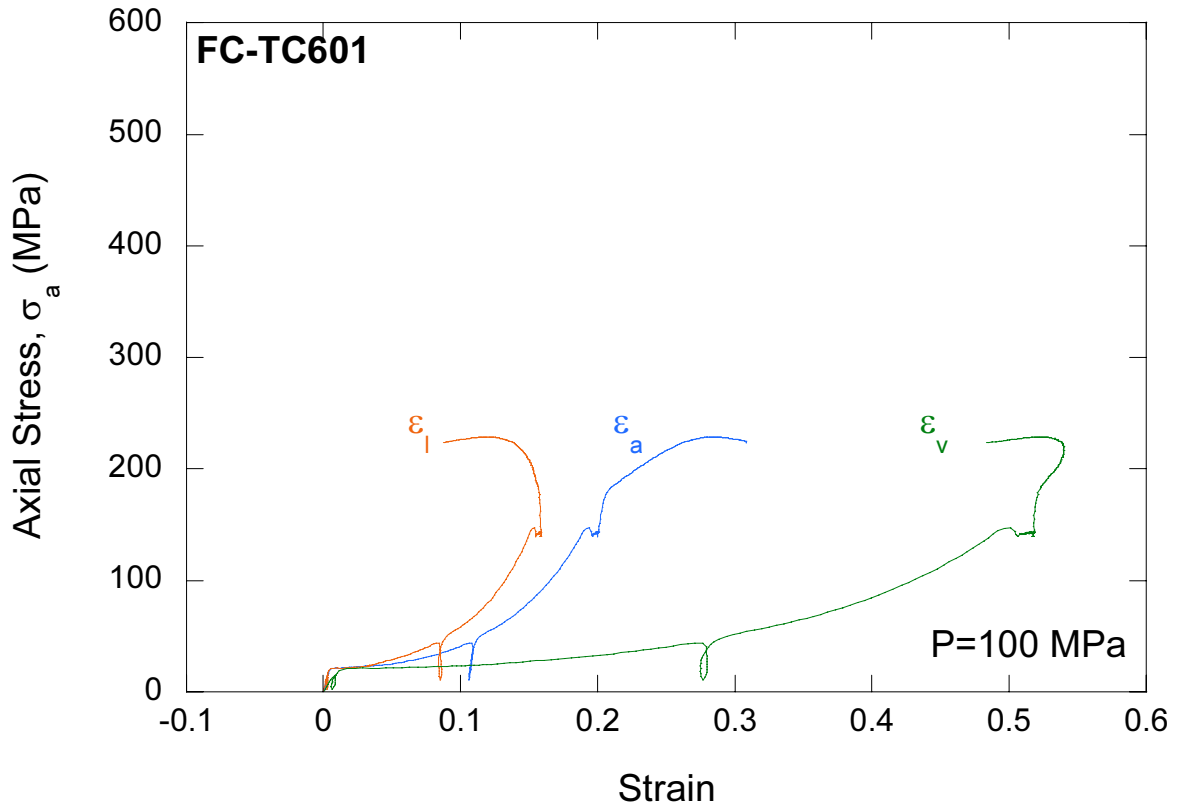


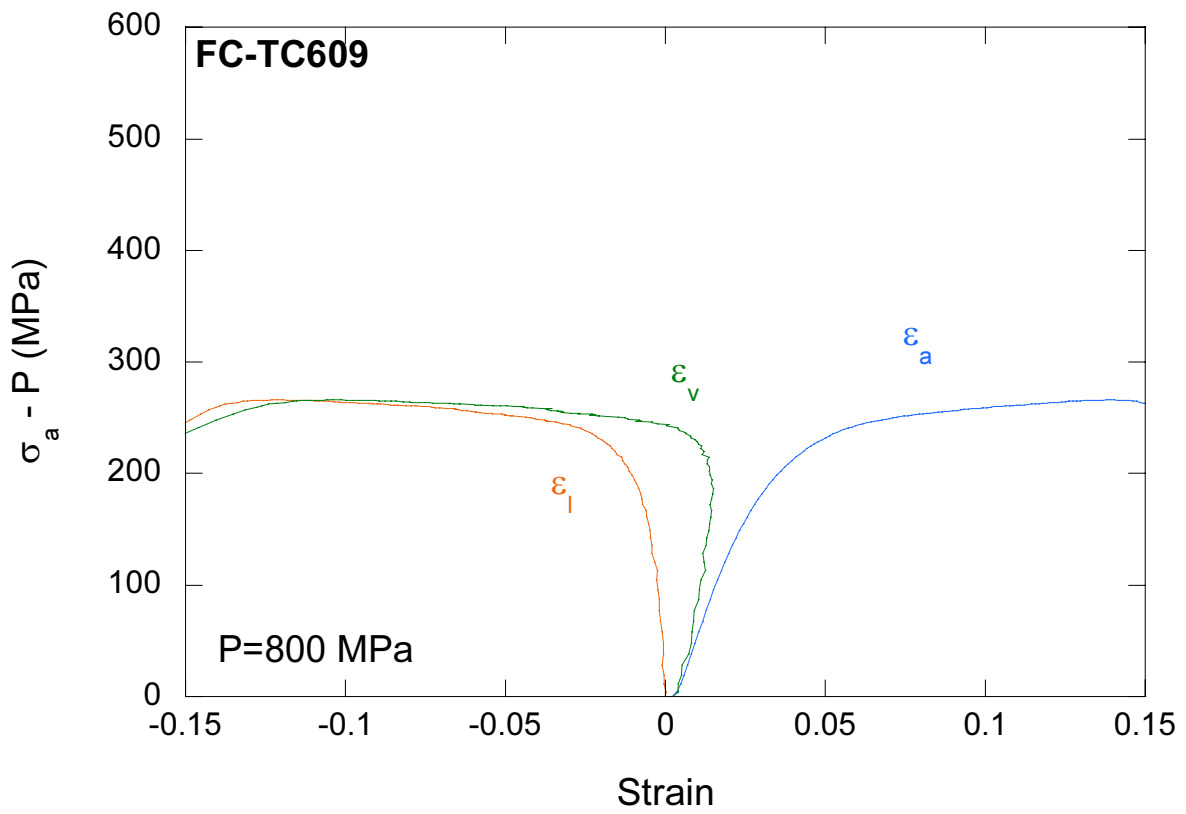
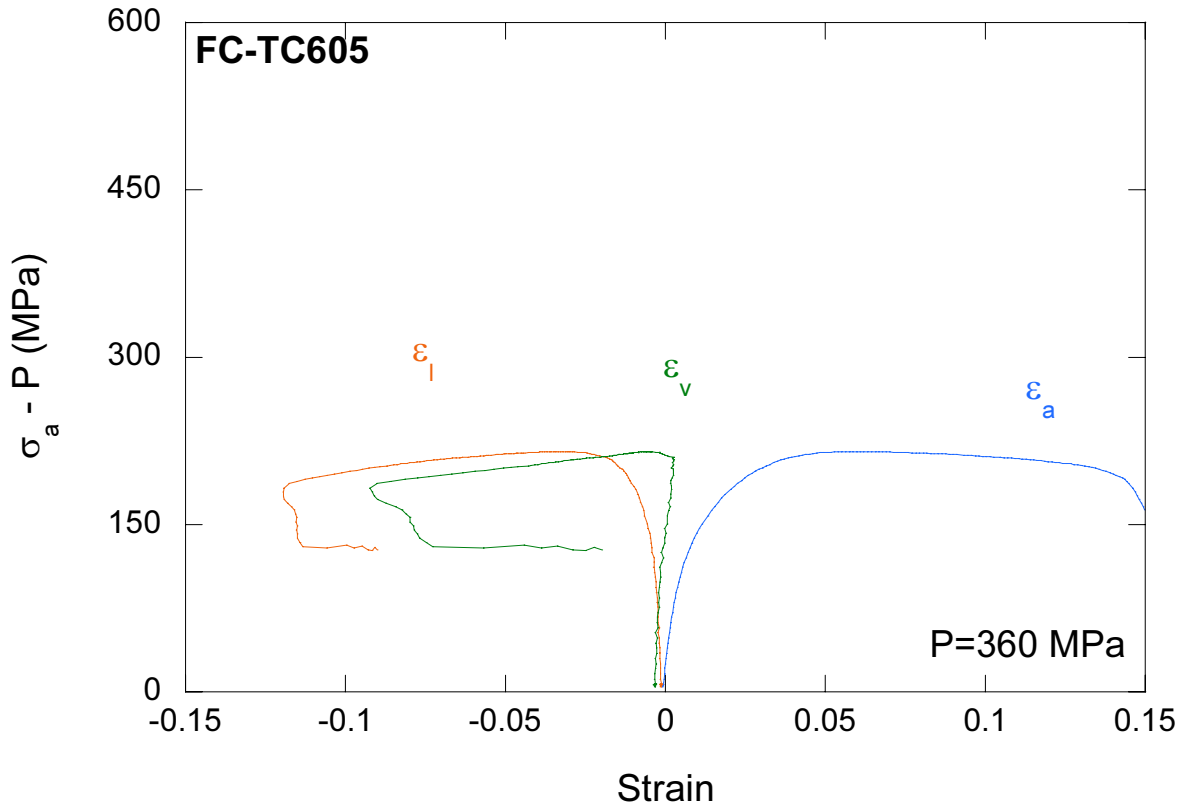








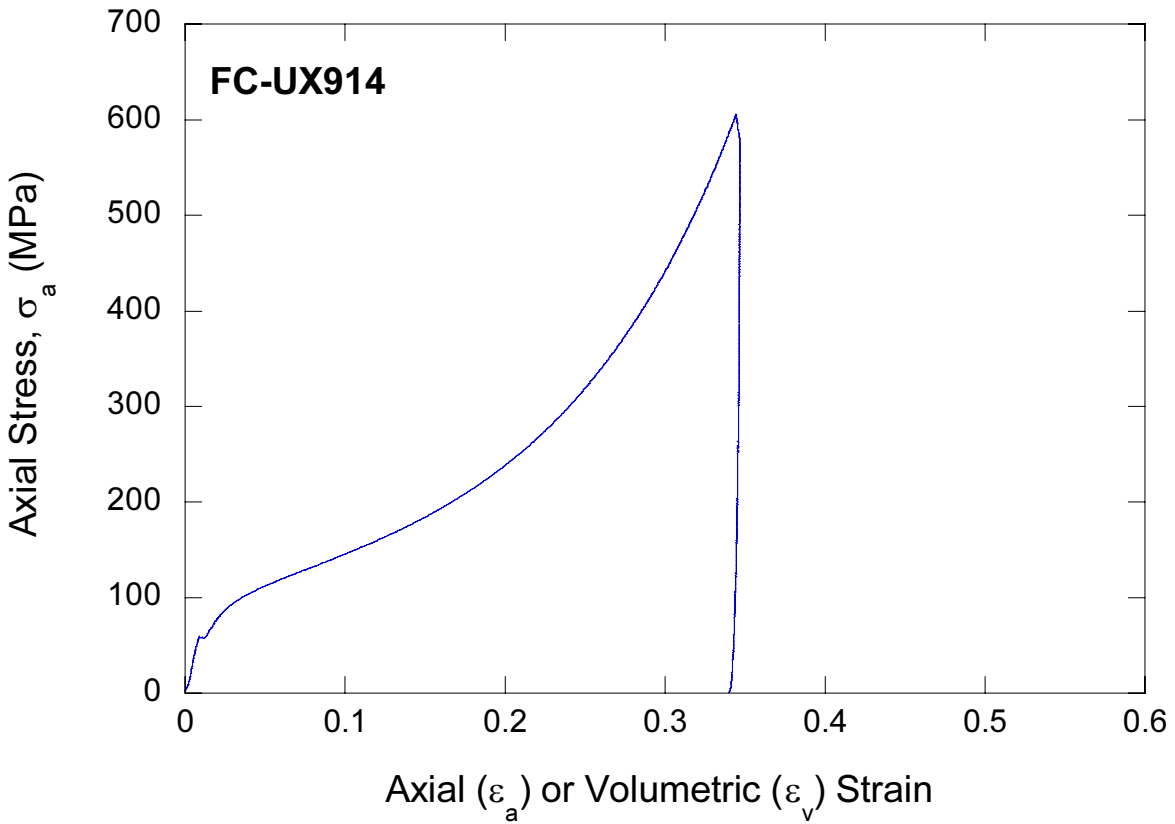
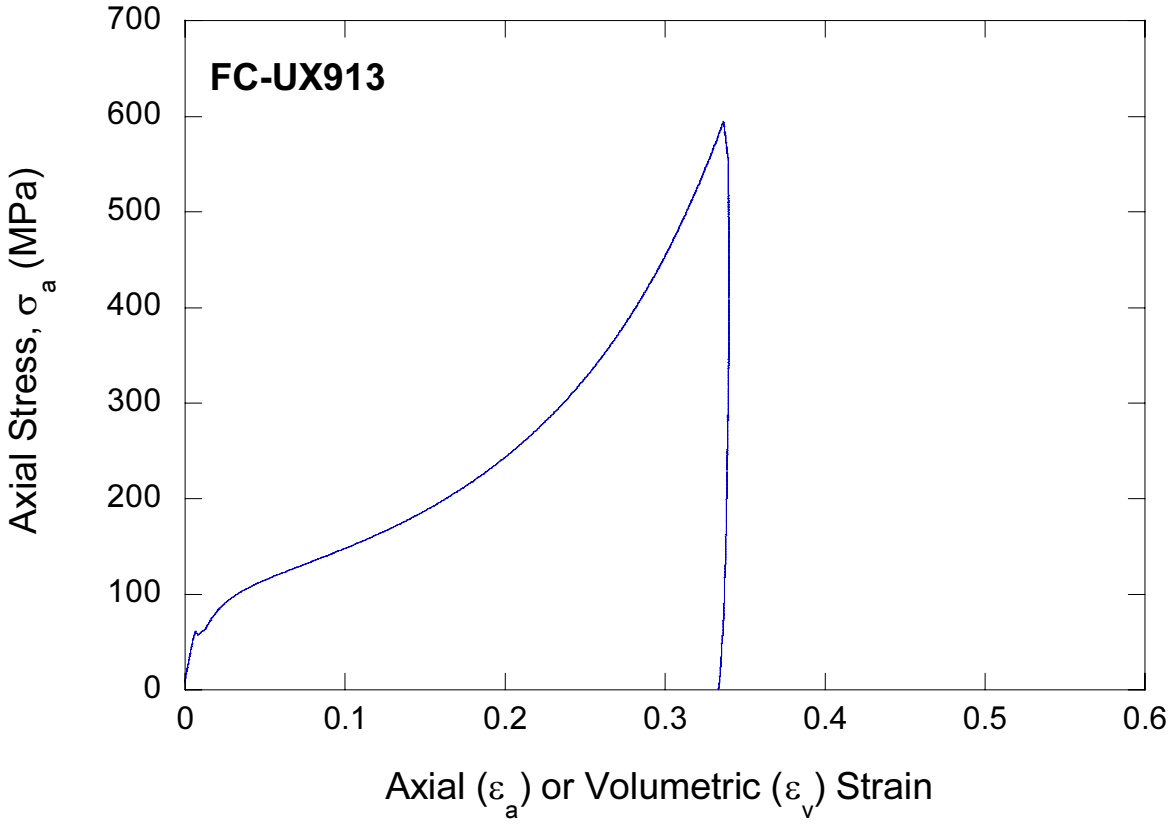


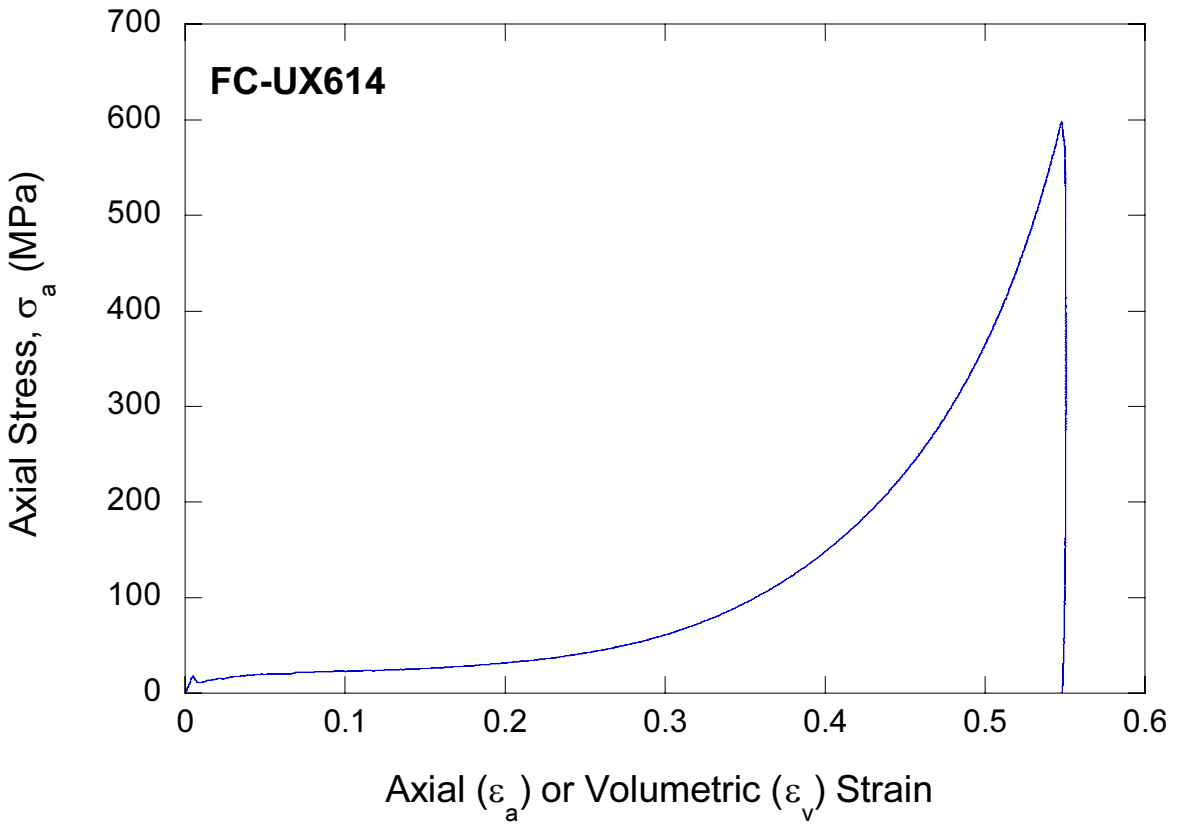
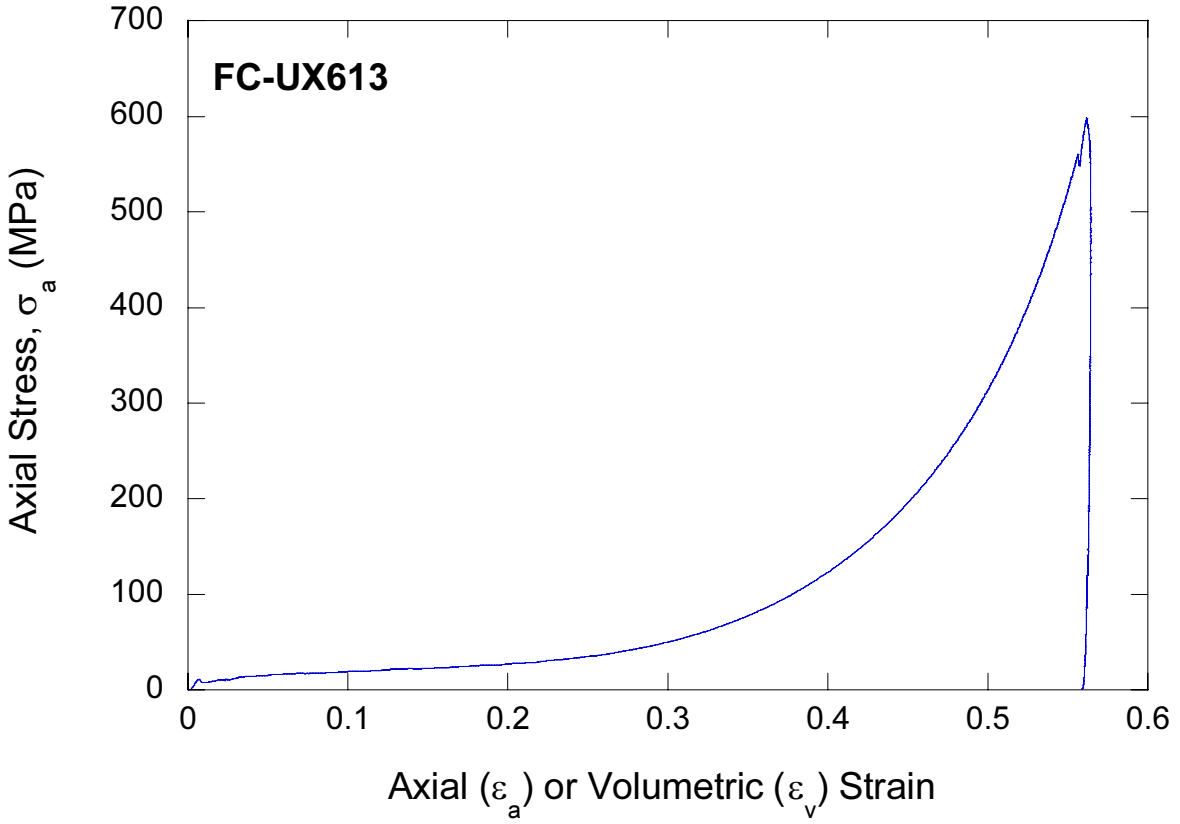


APPENDIX D

Stress-Strain Plots from Uniaxial Strain Tests (UXE) of Cellular Concrete

(σ_a -axial stress, ε_a -axial strain, and ε_v -volumetric strain)

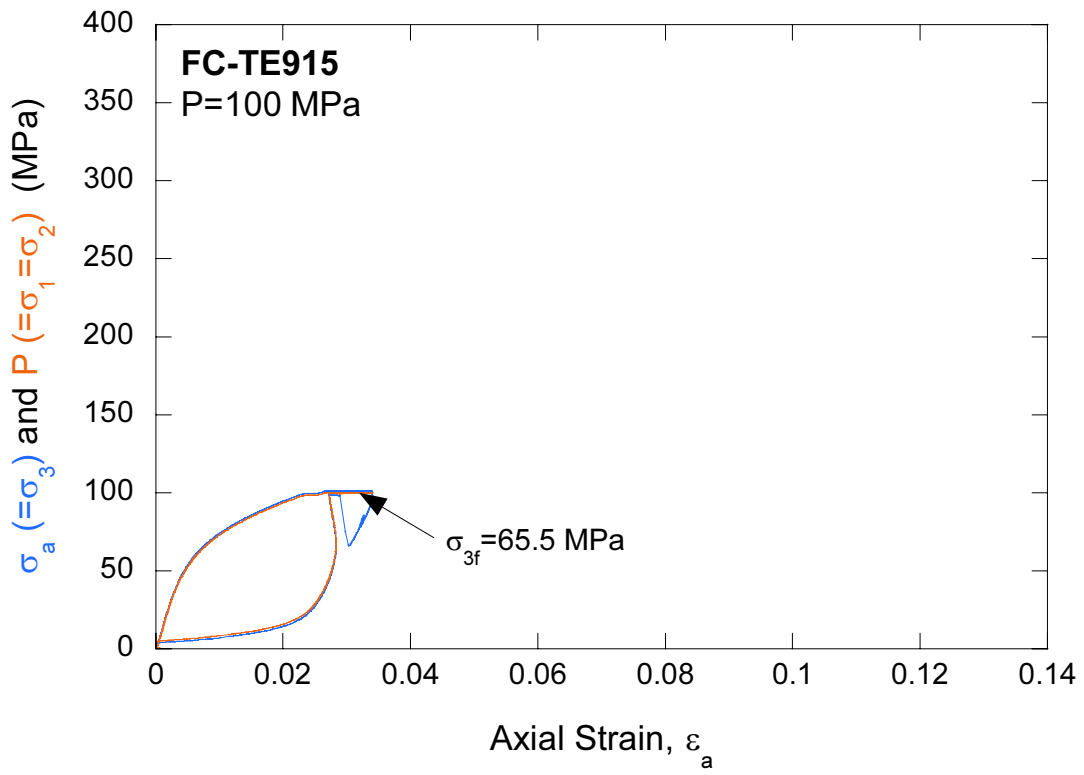
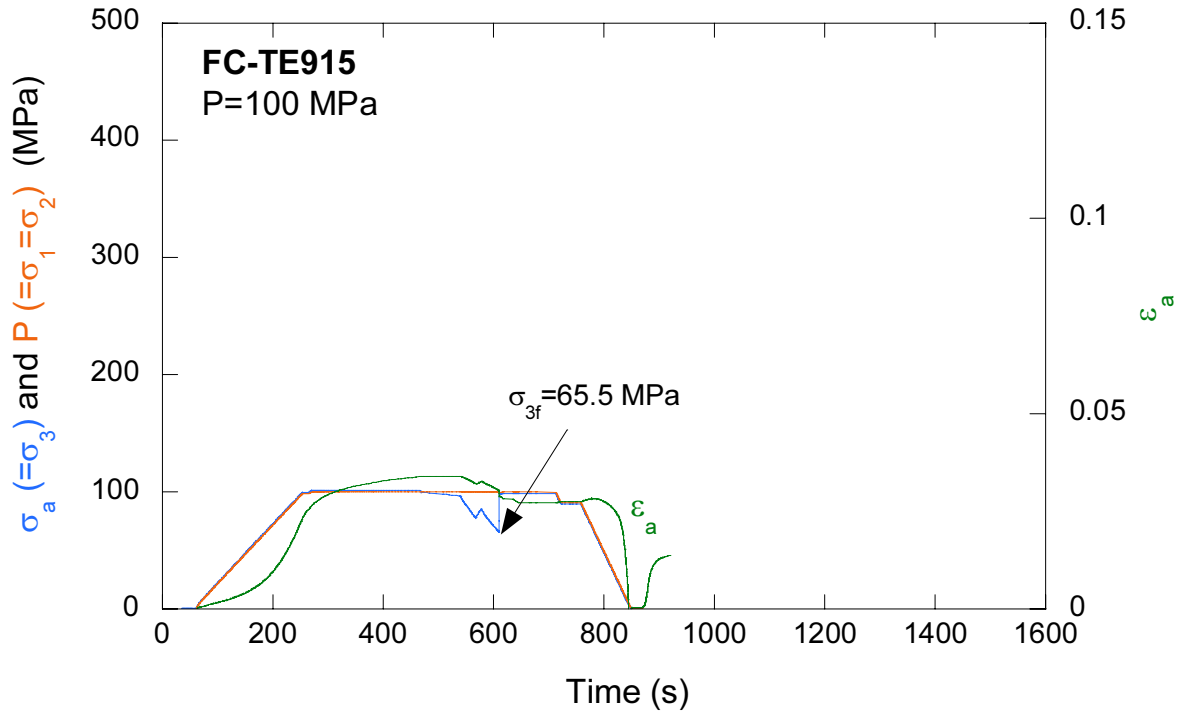


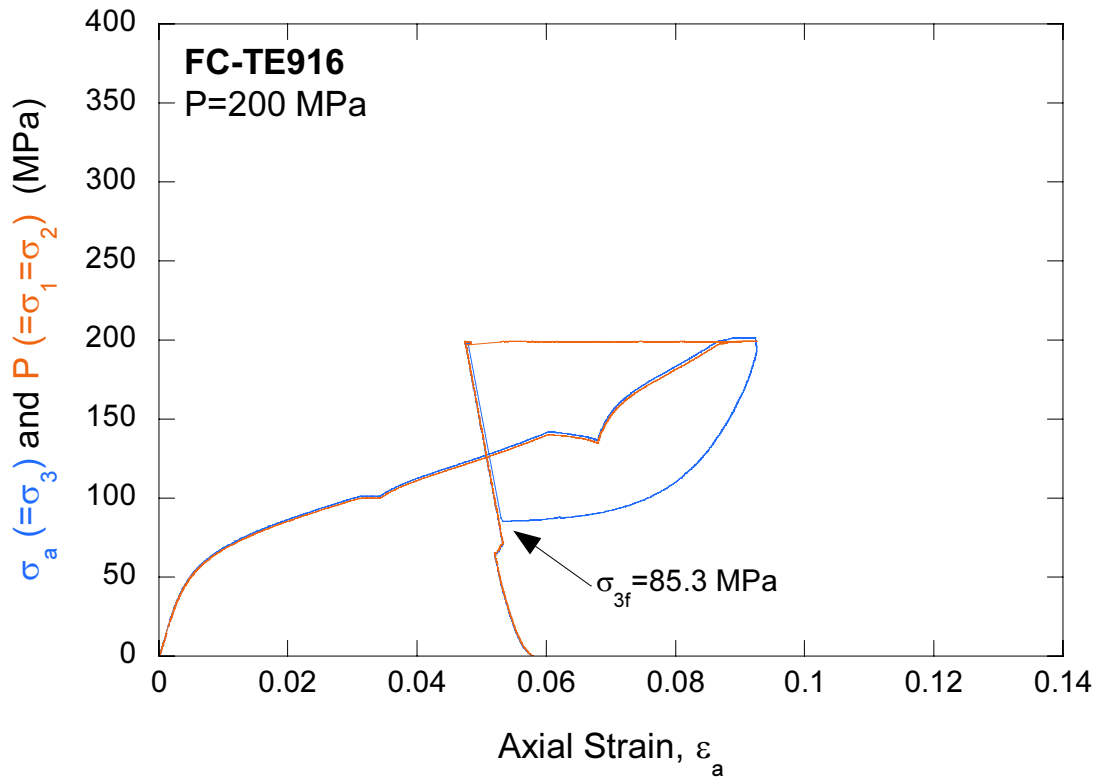
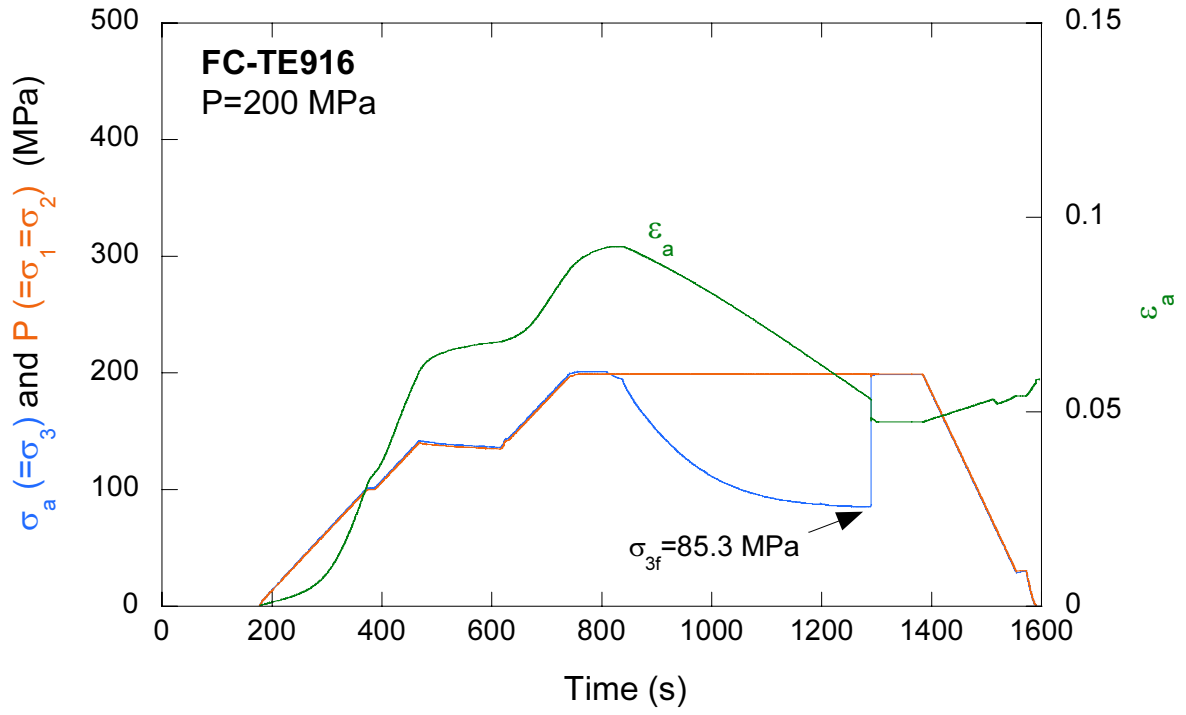


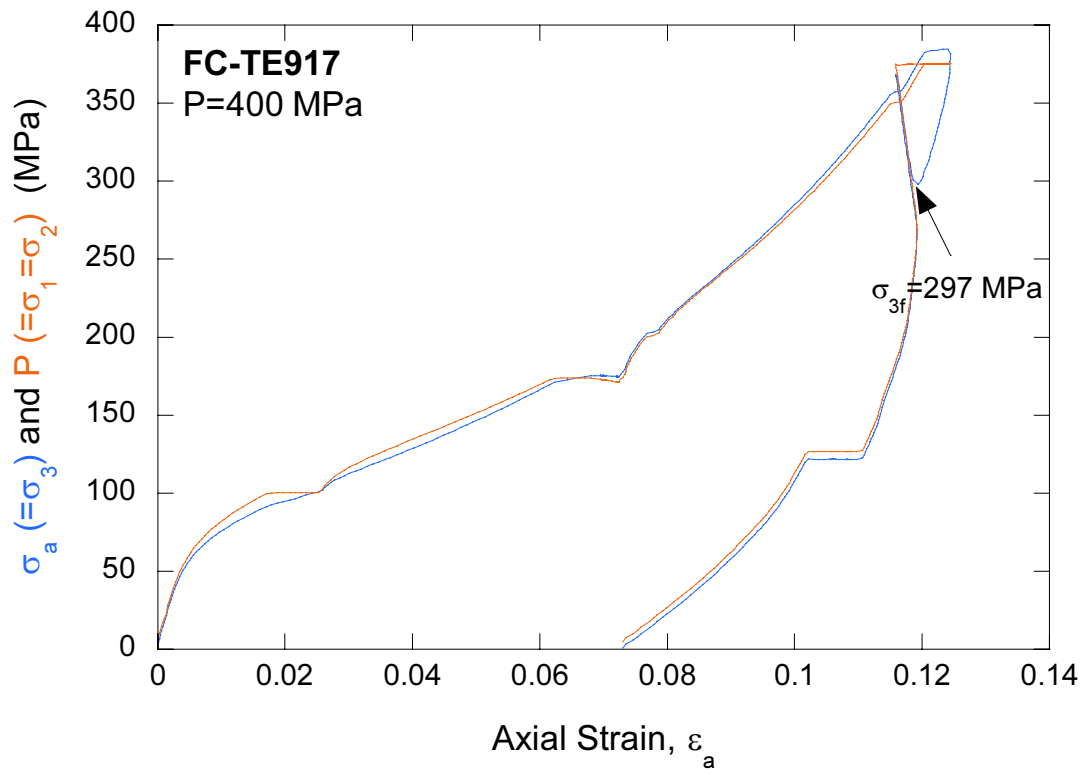
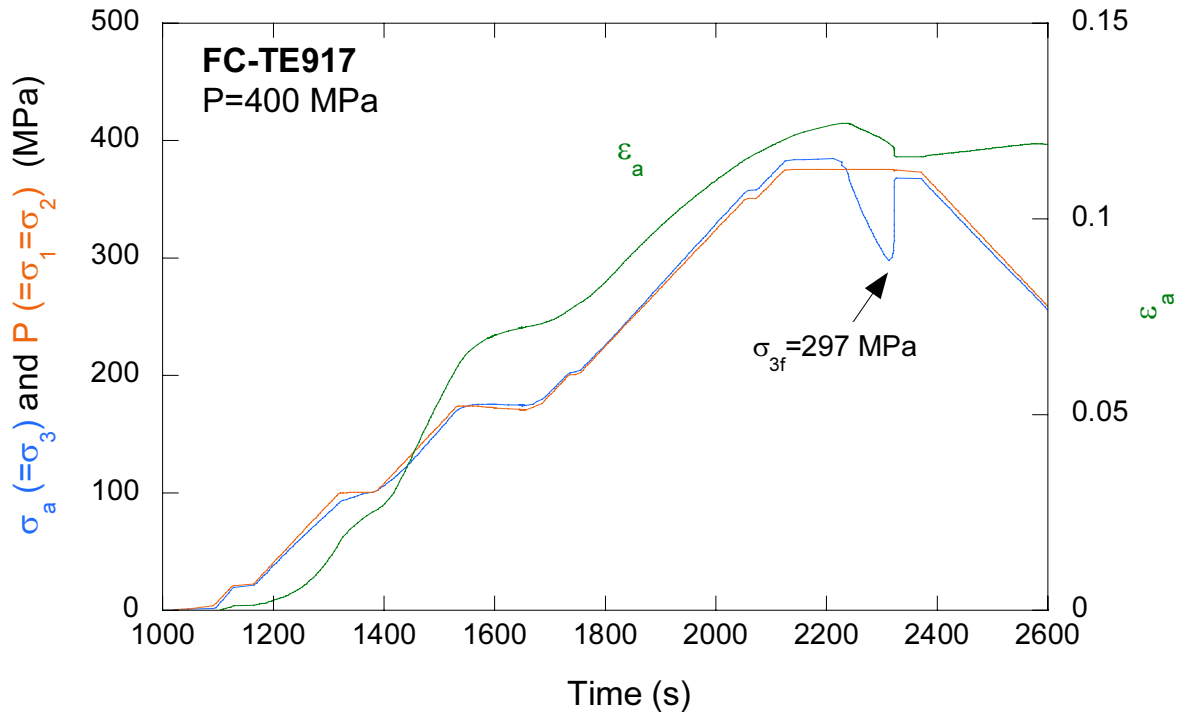
APPENDIX E

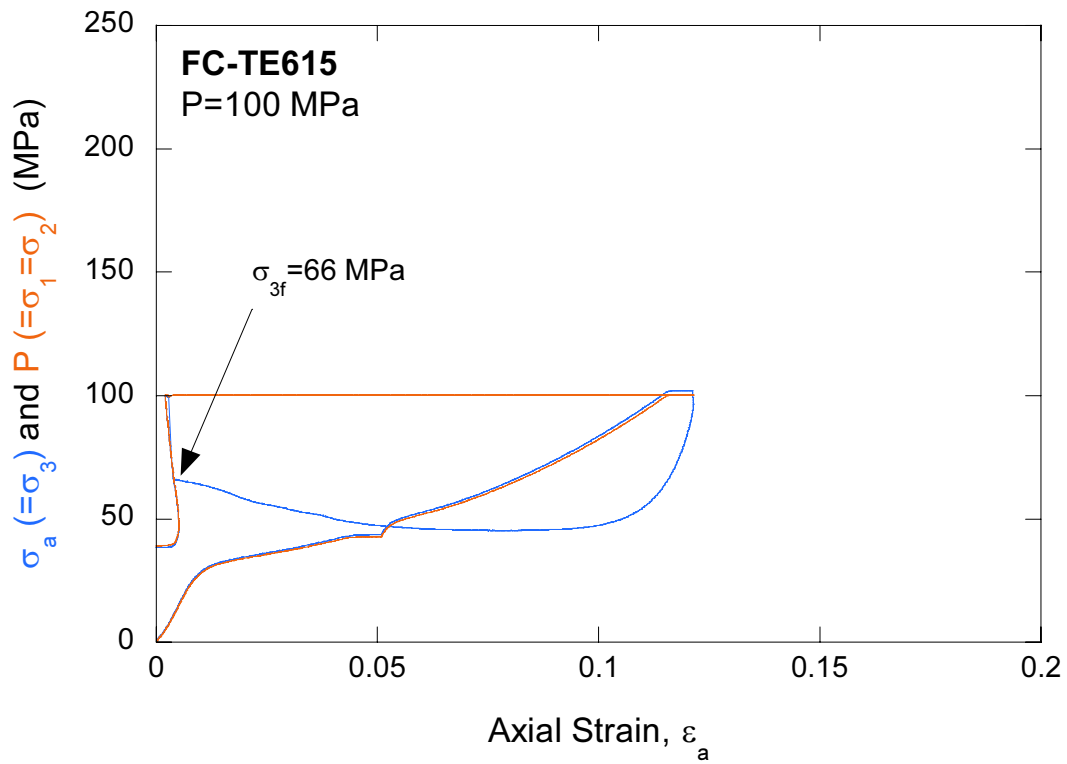
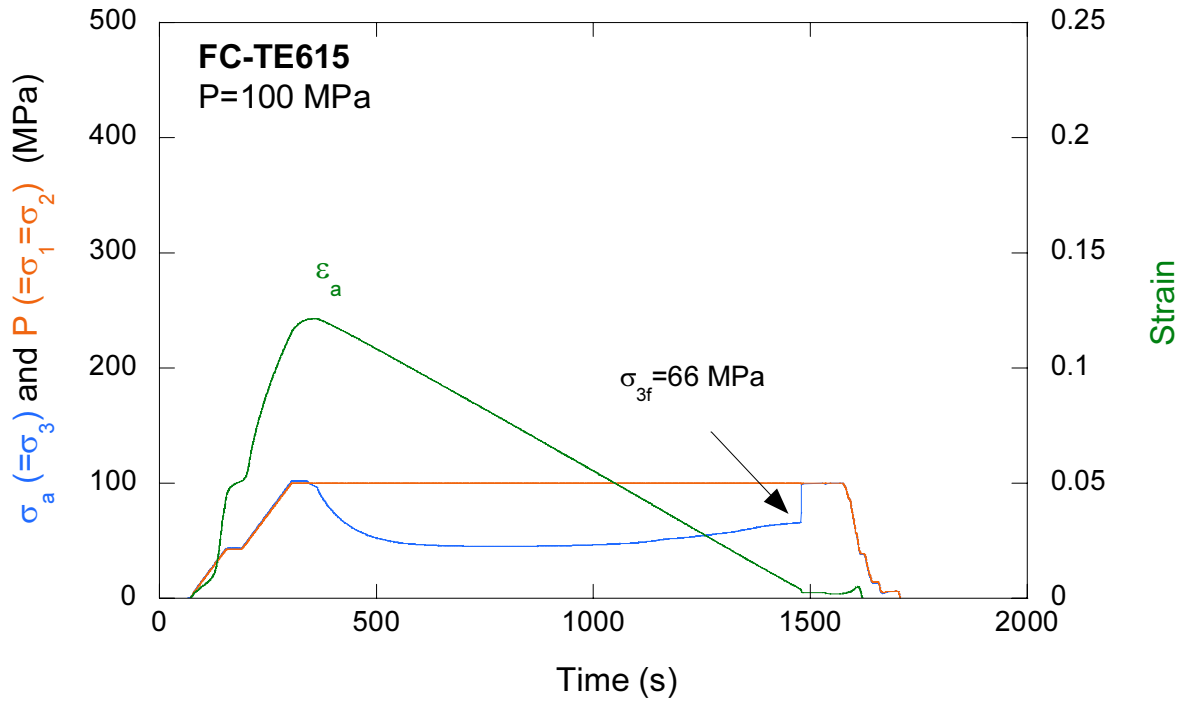
Stress-Strain-Time and Stress-Strain Plots from Triaxial Extension Tests (TXE) of Cellular Concrete

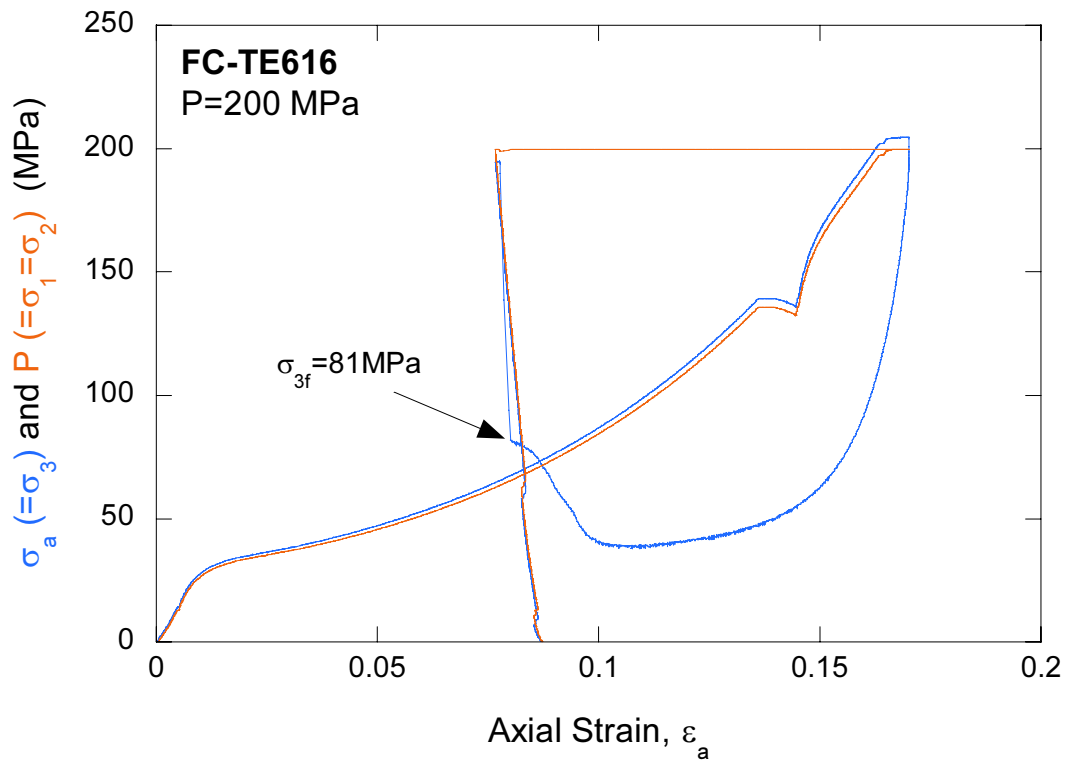
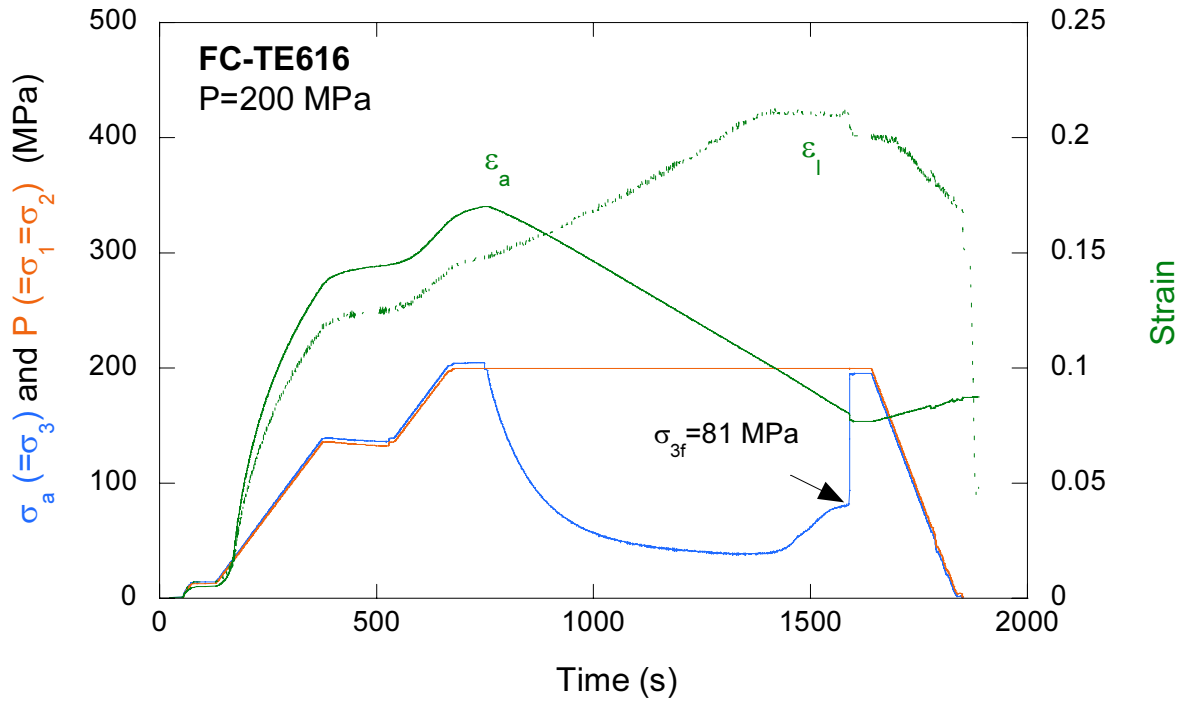
(σ_a -axial stress, σ_1 -major principal stress, σ_2 -intermediate principal stress, σ_3 -minor principal stress, σ_{3f} -triaxial extension strength, ε_a -axial strain, ε_l -lateral strain, and P-confining pressure)





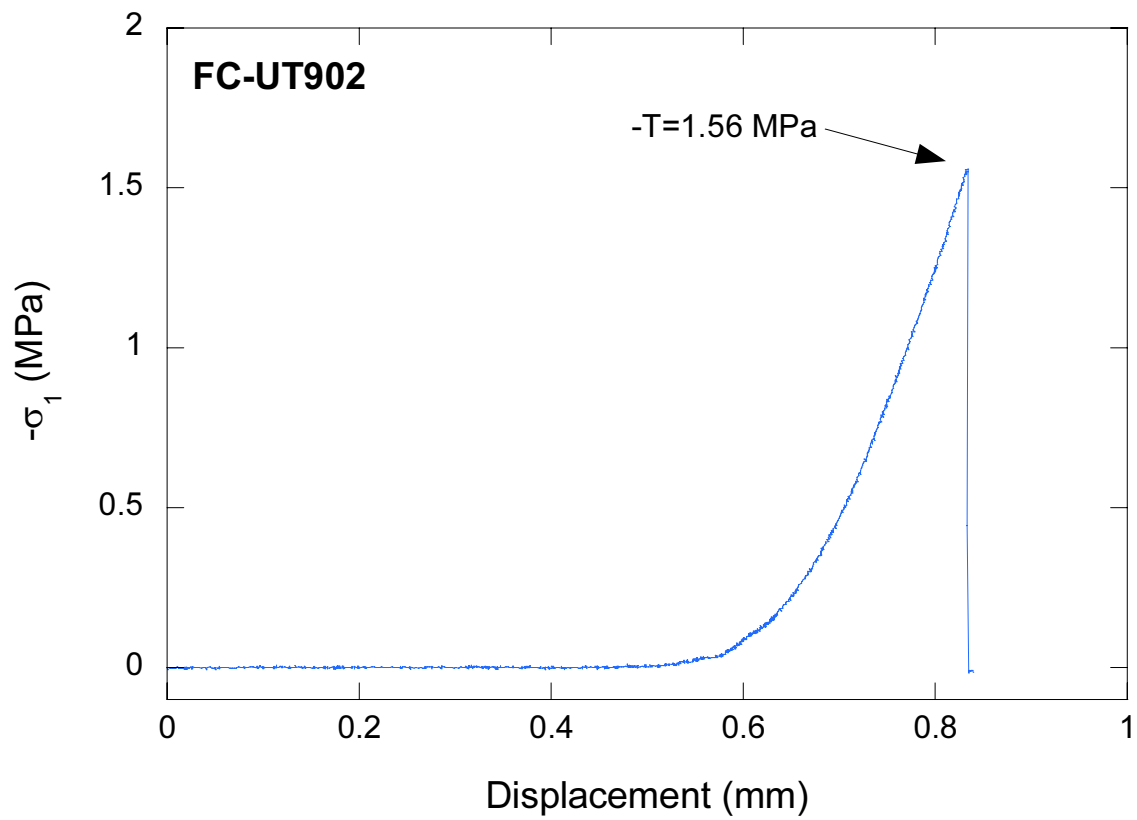
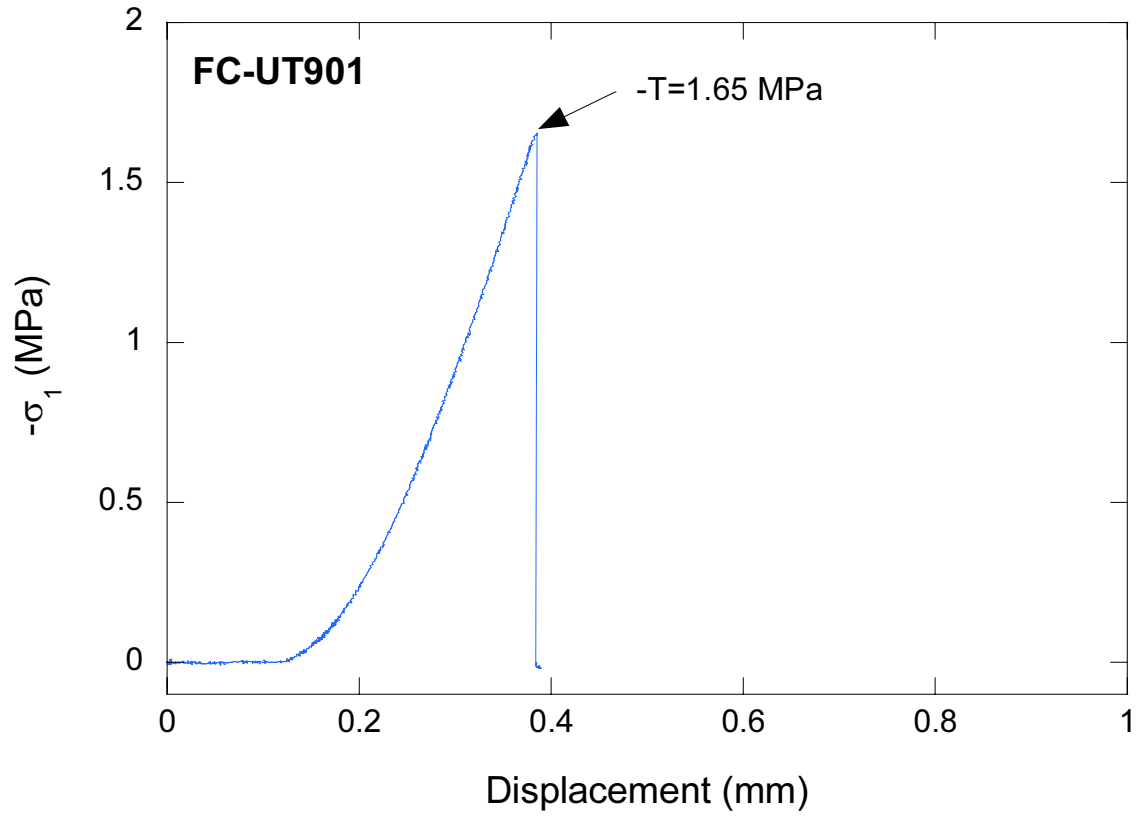


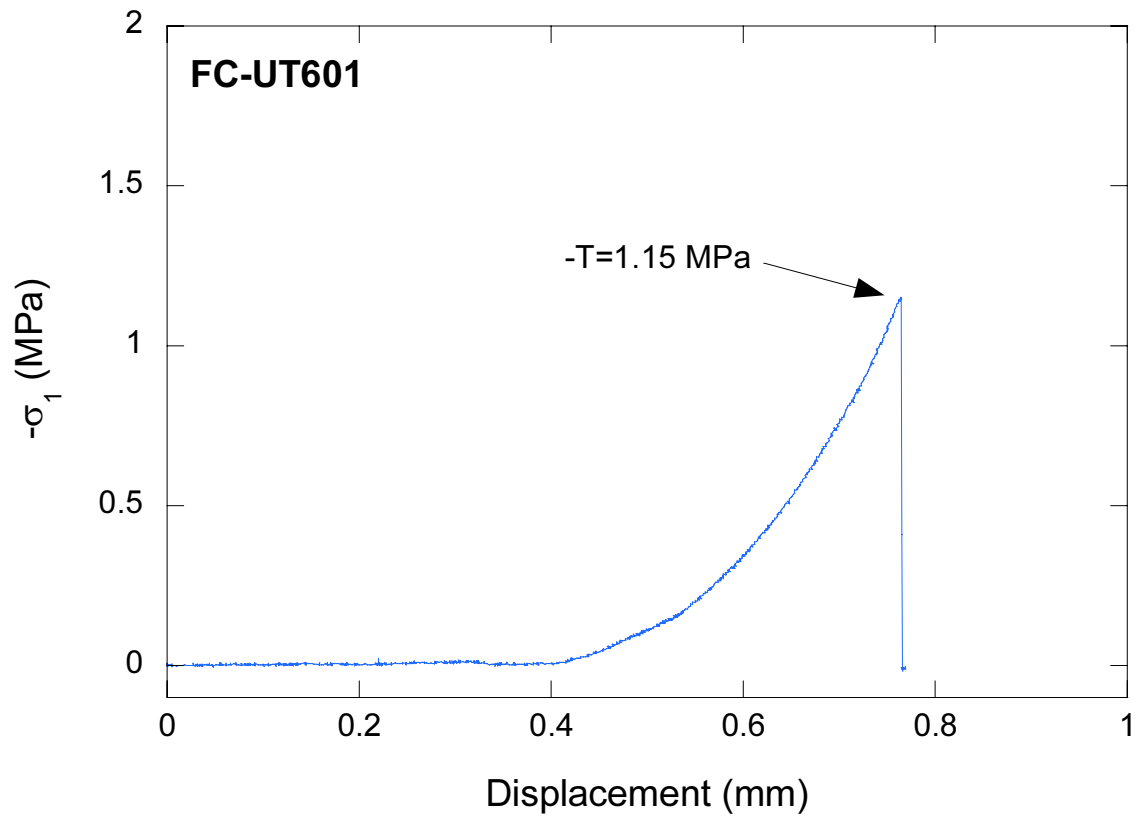
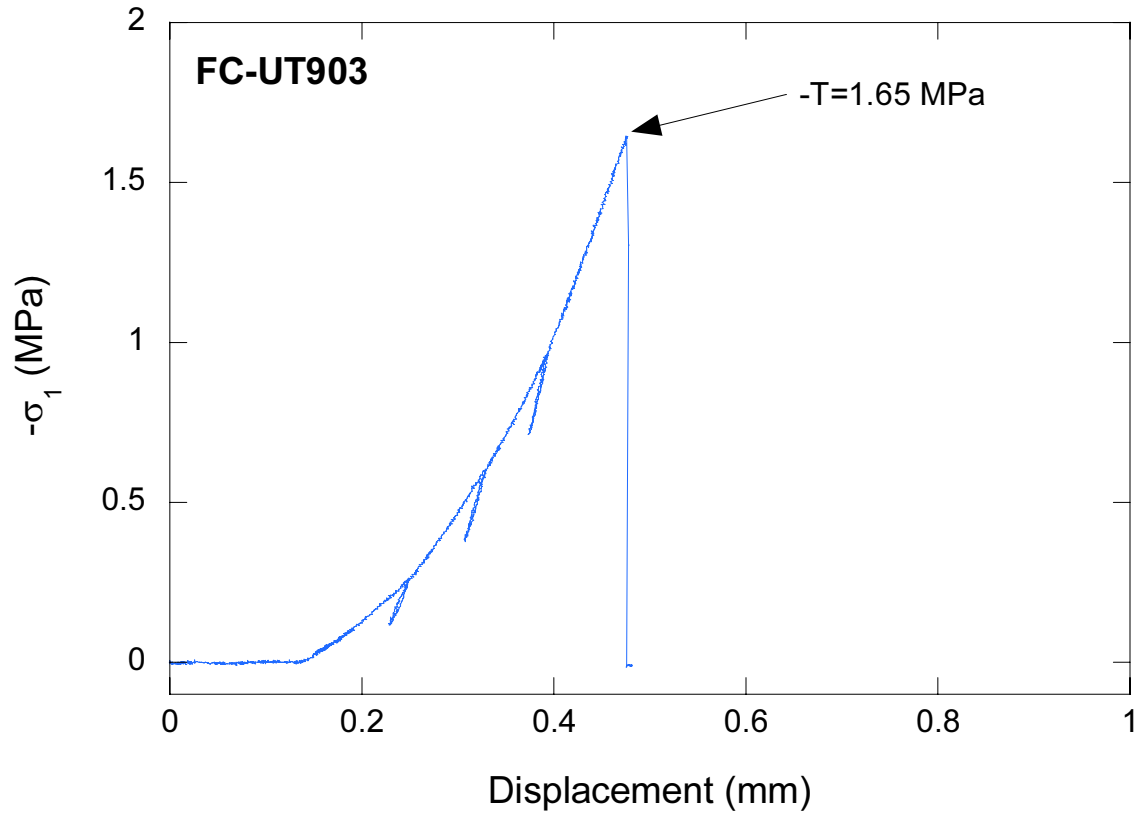


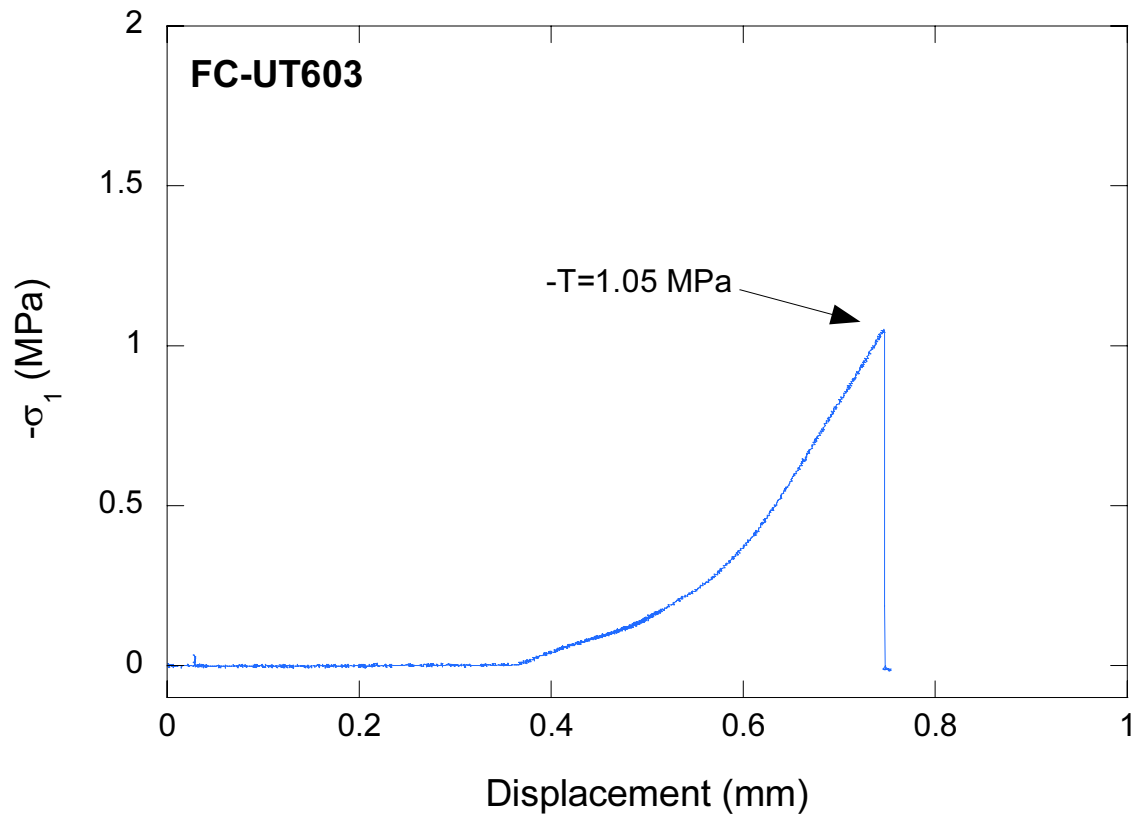
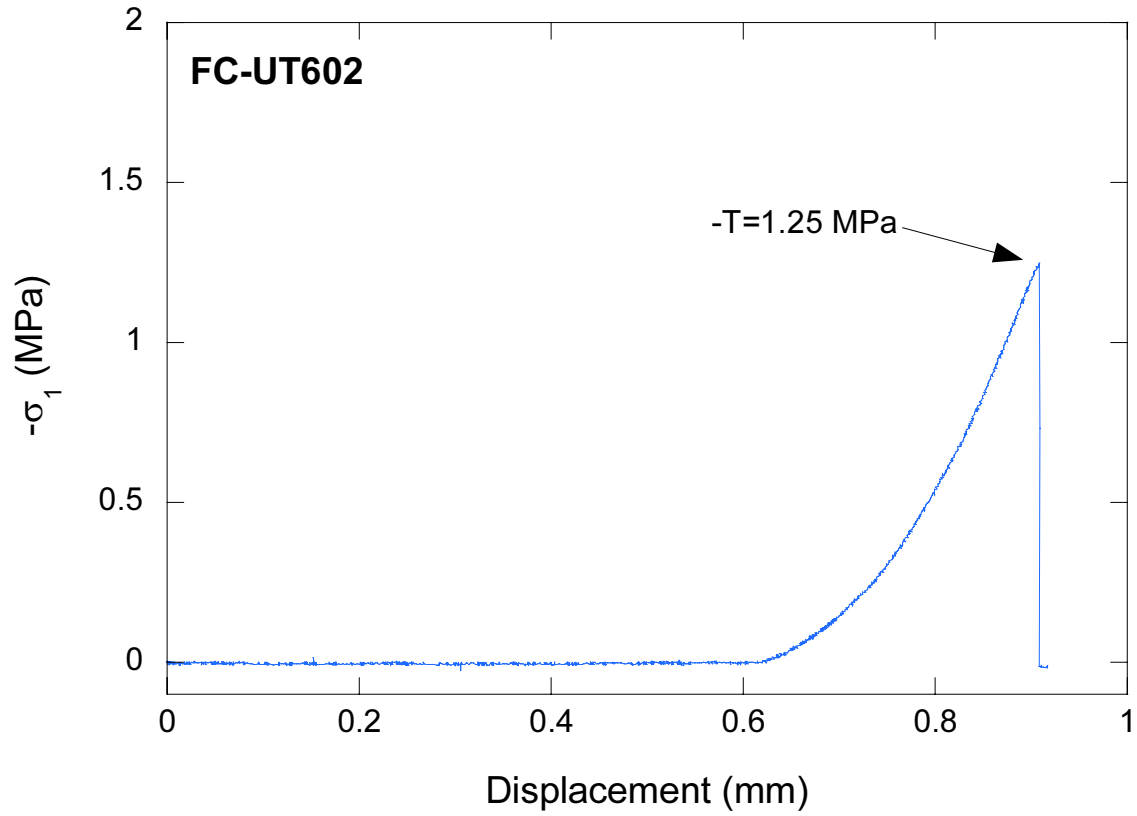


APPENDIX F

Stress-Displacement Plots from Uniaxial Tension Tests (UTT) of Cellular Concrete (-T : uniaxial tensile strength)







APPENDIX G

List of Data and Supplemental Files Archived in Webfileshare System

List of files archived in the WEBFILESHARE system (<https://wfsprod01.sandia.gov>).

Folder Name	File Name	Description
/TARGET/cellular-concrete	NSWCDD-Sand.doc	This SAND report
/TARGET/cellular-concrete	NSWCDD-Test Plan.doc	Test plan for geomaterial characterization of foamed concrete, Edward O'Connor, NSWCDD
/TARGET/cellular-concrete	NSWCDD-Cellular Concrete Status.doc	A draft of the end of the year report High Speed Ordnance Technology to the Office of Naval Research submitted in October 2003 for inclusion in the NSWCDD Surface Weapons Technology Program End of Year 2003 Progress Report, Timothy Spivak, NSWCDD/G22
/TARGET/cellular-concrete	NSWCDD-master.xls	<p>Master data file consists of the following seven worksheets:</p> <p>Specimen Dimension: cellular concrete specimen dimensions</p> <p>Triaxial (TxC) Hydro (HCT): Test data from triaxial compression tests</p> <p>Hydrostatic Compression (HCT): Test data from hydrostatic compression tests</p> <p>Uniaxial Compression (UCT): Test data from uniaxial compression tests</p> <p>Uniaxial Tension (UTT): Test data from uniaxial tension tests</p> <p>Uniaxial Strain (UXE): Test data from uniaxial strain tests</p> <p>Triaxial Extension (TXE): Test data from triaxial extension tests</p>
/TARGET/cellular-concrete	NSWCDD-Data-Sheets.zip	Laboratory data sheets consisting of original notes during testing.
/TARGET/cellular-concrete	NSWCDD-pictures.zip	Miscellaneous pictures taken during constitutive testing of cellular concrete
/TARGET/cellular-concrete	NSWCDD-Conversion-Equations.zip	Conversion equations used to obtain stress-strain data

DISTRIBUTION

Sandia National Laboratories

P.O. Box 5800

Albuquerque, NM 87185

1	MS 0316	P. Yarrington, 9230
1	MS 0482	T. C. Togami, 2131
1	MS 0701	P. J. Davies, 6100
1	MS 0751	A. F. Fossum, 6117
1	MS 0751	L. S. Costin, 6117
1	MS 0751	D. J. Holcomb, 6117
1	MS 0751	W. A. Olsson, 6117
5	MS 0751	M. Y. Lee, 6117
1	MS 0824	J. L. Moya, 9130
1	MS 0847	J. Jung, 9127
1	MS 1031	D. R. Bronowski, 6117
1	MS 1160	D. A. Dederman, 15412
1	MS 1395	B. Y. Park, 6821

1	MS 9018	Central Tech. Files, 8945-1
2	MS 0899	Technical Library, 9616
2	MS 0731	823/Library, 6850

Naval Surface Warfare Center, Dahlgren Division

NSWCDD - G22

17320 Dahlgren Road

Dahlgren, Virginia 22448

2	Edward O'Connor, NSWCDD-G22
1	Robert Gripshover, NSWCDD-G22
2	Allen D. Shirley, NSWCDD-G22
1	Timothy Spivak, NSWCDD-G22